

IZMIR KATIP CELEBI UNIVERSITY ★ GRADUATE SCHOOL OF SCIENCE
ENGINEERING AND TECHNOLOGY

NANOCOMPOSITES WITH GRAPHENE



Ph.D. THESIS

Sibel DEMİROĞLU MUSTAFOV

Department of Nanoscience and Nanotechnology

Thesis Advisor: Assoc. Prof. Dr. M. Özgür SEYDİBEYOĞLU

JANUARY 2018

IZMIR KATIP CELEBI UNIVERSITY ★ GRADUATE SCHOOL OF SCIENCE
ENGINEERING AND TECHNOLOGY

NANOCOMPOSITES WITH GRAPHENE



Ph.D. THESIS

Sibel DEMİROĞLU MUSTAFOV
(606113003)

Department of Nanoscience and Nanotechnology

Thesis Advisor: Assoc. Prof. Dr. M. Özgür SEYDİBEYOĞLU

JANUARY 2018

İZMİR KÂTİP ÇELEBİ ÜNİVERSİTESİ ★ FEN BİLİMLERİ ENSTİTÜSÜ

GRAFEN ESASLI NANOKOMPOZİTLER



DOKTORA TEZİ

**Sibel DEMİROĞLU MUSTAFOV
(606113003)**

Nanobilim ve Nanoteknoloji Anabilim Dalı

Tez Danışmanı: Doç. Dr. M. Özgür SEYDİBEYOĞLU

OCAK 2018

Sibel Demirođlu Mustafov, a **Ph.D.** student of IKCU Graduate School of Science Engineering and Technology student 606113003, successfully defended the thesis entitled “**NANOCOMPOSITES WITH GRAPHENE**”, which she prepared after fulfilling the requirements specified in the associated legislations, before the jury whose signatures are below.

Thesis Advisor: **Assoc. Prof. M. Özgür SEYDİBEYOĐLU**
İzmir Kâtip Çelebi University

Jury Members: **Prof. Dr. M. Mustafa DEMİR**
İzmir Institute of Technology

Assoc. Prof. Dr. Aylin ALBAYRAK
Dokuz Eylül University

Assist. Prof. Dr. Mustafa EROL
İzmir Kâtip Çelebi University

Assist. Prof. Dr. Nesrin HORZUM POLAT
İzmir Kâtip Çelebi University

Date of Submission : 05 December 2018

Date of Defense : 05 January 2018



*To my father who taught me the significance of education and supported me even
after he passed away*

FOREWORD

An advisor plays a considerable role in a PhD thesis. No thesis can be finished without guidance, inspiration and surely motivation. I would like to express my heartfelt gratitude to Assoc. Prof. Dr. M. Özgür Seydibeyođlu who has continuously been by my side giving me his broad knowledge, experience and kind support.

I would like to acknowledge Assist. Prof. Dr. Nesrin Horzum Polat for her mentorship. Her able guidance and opinions had encouraged me to conclude this thesis productively.

I would like to extend my gratitude to Assist. Prof. Dr. Mustafa Erol who helped me by presenting me to different executives and provided time and support for finishing my thesis.

This study has taken its present form also owing to some people who have been particularly supportive and helpful in the completion of this work. I express my honest gratitude to Dr. Amar Mohanty, Prof. Dr. Manju Misra and BDDC team (Guelph University, Canada) for giving me encourage to accomplish my research work.

I deeply thank all my friends (Merve Kaplan, Metehan Atagür, Ecem Akın, Tuđba Kılıç, Fatma Erdoğan, Tuđçe Uysalman, Saadet Güler) who took time off to understand my research problem and answer my queries.

Special thanks to my husband Kenan Mustafov who have been so understanding all through the days of my research and thesis writing. This thesis is the result of his enormous support.

I would like to gratefully thank to the İzmir Kâtip Çelebi University Scientific Research Projects Coordinatorship for providing me financial support by BAP-2015-TDR-FEBE-0011 project during my thesis.

I would like to acknowledge to Industrial Thesis Supporting Program (SAN-TEZ) project which was worked with the cooperation of İzmir Kâtip Çelebi University for financial support ensured in the course of this thesis.

05 January 2018

Sibel DEMİROĐLU MUSTAFOV



TABLE OF CONTENTS

	<u>Page</u>
FOREWORD	ix
TABLE OF CONTENTS	xi
ABBREVIATIONS	xiii
SYMBOLS	xv
LIST OF TABLES	xvii
LIST OF FIGURES	xix
SUMMARY	xxi
ÖZET	xxv
1. INTRODUCTION	1
1.1 Literature Review	1
1.1.1 Nanotechnology and nanomaterials	1
1.1.2 Carbon fiber	2
1.1.3 Lignin.....	4
1.1.4 Electrospinning.....	8
1.1.5 Lignin/PAN nanofibers.....	9
1.1.6 Thermal stabilization and Carbonization.....	10
1.1.7 Using nanomaterials in lignin-based carbon fibers	11
1.2 Hypothesis.....	12
2. EXPERIMENTAL	15
2.1 Materials	15
2.2 Extraction procedures of lignins from different resources.....	15
2.3 Characterization of lignins	18
2.3.1 SEM.....	18
2.3.2 Contact angle.....	18
2.3.3 FTIR.....	18
2.3.4 TGA	19
2.3.5 DSC	19
2.3.6 Elemental analysis	19
2.3.7 XPS.....	19
2.4 Fabrication of PAN, PAN/lignin, and PAN/lignin/graphene nanofibers and characterization of them.....	19
2.4.1 Solution preparation	19
2.4.2 Electrospinning of nanofibers	21
2.4.3 Rheological characterization of electrospinning solutions	23
2.4.4 Nanofiber characterization.....	23
2.4.4.1 Morphological and structural analysis.....	23
2.4.4.2 XRD	24
2.4.4.3 FTIR	24
2.4.4.4 Electrical conductivity.....	24
2.4.4.5 Statistical analysis	25
2.4.4.6 TGA.....	26
2.4.4.7 Atomic force microscopy (AFM).....	26
2.5 Thermal Stabilization and Carbonization	26
2.5.1 SEM of carbon nanofibers	27
2.5.2 RAMAN of carbon nanofibers.....	27

2.6 Electrochemical Sensor Analysis.....	27
2.6.1 Preparation of CNF/SPE (Carbon nanofiber modified screen printed electrode) and CNF-G/SPE (Graphene reinforced carbon nanofiber modified screen printed electrode)	27
2.6.2 Characterization of CNF/SPE and CNF-G/SPE.....	28
3. RESULTS and DISCUSSION.....	29
3.1 Extraction and Characterization of Lignins	29
3.1.1 SEM.....	30
3.1.2 Contact angle	31
3.1.3 FTIR of lignins.....	32
3.1.4 Elemental analysis of lignins	33
3.1.5 TGA of lignins	34
3.1.6 DSC of lignins	36
3.1.7 XPS of lignins.....	37
3.2 Fabrication and Characterization of Nanofibers	40
3.2.1 Effect of polymer concentration and environmental parameters on electrospinning process.....	40
3.2.2 Effect of graphene on electrospinning process.....	46
3.2.3 Experimental design.....	49
3.2.4 Electrical conductivity analysis	50
3.2.5 FTIR of nanofibers.....	51
3.2.6 XRD of nanofibers	54
3.2.7 TGA of nanofibers.....	56
3.2.8 AFM of nanofibers.....	58
3.3 Thermal Stabilization and Carbonization	58
3.3.1 SEM of carbon nanofibers.....	59
3.3.2 RAMAN of carbon nanofibers	64
3.4 Characterization of CNF/SPE and CNF-G/SPE.....	66
4. CONCLUSIONS.....	71
5. REFERENCES	73
CURRICULUM VITAE.....	85

ABBREVIATIONS

ABS	: Acetate buffer solution
AFM	: Atomic force microscopy
-CH₂-	: Methylene
>C=O	: Carbonyl group
-CN	: Nitrile groups
CNF	: Carbon nanofiber
CNF-G	: Graphene reinforced carbon nanofiber
CNTs	: Carbon nanotubes
CV	: Cyclic Voltammetry
DPV	: Differential Pulse Voltammetry
DMF	: N, N-dimethylformamide
DSC	: Differential Scanning Calorimetry
EDS	: Energy-dispersive X-ray spectroscopy
EDTA	: Ethylenediamine tetra-acetic acid
EIS	: Electrochemical impedance spectroscopy
FESEM	: Field emission scanning electron microscope
FTIR	: Fourier Transform Infrared Spectroscopy
GRP	: Graphene
GRPs	: Graphenes
HCl	: Hydrochloric acid
H₂SO₄	: Sulfuric acid
K₃Fe(CN)₆/K₄Fe(CN)₆	: Potassium ferricyanide
KCl	: Potassium chloride
NaCl	: Sodium chloride
PAN	: Polyacrylonitrile
PBS	: Phosphate buffer solution
PEO	: Poly (ethylene oxide)
SEM	: Scanning Electron Microscope
SPE	: Screen-printed electrode
T_g	: Glass Transition Temperature
TGA	: Thermogravimetric Analysis
T1	: First degradation temp.
T50%	: Temperature for 50% of weight loss
XPS	: X-ray Photoelectron Spectroscopy
XRD	: X-ray Diffraction



LIST OF TABLES

	<u>Page</u>
Table 1.1: General properties of different types of lignins.	6
Table 1.2: The costs of CFs from different precursor.....	7
Table 2.1: Numerous concentration of Electrospinning solutions.....	20
Table 2.2: Heating conditions of nanofibers	27
Table 3.1: The composition of different lignocellulosic materials	29
Table 3.2: Elemental analysis of lignin samples.....	33
Table 3.3: Thermal properties of lignins studied by TGA	34
Table 3.4: Glass Transition Temperatures T_g for Different Lignin Samples	37
Table 3.5: Elemental composition of the lignin samples as calculated by XPS.....	38
Table 3.6: Experimental design results	50
Table 3.7: Conductivity results of nanofibers	51
Table 3.8: Degree of nanofiber crystallinity by XRD patterns.....	56

LIST OF FIGURES

	<u>Page</u>
Figure 1.1: Manufacturing process of carbon fiber from PAN	3
Figure 1.2: Manufacturing costs of conventional PAN-based CFs	4
Figure 1.3: Representative schema of A) lignin precursors and B) lignin structure ...	5
Figure 2.1: ‘Chinese Textile Industry’ standard method	16
Figure 2.2: Schematic diagram of the lignin extraction for Turkish pine	17
Figure 2.3: Schematic illustration of the production of with and without graphene-polymer nanofiber by electrospinning.....	22
Figure 2.4: A) The electrospinning system with dehumidifier/AC, B) Dehumidifier and AC system equipment for electrospinning system.	23
Figure 2.5: Electrical conductivity set up consists of A) hollow cylinder and B) Potentiostat/Galvanostat	25
Figure 3.1: SEM images of lignin samples from A) Turkish Vine stem, B) commercial lignin, and C) Turkish pine.....	31
Figure 3.2: Contact angle images of the extracted lignin from a) vine stem b) commercial lignin and c) the extracted lignin from Turkish pine	31
Figure 3.3: FTIR spectra of three different lignins.....	32
Figure 3.4: Thermogravimetric analysis of three different lignins.....	35
Figure 3.5: High-resolution C 1s spectra of three different types of lignin. The explanation of the components Comp 1–4 is mentioned in the text.	39
Figure 3.6: High-resolution O 1s spectra of three different types of lignin. A) O1 peaks, and B) O2 peaks	40
Figure 3.7: Viscosity and lignin concentration relationship for the PAN and PAN/Lignin solutions with 10 and 20% wt. of total polymer concentration.....	41
Figure 3.8: SEM images of nanofibers of 10 PAN (left) and 10C1 (right).....	42
Figure 3.9: SEM images of nanofibers of 10C3 (left) and 10C5 (right).....	43
Figure 3.10: SEM images of nanofibers of 20PAN (left) and 20C1 (right)	44
Figure 3.11: SEM image of nanofibers of 20C3 (left) and 20C5 (right)	44
Figure 3.12: PAN/Lignin nanofibers of 20C1 without and with dehumidifier system during electrospinning	45
Figure 3.13: SEM image of nanofibers 20C1-1G (left) and 20C3-1G (right)	46
Figure 3.14: SEM image of nanofibers 20C5-1G.....	47
Figure 3.15: SEM image of nanofibers 20C1-5G (left) and 20C3-5G (right).	47
Figure 3.16: SEM image of nanofibers 20C5-5G.....	48
Figure 3.17: Shear rate and shear stress relationship for the 20C5 (1% and 5% wt.) solutions.....	49
Figure 3.18: FTIR multilayer spectra of the PAN nanofiber and PAN/lignin nanofibers with different lignin content.	52

Figure 3.19: FTIR spectra of the PAN/lignin and PAN/Lignin/GRP nanofibers with different lignin content.....	53
Figure 3.20: XRD spectrum of PAN/Lignin nanofibers at different concentrations.....	54
Figure 3.21: XRD pattern of PAN/Lignin nanofibers with and without graphene at several concentrations.....	55
Figure 3.22: TGA analyses of three types of nanofibers.....	57
Figure 3.23: AFM analyses of a) PAN/lignin/graphene and b) PAN/lignin of nanofibers.....	58
Figure 3.24: Sample preparation for thermal processing, (a) lignin powder, (b) electrospun PAN/Lignin nanofibers, (c) horizontal tube furnace (d) placement of carbon nanofibers in the ceramic boat after carbonization, (e) carbonized nanofibers.	59
Figure 3.25: 900 °C – 2 °C/min – 1 h, 20C1-1G (left) and 20C3-1G (right).....	60
Figure 3.26: 900 °C – 2 °C/min – 1 h, 20C5-1G.....	60
Figure 3.27: 800 °C – 2 °C/min – 2 h, 20C3 (left) and 20C3-5G (right).....	61
Figure 3.28: EDS of PAN/Lignin nanofibers.	62
Figure 3.29: EDS of PAN/Lignin/Graphene carbon nanofibers.	62
Figure 3.30: 900 °C – 1 °C/min – 1h -20C1-1G.....	63
Figure 3.31: Raman spectrum of graphene.....	64
Figure 3.32: Raman spectra of the carbonized nanofibers at different temperatures.	65
Figure 3.33: Nyquist plots of SPE, CNF/SPE and CNF-G/SPE.....	66
Figure 3.34: Cyclic voltammograms of three screen printed electrodes.....	67
Figure 3.35: DPV voltammograms of the acetaminophen for three screen-printed electrodes.....	68



NANOCOMPOSITES WITH GRAPHENE

SUMMARY

The carbon fiber used in the manufacturing of advanced composites has various applications in the automotive, aerospace, and electronics industry because of their comprehensive properties such as lightweight, flexibility, high strength to weight ratio, excellent chemical resistance, superior electrical conductivity and thermal conductivity.

Different kinds of carbon fiber precursors have been used and polyacrylonitrile (PAN) is the mostly utilized polymer type which is a petroleum-based, expensive and unsustainable. Remarkably, lignin is a highly accessible, low-cost, and renewable resource. Also, lignin is a byproduct of pulp and paper industry as well as cellulosic ethanol fuel production. So, the reuse of this byproduct is very significant for the bioeconomy. Accordingly, understanding the structure, types, and extraction methods of lignin are of great importance for transferring these biomass residues from a low-value material to a higher value product.

This work started with the extracted lignin from Turkish resources (Turkish Pine and Turkish Vine stem) by sulfuric acid treatment and to compare with commercial lignin. Additionally, we investigated lignin to identify its suitability as a carbon fiber precursor and to use for reducing the processing cost of carbon fiber production compared to other precursors.

In this thesis, sub-micron lignin-based nanofibers were produced by electrospinning of solutions obtained by dispersing lignin, polyacrylonitrile (PAN) and then graphene (GRP) in *N, N*-dimethylformamide (DMF). Lignin-based carbon nanofibers were investigated by focusing on the steps of manufacture. Resource types and corresponding pretreatments improve the processability of spinning and thermal treatments. Defect-free nanofibers with up to 5 wt. % lignin/PAN and 1% graphene were fabricated successfully. The succeeding step is the most significant process of stabilization, where nanofibers are oxidized, crosslinked, and thermally stabilized for the following step. After carbonization, lignin-based carbon nanofibers are obtained. When carbonized at 900 °C, PAN/Lignin/GRP carbon nanofiber presents carbon content of 94.3% and with average diameter ~ 100 nm. Effects of every single step on the lignin-based carbon nanofibers have been discussed comprehensively.

To sum up, the low cost of carbon nanofibers and graphene reinforced carbon nanofibers can be used in numerous fields, mainly for electronic devices containing biosensors and supercapacitors. In this thesis, the characterization of carbon nanofiber (CNF) and graphene reinforced carbon nanofiber (CNF-G) modification onto the screen printed electrode (SPE) has been verified via Electrochemical Impedance Spectroscopy (EIS) and Cyclic Voltammetry (CV). The charge transfer resistance, R_{ct} values obtained by electrochemical circle fit option of EIS have been utilized for

conductivity detection of modified electrodes. In the last part of this thesis, CNF and CNF-G modified electrodes were performed for an effective biosensor to detect acetaminophen.



GRAFEN ESASLI NANOKOMPOZİTLER

ÖZET

İleri kompozitlerin üretiminde kullanılan karbon elyaf, hafiflik, esneklik, ağırlık oranına karşın yüksek mukavemet, yüksek kimyasal direnç, üstün elektrik ve ısı iletkenliği gibi özelliklerinden ötürü otomotiv, havacılık ve elektronik sektöründe çeşitli uygulamalara sahiptir.

Farklı karbon elyaf hammaddelerinden en çok kullanılan ise petrol esaslı, pahalı ve sürdürülemez olan poliakrilonitril (PAN) dir. Dikkat çekici bir şekilde, lignin erişilebilir, düşük maliyetli ve yenilenebilir bir kaynaktır. Ayrıca, lignin selülozik etanol yakıt üretiminin yanı sıra hamur ve kâğıt sanayiinin bir yan ürünüdür. Dolayısıyla, bu yanürün yeniden kullanımı biyo-ekonomi için çok önemlidir. Ligninin yapısını, tiplerini ve ekstraksiyon yöntemlerini anlamak, bu biyolojik atığı düşük değerli bir materyalden yüksek değerli bir ürüne dönüştürmek büyük önem taşır.

Bu çalışma, sülfürik asit ile Türkiye'deki bitki kaynaklarından (kızılçam ve asma kökü) ligninin elde edilmesi ve ticari lignin ile karşılaştırılmasıyla başlamıştır. Ek olarak da, ligninin diğer öncü malzemelerle kıyaslayarak üretim maliyetini düşürmek için karbon elyaf öncü malzemesi olarak uygunluğunu belirlemek için araştırma yapılmıştır.

Bu tezde, mikron altı lignin esaslı nanoelyaf, lignin, poliakrilonitril (PAN) ve daha sonra grafenin (GRP) *N, N*-dimetilformamid (DMF) içinde disperse edilmesiyle elde edilen çözeltilerin elektroğirmesiyle üretilmiştir. Lignin esaslı karbon nanoelyaf, üretim aşamalarına odaklanarak araştırılmıştır. Kaynak türleri ve bunlara karşılık gelen ön işlemler, eğirme ve ısı işlemlerin işlenebilirliğini geliştirmektedir. Ağırlıkça % 5 lignin/PAN oranında ve % 1 grafene sahip olan düzgün nanoelyaf başarıyla üretilmiştir. Sonraki adım, nanoelyafın oksitlendiği, çapraz bağlandığı ve bir sonraki adım için termal olarak stabilize edildiği en önemli adım olan termal stabilizasyon sürecidir. Karbonlaşmadan sonra, lignin esaslı karbon nanoelyaf elde edilir. 900 °C'de karbonize edildiğinde, PAN / Lignin / Grafen karbon nanoelyaf, % 94.3'lük bir karbon içeriğine sahiptir ve ortalama çapı ~ 100 nm'dir. Lignin bazlı karbon nanoelyafı etkileyebilecek her bir basamak kapsamlı olarak ele alınmıştır.

Sonuç olarak, düşük maliyetli karbon nanoelyaf ve grafen takviyeli karbon nanoelyaf, biyolojik sensörler ve süperkapasitörleri içeren başta elektronik cihazlar olmak üzere birçok alanda kullanılabilirler. Bu tezde, karbon nanoelyaf (CNF) ve grafen esaslı karbon nanoelyaf (CNF-G)'in perde baskılı elektrot (SPE) üzerine modifikasyonu, Elektrokimyasal Empedans Spektroskopisi (EIS) ve Döngüsel Voltametri (CV) ile doğrulanmıştır. Modifiye elektrotların iletkenlik tespiti için, EIS'in elektrokimyasal daire uyumu seçeneği ile elde edilen yük transfer direnci, Rct değerleri kullanılmıştır. Bu tezin son bölümünde, asetaminofen tespit etmek için etkili bir biyosensör olarak CNF ve CNF-G modifiye elektrotlar kullanılmıştır.

1. INTRODUCTION

1.1 Literature Review

1.1.1 Nanotechnology and nanomaterials

Nanotechnology concerns to the science and technology regarding structures and materials which as a minimum one of the sizes is 100 nm or lower. Over several decades, researchers have improved instruments and techniques that assist better comprehension the significant prospects of the universe [1, 2]. Nanotechnology contains manipulating materials in nanometer range to get the advantage of their unique properties and to develop products in several industrial sectors such as biotechnology, defense, aerospace, and electronics [3, 4]. Furthermore, these nanomaterials with high surface-to-volume ratio can be utilized in drug delivery, composites, and energy storage [5].

While the scientists have to some degree agreed to the <100 nm standard for describing as a nanomaterial, the people worked in the industrial sector has accepted the dimension ranges from 300 nm up to 500 nm. However, the scope of the nanotechnology is wide and affects many various industrial sectors, an understanding of the related materials and methods is vital to make sure responsible industry improvement in some respects that both advances economic development and preserve the environment [6].

Nanomaterials, are an essential subclass of nanotechnology, have numerous specific characteristics such as incomparable chemical and physical properties. For example, melting of crystals in the nanoscale happens a lower temperature than that at the bulk. Thus, scholars produce valuable materials and instruments by ensuring of substance in the nanoscale and research new properties and phenomena acquired at that size [7].

Nanomaterials can be classified as zero dimension (i.e. nanoparticles), one dimension (i.e. nanotubes), two dimensions (i.e. nanoplatelets), or three dimensions (i.e.

particles). Besides, common kinds of nanomaterials contain quantum dots, nanotubes, nanowires, and fullerenes.

Decades of research have been performed on several novel nanomaterials. Carbon-based nanomaterials consist of fullerenes, carbon black, and carbon nanotubes (CNTs). Adding small amounts of nanomaterials such as carbon nanotubes may significantly develop functional properties of composites like their electrical conductivity. On the other hand, the addition of nanomaterials was informed to increase the productivity of numerous analytical techniques [6, 8].

1.1.2 Carbon fiber

Carbon fibers are carbon materials which consist of carbon allotrope or polymeric precursors with tremendous mechanical performance and electrical conductivity properties. They are made of a process that contains the preparation of precursor solutions, spinning (wet spinning, electrospinning etc.), thermal stabilization, carbonization, and then added of graphitization in some applications [9, 10].

Presently, more than 90 % of the commercial carbon fibers are manufactured from polyacrylonitrile (PAN), pitch and rayon. Figure 1.1 shows the manufacturing process of carbon fiber by using PAN [11]. The rate of growth in the carbon fiber-developed industry is too low to satisfy the fast arising requirement, largely as the primary precursor for carbon fibers, PAN, is costly and as a fossil fuel derivate not sustainable [10, 12]. That's why the high price of them limit their consumption for profitable applications such as aerospace and automotive although the commercial demand of carbon fibers increases continuously.

In carbon fiber generation, the issue part is spinning of the precursor material. Electrospinning has been utilized as a straightforward innovation to develop consistent submicron diameter fibers (termed as carbon nanofibers) from an extensive variety of materials. Arranged or adjusted fiber mats can be improved at random by this technique [13]. The developing technique of electrospinning provides a way to make continuous carbon fibers at sub-micrometer scale (typically 100–1000 nm), called carbon nanofibers [14].

Manufacturing Process of PAN Type Carbon Fiber

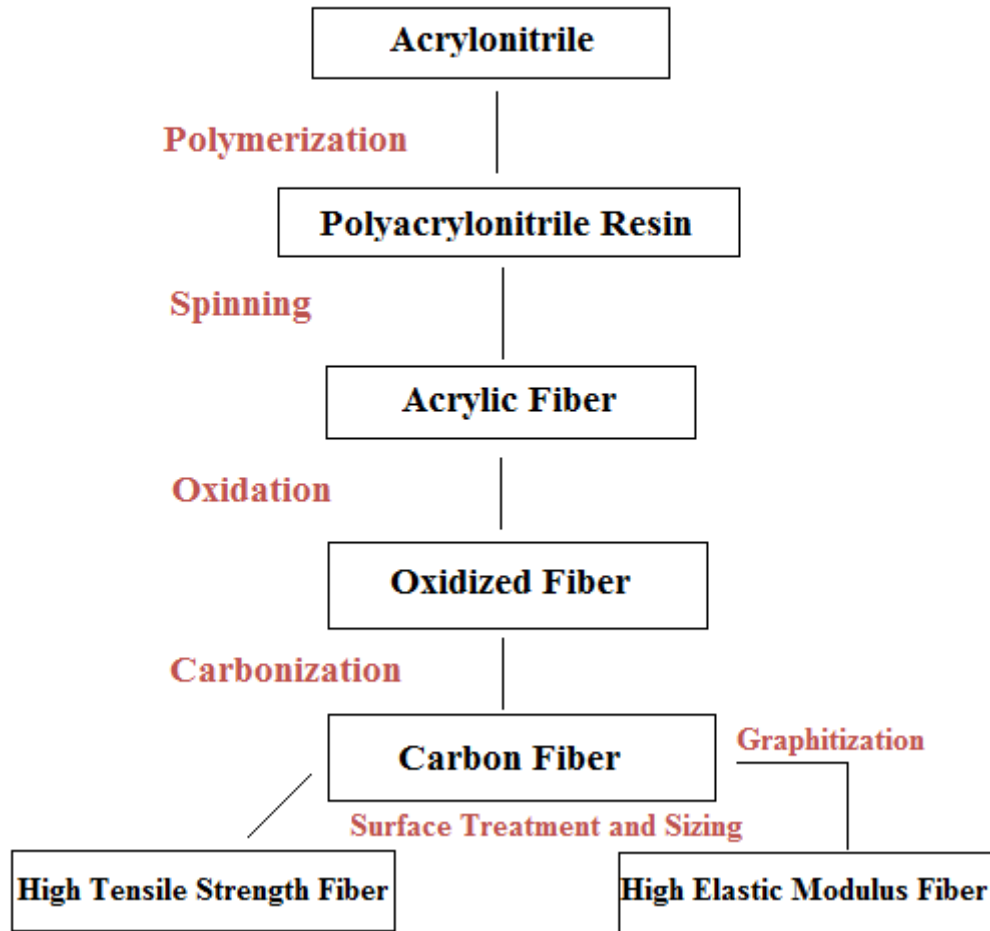


Figure 1.1: Manufacturing process of carbon fiber from PAN [11].

Carbon nanofibers were developed by means of nanofibers from the pitch and from polyacrylonitrile (PAN) with diameters of submicron and few hundreds of nanometer [15, 16]. PAN, is a petroleum-based polymer, is in need of a very slow heating process for carbonization which prolongs the processing time [13, 17]. Furthermore, the PAN is the largest part of the total manufacturing cost (Figure 1.2) [18].

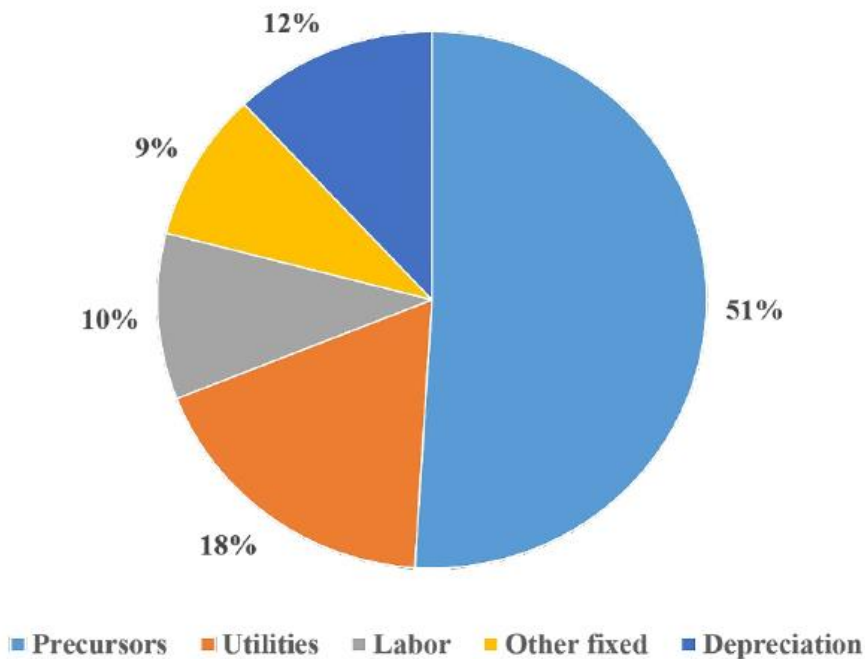


Figure 1.2: Manufacturing costs of conventional PAN-based CFs [18].

Currently, ecological contamination and a petroleum derivative substances deficiency influence the advancement of the world economy and environment. These reasons are due to the motivations us to seek replacements such as a low-cost, earth-abundant and eco-friendly materials [19]. As of late, an extensive variety of renewable resource-based materials have been researched for the generation of carbon materials [4]. To replace the fossil-based precursors utilized for carbon fiber fabrication like polyacrylonitrile (PAN), lignin has been thought as a bio-based and cheaper alternate raw material [20-23].

1.1.3 Lignin

Lignin, is basically a by-product of biorefinery process, has been investigated as a precursor for bio-derived carbon fibers from the 1960s [24, 25]. The great quantity of aromatic components in the molecular configuration of lignin comes through an effective prospect for a carbon fiber precursor [23]. Lignin has a very complex three-dimensional structure because of the random polymerization of phenylpropane monomers and significant C-C links are b-5, 5-5, b-1, and b-b linkages, and C-O linkages are a-O-4, b-O-4, and 4-O-5 [26, 27]. Lignin consists of peroxidase-mediated

dehydrogenation of three types of phenylpropane monomer units and linked by carbon-carbon and aryl-ether linkages with random cross-linked polymerization from radical-coupling reactions between phenolic radicals [28-31] (Figure 1.3).

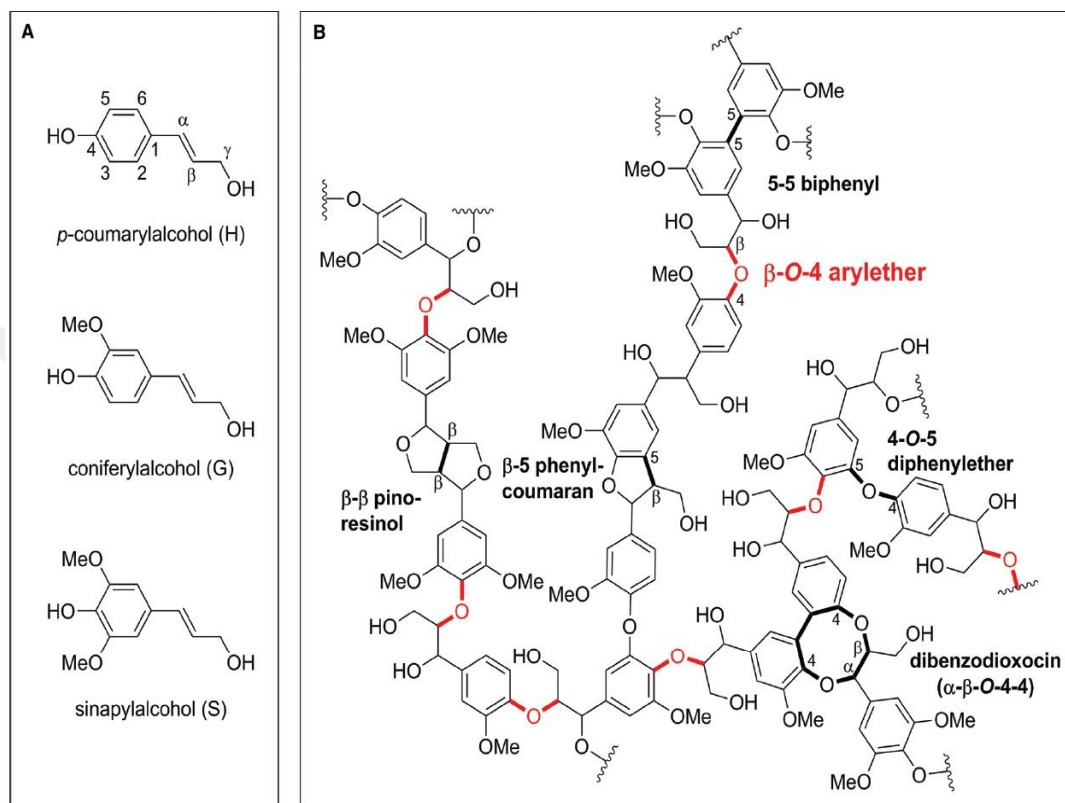


Figure 1.3: Representative schema of A) lignin precursors and B) lignin structure [31].

Not only chemical and physical properties but also the low cost and renewability of lignin have made it excellent precursor material for numerous applications. Lignin is utilized to make surfactants, emulsifiers, binder, paints, and polymeric materials [32-35]. However, there are some complications in conversion lignin to carbon fibers. One of them is its immense classification resulting from plant sources and extracting methods. There is a variety of lignin source present including pine straw, hemp, fiber flax, and wood pulp. Hence, their physical and chemical behavior is different with respect to the original source. Also, the chemical structure of lignin can be changed depending on extraction method.

Numerous processes have been developed over the course of many years to extract lignin such as kraft lignin, liginosulfonates, and organosolv lignins, which modify

chemical structure and facilitates based on the extraction circumstances. Although Kraft process is commercially common, the amount of extracted kraft lignin is very low [36]. A few different strategies for lignin processing also have vital applications in the potential of renewable fuel uses. While organosolv pulps are to some degree reduce the quality of Kraft pulps, modifications can enhance organosolv pulp facilities [37]. That's why, organosolv pulping has taken significant attention because of its potential use in the generation of biofuel such as biodiesel, cellulosic ethanol [38-40]. Table 1 indicated that the general properties such as molecular weight or T_g of lignins based on the source of biomass and processing circumstances [41, 42]. In any case, the high cost of the solvents when compared with Kraft lignin prevented those procedures to excite industrially appealing for pulp development.

Nonetheless, a few of them have found a restored enthusiasm for the most recent couple of years, essentially on the premise of second generation biorefineries, going for delivering fuels as well as chemicals from lignocellulosic biomass. Since original biorefineries, for the most part, centered around starch for the creation of bioethanol, the opposition with human nutrient has driven the exploration and industry to rather concentrate on non-sustenance lignocellulosic residues.

Table 1.1: General properties of different types of lignins [41,42].

Types of lignin	Molecular weight, Mw (g/mol)	Sulfur (%)	Chemicals used for lignin isolation	T_g ($^{\circ}$ C)
Kraft lignin	1000 – 3000	1-3	NaOH and Na ₂ S	140-150
Organosolv lignin	500 – 5000	0	acetic acid/formic acid, ethanol and water	90-110
Soda lignin	800 – 3000	0	Soda-anthraquinone, NaOH	140
Lignosulfonate lignin	15000-50000	4-6	HSO ₃ ⁻	130

Another difficulty is that its complex and disordered structure, as well as impurities in the final product, can affect low the thermal behavior and mechanical properties of carbon fibers. Especially, the thermal behavior is of vital importance when compared

with the mechanical properties of lignin. For instance, the glass transition temperature (T_g) plays a role in melt spinning and carbonization process.

Considering all the difficulties mentioned before, lignins have their advantages. It is clear that lignin has a cost advantage for the production of carbon fibers. As the aromatic structure of lignin (Figure 1.3) is similar to the structure in PAN-based carbon fibers (Figure 1.1). They can produce by means of same methods. Additionally, the thermoplastic character of lignin lets to fabricate precursor fibers through melt-spinning. To sum up, several investigators have entered the lignin research area to drive by the aim of lowering the cost of carbon fibers in the past many decades. Table 1.1 showed that the differences in cost for carbon fiber production depend on several precursors.

Table 1.2: The costs of CFs from different precursor [18, 43, 44].

Precursor	Precursor Cost (USD\$ kg-1)	Production Cost (USD\$ kg-1)	Total Cost (USD\$ kg-1)
Textile Grade PAN	4.4-13.2	12.2-25.4	16.6-38.6
Conventional PAN	10.2	24.4	34.6
Melt-spun PAN	6.3	17.4	23.7
Polyolefin	1.57-2.36	-	-
Lignin	1.1 (cover spinning)	5.2	6.3

As said by the literature, more than a few low-cost precursors have been stated to be effectively fabricated to carbon fibers [43]. The lignin-based carbon fiber was shown to be produced by Otani *et al* in early studies. Carbon fibers have however low modulus and low tensile due to micro voids [45]. The Oak Ridge National Laboratory (ORNL) in the United States developed lignin-based carbon fibers which have the average strength of 1.07 GPa and Young's modulus of 82.7 GPa. Nevertheless, the tensile strength of lignin carbon fibers is low compared to commercial PAN-based carbon fiber (3-7 GPa) [17, 46]. Such strength of carbon fibers can be improved by reducing the carbon fiber diameter. Much as there are a few serving difficulties in developing fibers of lignin, a few investigators get combined lignin with another

polymer to ease the fiber production method. Numerous ways of spinning, containing wet spinning, melt spinning, and electrospinning, have been explored to develop carbon fibers based on lignin/polymer [17, 23, 24, 47]. However, the product carbon fibers fabricated by melt spinning are moderately weak in comparison with those obtained from petroleum-based precursors [30].

Especially, utilizing PAN for an additive in electrospinning would, in theory, improve the mechanical functioning of lignin-based CFs (carbon fibers) since PAN is already called the most in effect precursor to develop CFs with high carbon yield and superior attributes [49]. Furthermore, after electrospinning method, the electrospun mats display high porosity and precise surface area, which cause them properly as the manufacture of superior materials such as sensors, medical materials, conductive materials [50, 51].

Nevertheless, it is hard to acquire continuous smooth fibers during electrospinning process as a result of its low molecular weight and chain entanglements. Developing the network of chain entanglements could be supplied for electrospinning progress by blending of lignin with another polymer which has high molecular weight [13, 17, 28]. In this way, the nanofibers of kraft, alkali kraft, and organosolv lignin could be fabricated after blending with numerous polymers such as polyvinyl alcohol (PVA) [52, 53], polyethylene oxide (PEO) [47, 54], polyhydroxybutyrate [55], PAN [51, 56-59], and polypropylene [60].

1.1.4 Electrospinning

Electrospinning states to a method of manufacturing fibers via electrostatic forces to method materials into fibers from blends or solutions and a comparatively low-cost process for fabrication of continuous fibers. The main setup for electrospinning consists of three basic parts: a high voltage power supply, a needle (spinneret), and a conductive collector. The needle is connected to a syringe to which the polymer blends are fed and is located on the top or beside of a collector which is the conductive plane. The conductive collector located at a constant distance from the needle, and a power supply which is used to exert a potential among the needle and collector [46, 61].

Applied to an electric field developed by means of high voltage, the droplet of polymer solution/blend at the tip of the needle is formed into a conical object, generally known as Taylor cone. Once the electrostatic force gets over the surface tension of the drop, a charged jet of solution throws out of the tip of the Taylor cone, and the electrospinning begins. So, the jet carries out an elongating and whipping technique shaping a thin and loop-shaped fiber [62]. Owing to the elongation and solvent evaporation, diameters of the fibers can be significantly diminished from micrometers to nanometers during the short period of time. The randomly oriented microfiber/nanofiber is deposited onto the plate collector or the rotating drum collector [63].

Depends on the electrospinning parameters, the morphology and diameter of the electrospun fiber can be changed. On the other hand, the fiber morphology based on processing parameters which contain: (a) solution properties such as viscosity, surface tension, electrical conductivity; b) operational conditions such as solution flow rate, the distance between needle and collector, applied an electric field, and ambient factors such as humidity and temperature. The importance of numerous parameters on the electrospinning technique has been examined in more than a few studies [64-69].

1.1.5 Lignin/PAN nanofibers

Blends of lignin with PAN as nanofiber precursors have been informed before. Basically dissolving PAN and lignin into blends with a consequent wet-spinning was possible to shape chemical crosslinking among two compounds [70]. These interactions were accomplished by other particular methods such as electrospinning and melt spinning.

Seo et al. reported the fabrication of PAN/lignin alkali nanofibers mats with the electrospinning technique. They cured the electrospun PAN/lignin nanofibers mats by E-beam irradiation. Although they produced PAN/lignin nanofiber of 300 nm diameter, the lignin content was 50 wt. % for better spinnability [57].

Liu et al. reported a work, in which carbon fibers were fabricated by gel-spinning the soda lignin/PAN blend. With this work, the interaction between PAN and lignin was given by the N-O bonds between two polymers. As indicated by Liu et al., with the expansion of lignin content, the activation energy of crosslinking responses was

diminished and mechanical properties of carbon fibers were improved, but the integration of lignins might give rise to imperfect structures of carbon fibers [72].

Dong et al. informed the PAN/lignin sulfonate (PAN/LS) fibers with the wet spinning process. The PAN contents altered from 0 to 100 wt. %. However, they reported the PAN/lignin fibers by wet spinning weren't obtained the chemical crosslinking between PAN and LS [57]. Bissett *et al.* reported two patents related to the method of manufacturing carbon fibers from lignin and PAN. They indicated that the blends were prepared by dissolving the polymers in which the lignin fractions provide 10 to 45% of the total polymer weight. The PAN/lignin-containing dopes were wet-spun after thermal stabilization and carbonized into carbon fibers through tensile strengths of 0.552 to 2.758 GPa [72, 73].

In another PAN/lignin nanofiber study, hardwood organosolv lignin was used with PAN as a precursor for producing carbon nanofibers. Yet, the organosolv lignin is relatively expensive in comparison with other processes for obtaining lignin since a large amount of organic solvent is used to remove impurities [56, 74].

1.1.6 Thermal stabilization and Carbonization

On the way to achievement materials with high carbon content, precursor fibers are subjected to thermal stabilization and carbonization. In the course of the stabilization process, precursor fibers are regularly heated to 200 - 300 °C in air. The main purpose of stabilization is to crosslink and prepares lignin structure that can prevent fiber melting during carbonization process at higher temperatures such as 900 or 1100 °C.

According to several groups which worked on the thermal stabilization of lignins, in the start of a process, hemolysis of C-O and C-C bonds, hydrogen abstraction, and reorganization take place as formaldehyde and then water are vaporized. The mechanism of leaving formaldehyde can happen the ways which are excited by hemolysis of C-O bonds or by hydrogen separation. By means of air in this process, oxygen may induce other readjustments and oxidizes lignin configurations [75, 76].

After the thermal stabilization, the stabilized fibers with the capability to tolerate high temperature are carbonized at 800-1200 °C in a stream of nitrogen or argon. During the carbonization process of lignin fiber, while the possible degradation products are

carbon monoxide, carbon dioxide, water vapor and maybe methane, the amounts of hydrogen and oxygen reduction. After carbonization process, the carbon content is likely excess of 92 % and this value can be increased based on carbonization temperature [77, 78, 79]. Because of the high temperature in the course of carbonization, the chemical structures of lignins alter considerably. The structure of carbonized fibers was commonly displayed through Raman spectra. In RAMAN, when the carbonization temperature enhances, the R-value (demonstrating the degree of disorder) reduced. Furthermore, fiber diameters diminished after carbonization [78, 80].

1.1.7 Using nanomaterials in lignin-based carbon fibers

The electrochemical functioning of the polymer-based carbon fibers could be increased along comprising the nanomaterials such as carbon nanotubes [59], graphene [81] or graphene oxide [82] in order to enhance mechanical and electrical properties. For instance, lignin-based carbon nanofibers reinforced with CNTs were fabricated by gel spinning. Interestingly, the tensile strength of these carbon nanofibers was 1.72 GPa with the adding of CNTs, while they improved the ordered size of carbon nanofibers [71].

There are also several studies using nanomaterials except for carbon nanotubes, graphene or graphene oxide to improve lignin-based carbon fibers. Novel lignin-based nanofibers decorated with monometallic and bimetallic nanoparticles, including Pt, Au, Pd, and their bimetallic conjugates were synthesized by Gao *et al.* The metallic nanoparticle deposited lignin-based nanofibers were then carbonized into lignin-based carbon nanofibers. This study indicated that the Pd nanoparticle immobilized lignin-based nanofibers and carbon nanofibers displayed catalytic activity concerning the NaBH₄ reduction of p-nitrophenol [83].

Particularly, graphene, an individual layer of aromatic carbon, has one of the powerful in-plane bonds among whole materials, in addition to as greater electrical and thermal conductivity.

Graphene, is the sp^2 hybridized forms of carbon, is considered to be the thinnest material-one atom thick. In spite of being the thinnest material identified to be present, graphene sheets also are independently very strong [84].

A single 2D sheet of graphene is a hexagonal structure with each atom modeling three bonds through each of its closest neighbors. These are called the σ bonds arranged towards these neighboring atoms and composed of three of the valence electrons. These covalent carbon-carbon bonds are almost equivalent to the bonds holding diamond along giving graphene similar thermal and mechanical properties like the diamond.

Graphene sheets can be arranged and functionalized to provide various sorts of graphene-based nanoscale materials. Due to having different structures, spectroscopic techniques such as Raman, Scanning Electron Microscope (SEM), and X-ray Photoelectron Spectroscopy (XPS) are being used to detect the surface and chemical properties of graphene.

To sum up, the cost advantages and performance of graphene are greater than carbon nanotubes in sensors, nanocomposites, and energy storage devices although carbon nanotubes have structural flexibility [85]. Thus, graphene reinforced-lignin based nanofibers are promising candidates as efficient biosensor materials for the increase of electrical conductivity in nanofibers.

1.2 Hypothesis

The main hypotheses of this work are:

- Extracted lignins from different Turkish resources and compared with commercial lignin which has distinct thermal properties and chemical properties.
- Lignin has the potential to obtain nanofibers through electrospinning technique if it can be solubilized in proper polymer and organic solvents such as dimethylformamide. The cost advantages of lignin challenge CNFs in nanocomposites sensors, tissue scaffolds, energy transformation, and storage device applications.

- Graphene filled-lignin based nanofibers are promising candidates as efficient biosensor materials for the increase of electrical conductivity in nanofibers.
- The selection of suitable thermal conditions for carbonization of lignin nanofibers with and without graphene helps to transform them into carbon nanofibers.
- The modified electrodes with lignin-based carbon nanofibers and graphene filled-lignin based carbon nanofibers are using in the biosensor to detect biomolecules.





2. EXPERIMENTAL

This study has three main parts. The first part is the extraction and comparison of extracted lignins with commercial lignin. The second part is the fabrication of PAN/Lignin and PAN/Lignin/Graphene nanofibers. The last part is the thermal stabilization and carbonization of these nanofibers for obtaining the electrode materials.

2.1 Materials

Protobind 2400 lignin was obtained from ALM Private Limited, Punjab, India. Biomass resources for Turkish pine and Turkish vine stem were collected from local fields near the Aegean region, Turkey. Chemicals used for extraction of lignin such as EDTA (Ethylenediamine tetra-acetic acid), acetone, alcohol ethanol, HCl (hydrochloric acid), and H₂SO₄ (sulfuric acid) were obtained from Sigma–Aldrich Inc., USA. Polyacrylonitrile (80 000 g/mol) was received from Dow Aksa Pvt. Ltd (Turkey), and graphene (GRP) with an average thickness of 12 nm were purchased from Graphene Supermarket. *N, N*-dimethylformamide (DMF) was obtained from Sigma-Aldrich Co. and used as the solvent for the electrospinning. Screen printed electrode (SPE) was obtained DropSens, S. L., Spain. 5 mM of potassium ferricyanide (K₃Fe(CN)₆/K₄Fe(CN)₆) with 0.1 M KCl (Potassium chloride), Acetaminophen, Acetate buffer solution (ABS) (pH: 4.80) containing 20 mM NaCl (Sodium chloride), 20 mM phosphate buffer solution (PBS, pH: 7.4) were prepared by dissolving chemicals purchased from Merck (Germany). Also, ethanol was obtained from Sigma–Aldrich Inc., USA, and de-ionized water were used for preparing solutions.

2.2 Extraction procedures of lignins from different resources

The process of lignin extraction from different biomass resources was carried out through "Chinese Textile Industry" standard method [86]. Herein, experimental process was explained for Turkish pine but afterward, the same method was used to extract lignin from Turkish vine stem. This standard process is shown in Figure 2.1.

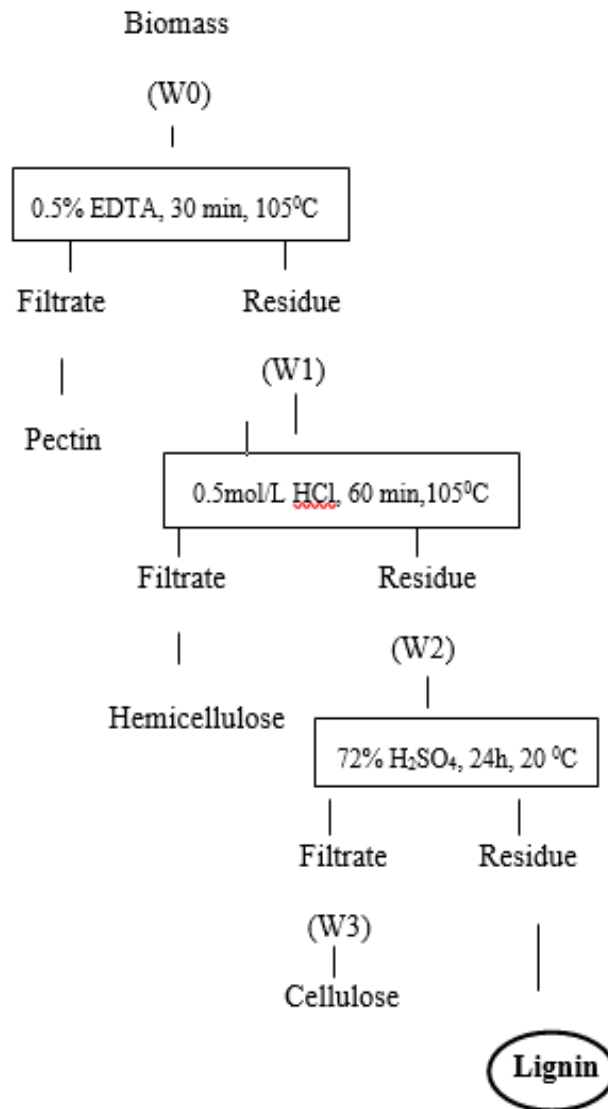


Figure 2.1: ‘Chinese Textile Industry’ standard method [86].

Extraction process started first by pulping, where the biomass was cut and grind into small pieces in a blade mill to around 200 meshes and the powder was placed in the 70 °C oven, drying to constant weight (W0). The dried powder was washed with 70 % alcohol and added EDTA solution to extract the pectin from biomass, filtered via sintered glass crucible and washed after drying to constant weight (W1). Using acetone to wash the residue (W1) and dried. Later, it was added hydrochloric acid to hydrolyze and then filtered to separate hemicellulose from the mixture, washed and dried to constant weight (W2). The residue (W2) was washed with acetone, dried, treated with

sulfuric acid, afterward filtered mixture, washed with distilled water to remove residual lignin and dried to constant weight (W3) (see Figure 2.2)



Figure 2.2: Schematic diagram of the lignin extraction for Turkish pine.

The ratios of the cellulose, hemicellulose, lignin, and pectin content were calculated by the equation 1-4 [87].

$$Pectin (\%) = \frac{W_0 - W_1}{W_0} \times 100 \quad (1)$$

$$Hemicellulose (\%) = \frac{W_1 - W_2}{W_0} \times 100 \quad (2)$$

$$\text{Lignin (\%)} = \frac{W_3}{W_0} \times 100 \quad (3)$$

$$\text{Cellulose (\%)} = \frac{W_2 - W_3}{W_0} \times 100 \quad (4)$$

2.3 Characterization of lignins

The structural, chemical and thermal characterization of lignins were examined by Scanning electron microscopy (SEM), Fourier transform infrared spectroscopy (FTIR), Water Contact Angle measurements, Thermogravimetric analysis (TGA), Elemental analysis CHNS, X-ray Photoelectron Spectroscopy(XPS) and Differential scanning calorimetry (DSC).

2.3.1 SEM

SEM images were recorded by Phenom proX desktop scanning electron microscope using gold-coated samples and were analyzed the surface structure of lignins.

2.3.2 Contact angle

Contact angle measurements were carried out using an easy drop instrument (ThetaLite101, Biolin Scientific). A water drop (~3 μ l) was added to each sample surface using a Hamilton syringe at room temperature and obtained the changes in hydrophobicity of the surfaces.

2.3.3 FTIR

The FTIR measurements of extracted lignin patterns are taken using Thermo Scientific Nicolet 6700 equipped with an ATR mode. The FTIR spectra were noted in the wavenumber range of 4000 to 400 cm^{-1} in the absorbance mode. The materials were observed with a resolution of 4 cm^{-1} and each sample was recorded 64 scans.

2.3.4 TGA

Thermogravimetric analysis (TGA) was utilized to detect the thermal stability, decomposition temperature for each lignin. TGA analyses were measured using TA Instruments Q500 setup operating under nitrogen. Samples on a platinum pan for each measurement were maintained at -5 mg, and scans were applied from 25 to 800 $^{\circ}\text{C}$ at

10 °C/min. TGA was replicated three times, and the results of the analysis were reproducible.

2.3.5 DSC

Thermal properties of lignins were assigned with Differential Scanning Calorimetry (TA Instruments Q200) with $3,0 \pm 0.50$ mg of lignin samples were put in a hermetic pan and heated from 0 to 200 °C at 10 °C/min in the nitrogen environment. Lignin samples were run in triplicate and the average deviation was defined. The glass transition temperature (T_g) of lignin-based on its resource and extraction method [88]. Consequently, three different lignins were applied to calculate T_g and to understand the effect of temperature and time on the DSC results. The average moisture amount of lignin samples was measured before the experiments and was kept nearly amount for all of the lignin samples (Denver Instrument–IR 35 moisture analyzer).

2.3.6 Elemental analysis

The weight percentage of elements CHNS was obtained from an elemental analyzer (Thermo Scientific FLASH 2000 CHNS/O analyzer). Each sample of lignin was measured in three times by Elemental analyzer.

2.3.7 XPS

The composition of chemical elements on lignin has been examined by X-ray photoelectron spectroscopy. XPS measurements were performed with a Thermo Scientific K-Alpha electron spectrometer using a monochromated Al K_α X-ray source run at 100 W.

2.4 Fabrication and characterization of PAN, PAN/lignin, and PAN/lignin/graphene nanofibers

2.4.1 Solution preparation

Three types of solutions (PAN, PAN/lignin, and PAN/lignin/GRP) were made ready for electrospinning process. Solutions of nanofibers with numerous concentrations (Experimental Design parts) were prepared by magnetic stirring at room temperature. Earliest experiments on electrospinnability of lignin/PAN in DMF solutions with different polymer concentrations ranging from 12 to 25 wt. % displayed that solutions

with the concentration of polymer play a significant role in the electrospinning parameters based on the viscosity of solutions [51, 56].

In this work, the certain amounts of lignin and PAN were weighed. Table 2.1 shows numerous concentrations of electrospinning solutions and their sample codes.

Table 2.1: Numerous concentrations of electrospinning solutions.

Lignin/PAN Ratio (wt.%)	Graphene (wt.%)	Total Polymer Concentration (wt. %)	Sample Code
0	0	10	PAN
1	0	10	10C1
3	0	10	10C3
5	0	10	10C5
0	0	20	20PAN
1	0	20	20C1
3	0	20	20C3
5	0	20	20C5
1	1	10	10C1-1G
3	1	10	10C3-1G
5	1	10	10C5-1G
1	1	20	20C1-1G
3	1	20	20C3-1G
5	1	20	20C5-1G
1	5	10	10C1-5G
3	5	10	10C3-5G
5	5	10	10C5-5G
1	5	20	20C1-5G
3	5	20	20C3-5G
5	5	20	20C5-5G

The powders were mixed by using a stirrer and the weight ratio of PAN to lignin in the solutions were 1:1, 1:3, and 1:5, respectively. The appropriate volume of Dimethylformamide (DMF) was added to the mixed powders to obtain the preferred total polymer concentration of 10 % and 20 wt./v %. The concentration of 10 and 20 wt.% was chosen to prepare PAN/lignin solutions throughout the electrospinning experiments to find a suitable concentration of PAN/lignin.

To prepare for the PAN/lignin/GRP solutions, the concentrations ranging from 1 to 5 wt. % of GRP were added separately to the PAN/lignin solutions. After adding of GRPs, GRPs were dissolved in PAN/lignin solutions under 30 min of sonication (Hielscher Ultrasonics) and then mixed by using a magnetic stirrer until homogeneous.

2.4.2 Electrospinning of nanofibers

The electrospun mats were produced in a NANON-01A (MECC Co. Ltd. Japan) in which electrospinning setup has a vertical orientation. A 10 ml plastic syringe (22-gauge needle) was used. The collector was covered with an aluminum foil in the course of the process.

The distance was 22 cm between the needle and the collector. A working voltage of 24 kV and a flow rate of 0.3 mL/h (by way of a computer-controlled syringe pump) were used in all electrospinning experiments (Figure 2.3). The electrospinning experiments were completed at 25–30 °C and the humidity was constant during the experiments (35–45%).

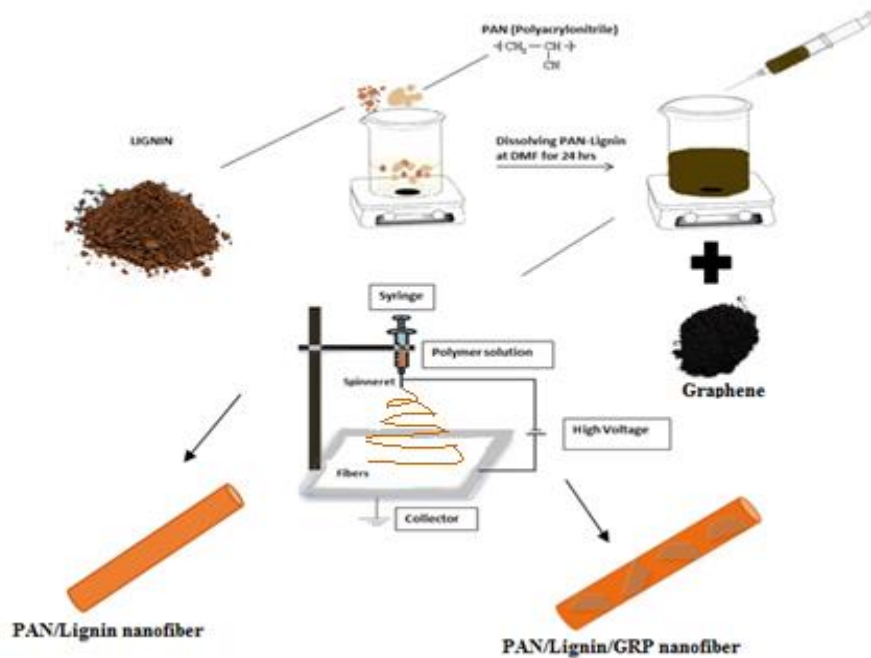


Figure 2.3: Schematic illustration of the production of with and without graphene-polymer nanofiber by electrospinning.

A wide variety of parameters impact the electrospinning process. Apart from processing parameters such as voltage, flow rate and ambient parameters such as humidity, temperature can play an important role in defining the electrospinnability of the environment. For this reason, this system used to reduce humidity and temperature in the electrospinning set up (NANON-01A).

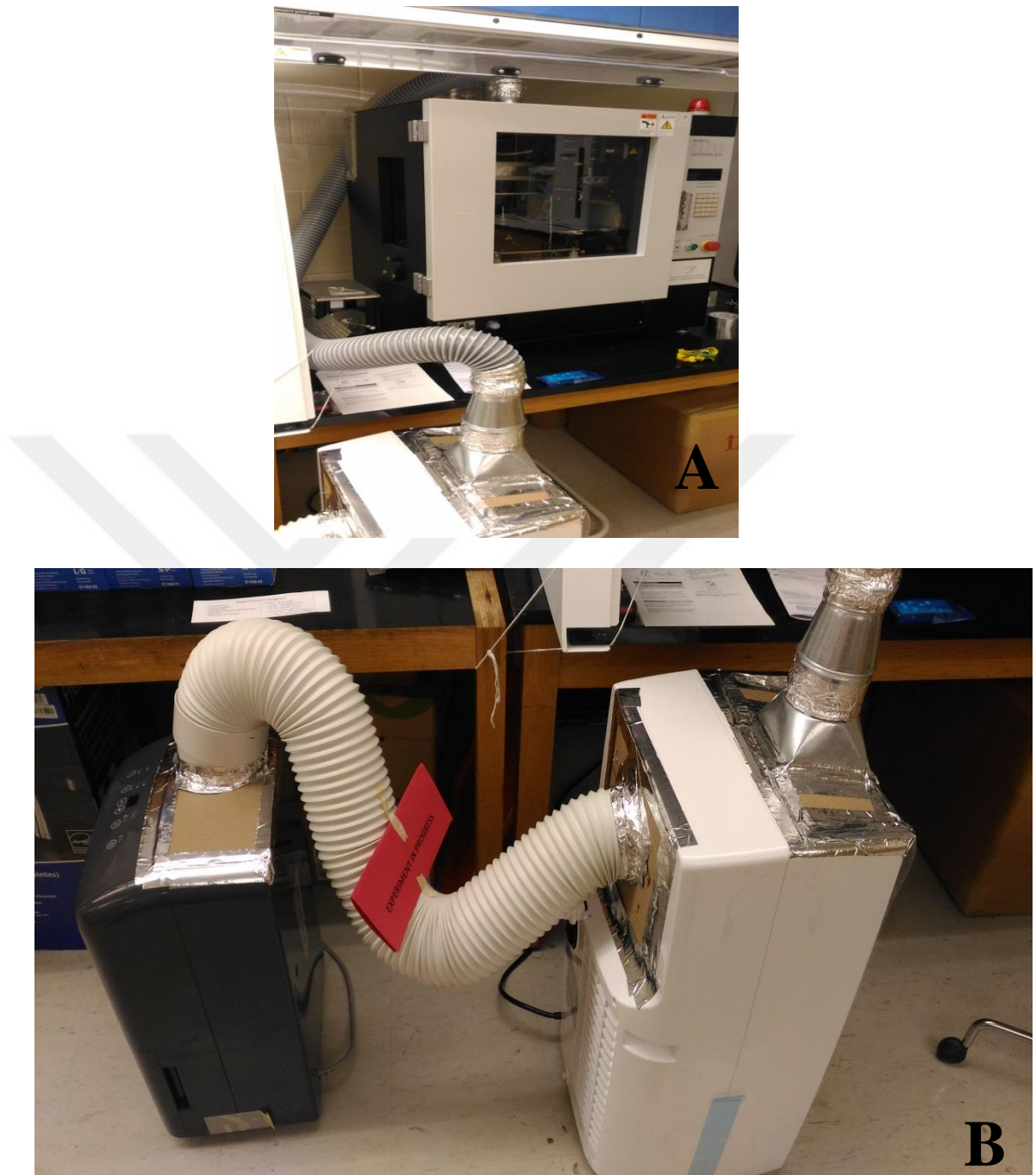


Figure 2.4: A) The electrospinning system with dehumidifier/AC, B) Dehumidifier and AC system equipment for electrospinning system

When the temperature and humidity increased inside the electrospinning system, this equipment was turned on to fix the temperature and humidity in the course of the whole electrospinning process (Figure 2.4).

2.4.3 Rheological characterization of electrospinning solutions

A rheometer (Anton Paar Modular Compact Rheometer MCR–302) was utilized to observe the rheological properties of PAN, PAN/Lignin, and PAN/Lignin/Graphene blends. The viscosity was calculated using a rheometer, as a function of the shear rate range of 0,1-100 s⁻¹ in concentric cylinder configuration. The blended solutions were measured within 24 h later. The average values of three measurements are reported.

2.4.4 Nanofiber characterization

2.4.4.1 Morphological and structural analysis

The morphology and diameter of PAN, PAN/lignin, and PAN/lignin/GRP nanofibers were assessed by using Zeiss Gemini 300 VP field emission scanning electron microscope (FESEM) working at 5 kV. A few piece of the nanofiber was put on carbon tape and then covered with Au. The mean nanofiber diameter was surveyed using an image analyzer (Image J software). About 40 measurements in each sample were used for the calculation of the diameter distribution.

2.4.4.2 XRD

The structural characterization of PAN, PAN/lignin, and PAN/lignin/GRP nanofibers was achieved by X-ray diffraction (Panalytical Empyrean XRD System, Ni-filtered CuK α , k:1.54 Å⁰) in a 2 θ angle range of 10⁰ to 50⁰, with a step size of 0.005. The percentages of crystallinity were calculated with the Diffrac. Suite Eva software for each nanofiber samples.

2.4.4.3 FTIR

FTIR data were verified on a Thermo Scientific, model Nicolet IS5 with ATR mode. A total of 64 scans were recorded with a resolution of 4 cm⁻¹. The FTIR was completed in the spectral range of 400-4000 cm⁻¹ with absorbance mode. The characteristic absorbance bands for PAN, PAN/Lignin, and PAN/Lignin/GRP nanofibers were approved by FTIR.

2.4.4.4 Electrical conductivity

Experiments of the electrical conductivity were carried out at room temperature using

an Autolab PGSTAT302N equipped with a FRA32 M impedance analysis module from Metrohm Autolab B.V. Netherlands. Conductivity measurements were performed by means of a frequency response from 0.1 to 100 kHz under potentiostatic mode at 10 mV.

Nanofibers were vacuum oven-dried at 80 °C for 24 hours and placed in a hollow cylinder with an inner diameter of 10 mm, which was then pressed between two pistons that form the electrodes. Results were obtained with Nova 1.8.17 software. Figure 2.5 showed how the electrical conductivity of PAN, PAN/lignin, and PAN/lignin/GRP nanofiber were measured by using experimental setup.

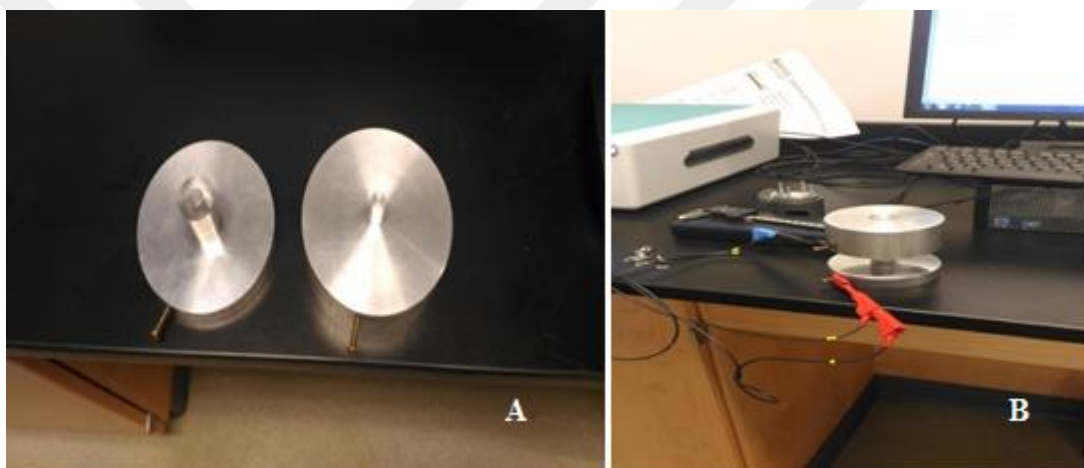


Figure 2.5: Electrical conductivity set up consists of A) hollow cylinder and B) Potentiostat/Galvanostat.

2.4.4.5 Statistical analysis

In this work, PAN/Lignin/GRP nanofibers were prepared by electrospinning. So as to minimize the response, an experimental design was utilized. Statistical analysis of the electrospinning process was performed by ANOVA using Minitab VR 16.2.4. The factors studied were the ratio of lignin/ PAN (X1), percentage of graphene (X2), and polymer concentration (X3). All variables and their respective range were shown in the further section. A 2^3 resolution V fractional factorial design with 8 experimental runs in one block. The purpose of this factorial design was to examine the effects of the design variables on the response of conductivity and diameter of PAN/lignin/GRP nanofibers.

In order to evaluate the goodness of fit of the analysis, each term of the model is examined statistically which established the meaning of F-values with $p \leq 0.05$.

2.4.4.6 TGA

Thermogravimetric analyses (TGA, Q600, TA Instruments) were led to evaluate the thermal stability of the nanofiber mats. Approximately 10 mg samples in a pan and heated from room temperature to 900 °C at a rate of 10 °C/min under nitrogen atmosphere. The thermal behavior for PAN/Lignin, and PAN/Lignin/GRP nanofibers were detected by TGA.

2.4.4.7 Atomic force microscopy (AFM)

Nanosurf Flex Axiom AFM was used to gather the surface data and phase separation properties of the electrospun nanofibers. Tapping mode AFM was utilized to determine the surface morphology and the cantilever is located at the sample surface within a selected area of interest.

The scan area of each image was chosen 10 μm with and three measurements on same nanofiber were done.

2.5 Thermal Stabilization and Carbonization

Carbonization of nanofibers was started with thermal stabilization step which nanofibers are heated in air and temperature is ramped from 25 °C to 225 °C at a heating rate of 1 °C /min and held at 225 °C for 2 hours. Thermal stabilization prior to carbonization causes the nanofibers to have increased resistance to higher thermal treatment because of the formation of crosslinks.

In carbonization step, the nanofibers were heated in nitrogen to the different temperature to carbonize. Table 2.2 indicates the heating conditions utilized for nanofibers and the residence time at max temp. and heating rates used for each nanofiber. Thermal stabilization was performed in a Sentro Tech Corp furnace and carbonization was carried out in a Carbolite 1200 °C G-range horizontal tube furnace. The horizontal tube was constantly purged with a 3 L/min flow of nitrogen.

Table 2.2: Heating conditions of nanofibers.

Temperature ($^{\circ}\text{C}$)	Heating rate ($^{\circ}\text{C}/\text{min}$)	Residence time at Max. T (h)
900 $^{\circ}\text{C}$	2 $^{\circ}\text{C}/\text{min}$	1 h
800 $^{\circ}\text{C}$	2 $^{\circ}\text{C}/\text{min}$	2 h

2.5.1 SEM of carbon nanofibers

The morphology of the carbonized mats was examined by Scanning Electron Microscopy using Zeiss Gemini 300 VP field emission scanning electron microscope (FESEM) and carbonized mats were covered with gold. The elemental composition of these carbonized mats was examined with Energy Dispersive X-ray Spectroscopy (EDS) and analyzed using the Phenom ProX SEM. Carbonized mats were not coated gold.

2.5.2 RAMAN of carbon nanofibers

Raman measurements were conducted on the carbon nanofibers by using Renishaw. Raman spectrometer at room temperature with a laser diode emitting at 514 and 785 nm, operating in the confocal mode. It was used to detect the presence of graphene in the carbon nanofibers. In order to avoid the overheating of the surface of carbon nanofibers, the energy of the laser has been set at 0.1 mW.

2.6 Electrochemical Sensor Analysis

2.6.1 Preparation of CNF/SPE (Carbon nanofiber modified screen-printed electrode) and CNF-G/SPE (Graphene reinforced carbon nanofiber modified screen-printed electrode)

8 mg/mL of CNFs (20C5) and CNF-Gs (20C5-1G) were homogenized by sonication for 2 h in ethanol and then stirred by a magnetic stirrer for another 1 h until obtained solutions. These obtained solutions were used for modification of SPEs (Screen printed electrodes). 5 μL of the obtained CNFs and CNF-Gs were dropped on the SPEs separately. These electrodes were left for drying in the air. After 1.5 hours, CNFs/SPE

and CNF-Gs/SPE were washed with PBS (pH:7.4) and kept for a couple of minutes at room temperatures.

2.6.2 Characterization of CNF/SPE and CNF-G/SPE

The bare SPE, CNF/SPE, and CNF-G/SPE were activated in the acetate buffer solutions (ABS) by means of applying 0.8 V for 60s. AUTOLAB PGSTAT204 potentiostat/galvanostat system was used Electrochemical Impedance Spectroscopy (EIS) and Cyclic voltammetry (CV) measurements for characterization of modified electrodes. The three electrode system consisting of the working electrode, reference electrode, and counter electrode were connected with the Nova 1.10 software.

The EIS was performed in redox solution containing $[\text{Fe}(\text{CN})_6]^{3-/4-}$ with KCl between the frequency range of 10^{-2} Hz to 10^5 . The voltage of +0.24 V and the sinusoidal signal of 10 mV was implemented in the course of the EIS measurements.

The CV was made in the potential range of 0 V to +1.2 V at a scan rate of 50 mV/s and used $[\text{Fe}(\text{CN})_6]^{3-/4-}$ with KCl as a redox solution. All measurements were replicated three times and done at room temperature.

Differential Pulse Voltammetry (DPV) measurements were used to determine the commercial pharmaceutical drug containing acetaminophen. The A-ferin forte tablet (Bilim Pharmaceuticals, Turkey) was ground to powder and dissolved in PBS (pH:7.4). The final concentration of acetaminophen was detected in the working range. The DPV responses were recorded between the potentials + 0.20 V and + 1.20 V, the pulse amplitude 50 mV and pulse width 50 ms.

3. RESULTS AND DISCUSSION

3.1 Extraction and Characterization of Lignins

Wood fundamentally consists of cellulose, hemicelluloses, and lignin. Its types can be classified by two kinds: softwood and hardwood. Hardwoods are angiosperm plants although softwoods are gymnosperm plants. The chemical composition of these types differs significantly [89].

The results of Turkish pine and Turkish vine stem were compared to other lignocellulosic raw materials and wastes indicated in Table 3.1. According to Eq (3), Turkish pine and Turkish vine stem consist of 22,9 % and 30,2% lignin, respectively.

Table 3.1: The composition of different lignocellulosic resources.

	Hemicellulose (%)	Cellulose (%)	Lignin (%)	Reference
Turkish pine	25,6	39,7	22,9	
Turkish vine stem	27,3	32,4	30,2	
Softwood stems	25-35	45-50	25-35	[90]
Rice straw	18-25	35-45	10-25	[91]
Hardwood stems	20-40	40-55	18-25	[90]
Bagasse	16.52	54.87	23.33	[92]
Wheat straw	20-32	38-45	7-10	[93]

The values reported in Table 3.1, the contents of cellulose are comparatively greater than that of lignin in each wood and non-wood species. Considering Table 3.1, the amount of lignin in softwood stems is higher than in hardwood stems while extracted

lignin from Turkish vine stem significantly upper than that of Turkish pine. It is reasonable to presume that Turkish vine stems can be taken either semi-hardwood or softwood because Turkish pine is softwood.

Lignin was extracted from various biomass in this study and compared with commercial lignin (Protobind 2400) as lignin includes different functional groups based on the biomass and the extraction method. For instance, the extracted lignin by using acid treatment has great amounts of carbonyl groups [94]. To study the effect of extraction method and biomass source on the structure and thermal properties of lignin, the characterization methods were used to determine the differences between the commercial lignin and the extracted lignin.

3.1.1 SEM of lignins

The structure of lignin has irregular shaped and small size particles. Industrial extraction procedures considerably change the chemical structure of lignin while the laboratory scale extraction procedures that give rise to lower alter the natural lignin structure. To figure out the structural differences between commercial and extracted lignin, we were examined the images obtained by SEM. However, Figure 3.1 indicates that the extracted lignins have damaged cell wall in comparison with commercial lignin. These results showed that the extraction method using acid treatment may also damage the morphology and the structure of lignin.

It is evident from Figure 3.1 that another important difference for commercial lignin is particle size. While the average size of commercial lignin (Protobind 2400) is about 10-15 μ , the particle size of extracted lignins is much bigger than commercial lignin because of isolation method [28]. Also, these differences can be related to their origin, which influences functional groups.

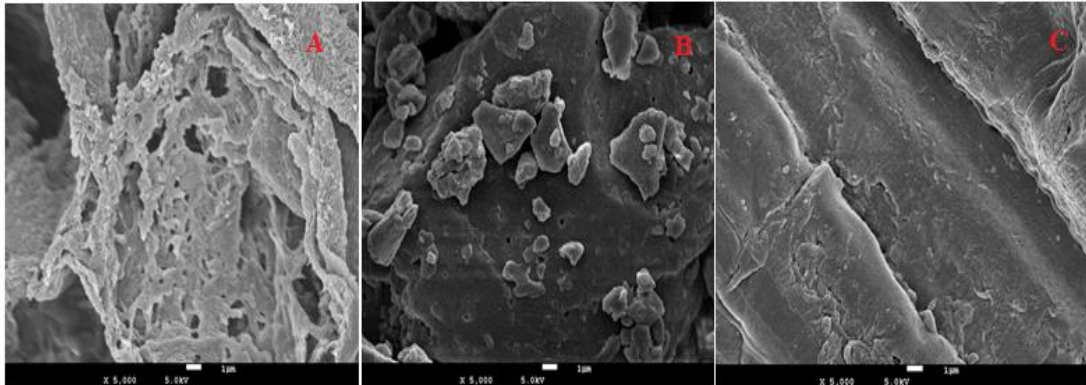


Figure 3.1: SEM images of lignin samples from A) Turkish Vine stem, B) Commercial lignin, and C) Turkish Pine

3.1.2 Contact angle

Contact angle measurements of commercial lignin and extracted lignin were performed to understand the surface properties of them. Lignin consists of hydrophilic and hydrophobic groups. However, the extraction method can strengthen either characteristic for hydrophobicity and hydrophilicity. That's why contact angle was carried out to understand the effects of acid treatment.

The results from contact angle measurements indicate that the extracted lignins from Turkish vine stem and Turkish pine are more hydrophilic than commercial lignin depending on the different sources and extraction methods (Figure 3.2). The increased hydrophilicity in the extracted lignins can be due to the display of OH groups from the lignin structure or the addition of polar sulfate groups from the extraction method [95, 96]. Also, the differences in contact angle for both type of extracted lignin may be owing to the enlarged roughness of the samples.

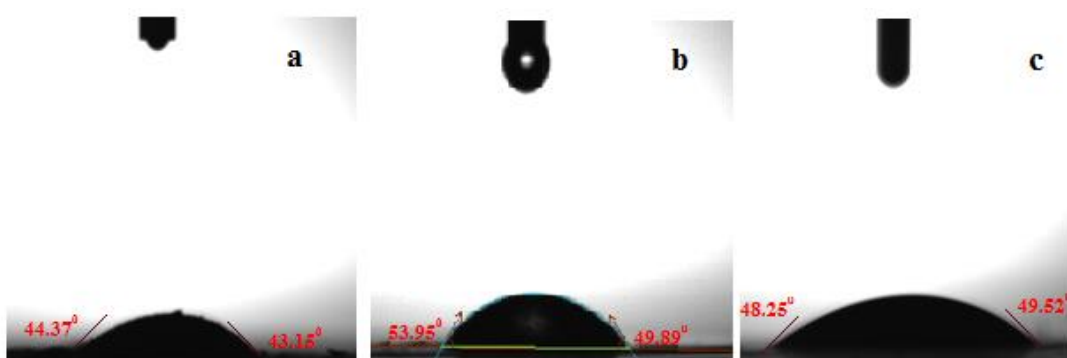


Figure 3.2: Contact angle images of a) the extracted lignin from Turkish vine stem b) commercial lignin, and c) the extracted lignin from Turkish pine.

3.1.3 FTIR of lignins

The chemical structure of the three lignin samples was performed by means of FTIR in Figure 3.3. As can be seen, the spectra of all lignin are very similar to each other. Every lignin has a strong broad absorption band among $3500 - 3100 \text{ cm}^{-1}$ was because of the presence of hydroxyls. This band is due to the presence of alcoholic and phenolic hydroxyl groups concerned with hydrogen bonding [97]. The extracted lignin has a band at 2930 cm^{-1} with a shoulder at 2845 cm^{-1} while the commercial lignin has a sharp band at 2920 cm^{-1} . The appearance of these bands is an indication of the existence of C-H stretching vibrations of aromatic methoxyl groups and methylene in lignin structure [98, 99].

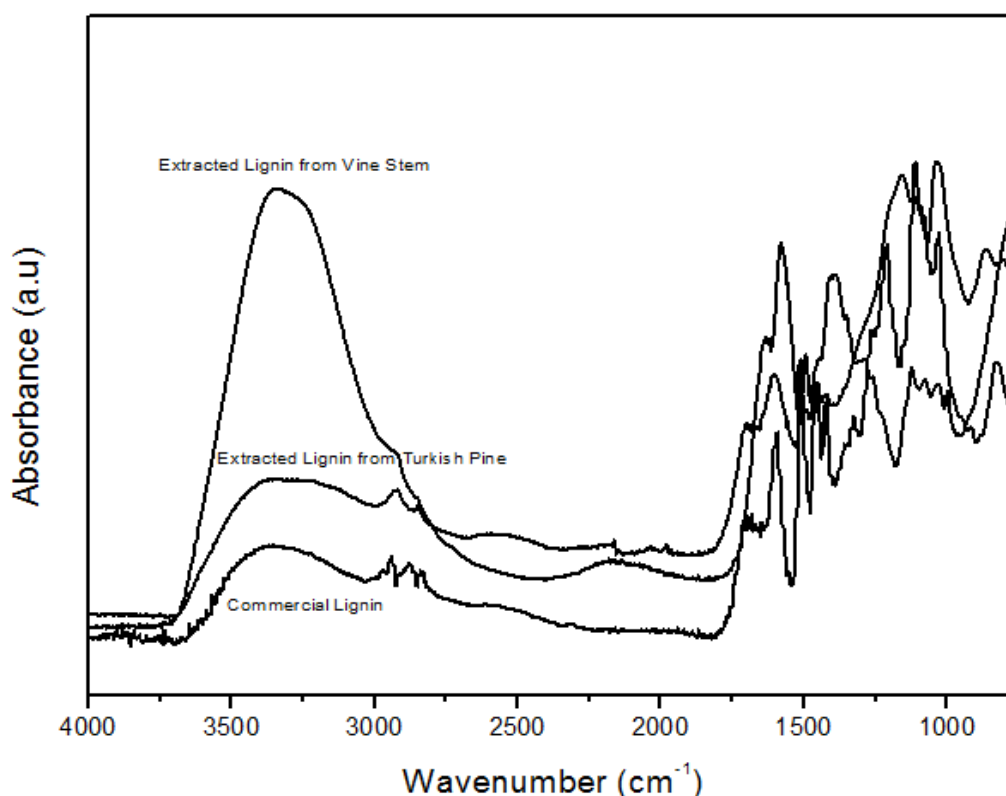


Figure 3.3: FTIR spectra of three different lignins.

The band at 1705 cm^{-1} in commercial lignin ascribed to the stretching vibrations of C=O present in the carbonyl [100]. The absorption bands at $1626\text{-}1608\text{ cm}^{-1}$ were attributed to C=C double bonds in lignin [101]. The bands from $1455\text{ to }1500\text{ cm}^{-1}$ were considered the C-H deformations and aromatic C-H in-plane deformation with an aromatic ring stretching [96]. These bands are very similar for all lignins, even though their intensities may be shifted. Lignin consists of three structural units, namely guaiacyl (G), p-hydroxyphenyl (H), and syringyl (S) [102]. Guaiacyl (G) and syringyl (S) are the main units of lignin, nevertheless, the percentage of S/G diverges from one to another resource. The band at 1328 cm^{-1} present in commercial lignin corresponds to C-O of the syringyl ring although it is absent in extracted lignins. Syringyl and guaiacyl units in lignin were identified at $1325, 1220, 1025, \text{ and } 829\text{ cm}^{-1}$ conforming to syringyl and condensed guaiacyl absorptions, C-C, C-O and C-O stretch, CH vibrations [103]. The guaiacyl band was contemplated between $1210\text{ and }1220\text{ cm}^{-1}$ for all lignins, but commercial lignin was shifted to lower wavenumbers than extracted lignins. Although the alkyl ether vibrations ($\beta\text{-O-4}$) at 1040 cm^{-1} current in all lignin, this band was weak in extracted lignin from vine stem and strong in extracted lignin in Turkish pine [104].

FTIR spectra indicate that lignin is presented in both the extracted samples of Turkish pine and Turkish vine stem. The main changes in the functional groups between commercial lignin and extracted lignins are due to the extraction method of lignin.

3.1.4 Elemental analysis of lignins

Table 3.2: Elemental analysis of lignin samples.

Lignin source	N (%)	C (%)	H (%)	S (%)
Commercial lignin	0.550	61.850	6.210	0.980
Turkish pine	0.009	45.410	3.664	3.932
Turkish vine stem	0.457	49.175	3.911	3.515

Elemental analysis of lignin in terms of nitrogen, carbon, hydrogen and sulfur amount was investigated. From the results of the elemental analysis (Table 3.2), it can be seen that very low nitrogen amount (0.008%) was observed in extracted lignin from Turkish pine. Although the extracted lignin from vine stem was extracted by the same method, nitrogen amount observed in vine stem was 0.45 %. This may be due to the distinct resource. On the other hand, the amount of sulfur was apparently higher than commercial lignin was owing to the sulfuric acid treatment in the extraction process.

While a low amount of sulfur (0.9 %) in commercial lignin was detected, commercial lignin has the highest carbon amount 61.85 %. Carbon amount is close to the amount found in present literature, which is described by Sahoo et al [105]. They stated that the carbon amount of commercial lignin (Protobind 2400) to be 62.6 %.

3.1.5 TGA of lignins

Thermal stability and the degradation temperature of the lignins were performed by TGA. The resulting values of TGA analysis are shown in Figure 3.4. Table 3.3 indicates the temperature of the first degradation, which is the temperature that corresponds to around 10 % weight loss of the lignin and the temperature at which 50 % of weight (T50 %) has been lost, for each lignin.

Table 3.3: Thermal properties of lignins studied by TGA.

TGA	T1 (°C)	50% (°C)	Residues (%)
Commercial lignin	181	380	24
Extracted lignin from Turkish vine stem	176	485	31
Extracted lignin from Turkish pine	178	542	42

T1: First degradation temp.; T50 %: Temperature for 50 % of weight loss (°C)

The structure of lignin is consisted of primarily aromatic rings having numerous branching, these chemical bonds lead to a large range of degradation temperature from 100 to 800 °C [106]. Degradation of the lignin can be partitioned into three phases. In phase one, the first weight reduction step happened at 30–120 °C owing to the

evaporation of water assimilated. The second phase is viewed to occur around 180–350 °C and is ascribed to the degradation of parts of carbohydrates in the lignin, which is changed over to unpredictable gasses, for example, CO₂ and CO. The final degradation happened over an extensive variety of temperatures over 350 °C [107].

Figure 3.4 shows that the first weight loss that happened from 25 °C to 120 °C is owing to the loss of residual moisture content in lignin. It could be seen from this figure, the extracted lignins have more water content than commercial. This probably due to the extraction method or mostly related to the plant source. The results of TGA, shown in Figure 3.4, exhibit that temperatures at which the lignins start to degrade are situated around 175 °C except for commercial lignin for which the degradation is beginning at considerably higher temperature.

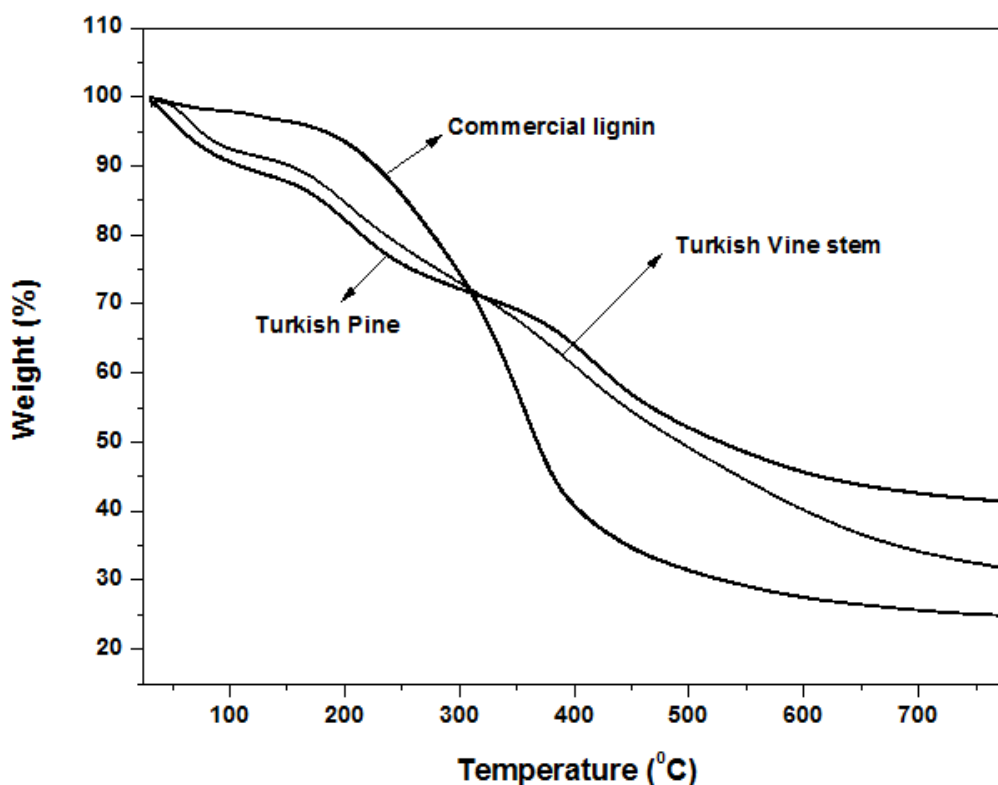


Figure 3.4: Thermogravimetric analysis of three different lignins.

The TG curve of extracted lignins demonstrates three stages of degradation of components, whereas two-stage degradation was detected for commercial lignin. Degraded volatile products got from lignin including alcohols aldehyde acids, phenolics alongside the development of vaporous outcome are getting evacuated. It

can be proposed that the lignin's thermal facilities are subject to their source. Sahoo et al. presented similar thermal behavior when they investigated different lignins for industrial uses [105].

For the mass loss of 50 %, the temperature was 380 °C for commercial lignin, whereas for extracted lignin from Turkish vine stem and Turkish pine they were 485 °C and 542 °C, respectively. Consequently, commercial lignin decays much faster than extracted lignins. Figure 3.4 displays that lignin degradation is proceeding within a great range of temperatures (170–800 °C), which could be ascribed to the complexity of the lignin configurations. All the result contained the degradation temperature of aromatic structures (Figure 3.4), approving the reliability of lignin samples, as stated by the literature data, this great range of degradation temperatures by dissimilar thermal stabilities of numerous functional groups having oxygen atoms in lignins and the thermal degradation of which is taking place at different temperatures [108].

The TGA results acquired in this study confirmed a better thermal stability of extracted lignins might be because of strong crosslinking of their structures.

3.1.6 DSC of lignins

Glass transition temperature (T_g) for three types of lignin were detected with DSC where the heat of reaction was carried out (Table 3.4). T_g of lignins is likewise extremely affected by the water content. Hence, T_g has been controlled by DSC checks after widely drying lignins (24 h, 60 °C, a vacuum oven) in the request to discharge all the water content.

The T_g of lignin is frequently difficult to notice owing to the complex arrangement of this polymer. Numerous lignin arrangements are accounted for to have T_g values in the vicinity of 90 and 180 °C, relating the higher values as a rule to softwood kraft lignins and the lower ones to organosolv lignins [109].

Table 3.4: Glass Transition Temperatures T_g for Different Lignin Samples.

Samples	T_g (°C)
Commercial lignin	149.51

Extracted lignin from Turkish pine	153.61
Extracted lignin from Turkish vine stem	150.58

All non-modified lignin has a comparatively high glass transition temperature because the condensed rigid phenolic moieties and strong intermolecular hydrogen bonding interactions confine the thermal mobility of lignin molecules and bring about its high T_g [110]. In this study, similar T_g value was found for all types of lignin, which are higher than those determined for organosolv lignins [111]. As can be seen in Table 3.4, there is no big difference among three lignins depends on the T_g values.

This variation in T_g can be described by the free volume concept as defined by Mohammed et al., which shows that free volume is the space in a solid or liquid sample not occupied by polymer molecules. Thus, T_g could be represented by such activation energies through the utilization of free volume. Furthermore, this property is influenced by extremely on molecular weight since polymers with higher molecular weight could necessitate more energy to reach this transition. So, T_g can be increased with higher molecular weight [112].

3.1.7 XPS analysis of lignins

The surface composition of samples of commercial lignin and the extracted lignin was studied by X-ray photoelectron spectroscopy. However, XPS is generally used to verify and compare modifications, instead of defining the chemical structure in analyzing lignin.

Carbon, oxygen, and nitrogen atoms are the basic components of lignin. Table 3.5 presents the elemental composition of all lignin samples by using survey spectra in the binding energy. In Table 3.5, the O/C ratio calculated for lignin samples are 0.51, 0.20 and 0.45, relatively similar to the theoretical value for lignin dedicated by Johansson *et al.* as 0.34 [113].

Table 3.5: Elemental composition of the lignin samples as calculated by XPS analysis.

Sample	C1	C2	C3	C4	O/C
Turkish Pine	7.17	11.12	7.16	1.35	0.51
Commercial lignin	10.17	13.44	17.52	-	0.20
Turkish Vine stem	9.28	10.57	9.09	0.96	0.45

According to obtained XPS results, C 1s and O 1s peaks were determined in detail and showed in Figure 3.5, and Figure 3.6.

Different valence states of carbon are a reason for having different binding energies in the XPS spectra. For this reason, C 1s consists of four components in the lignin, which is C₁ (Comp1), C₂ (Comp2), C₃ (Comp3), and C₄ (Comp4) in Figure 3.5. Component C₁ indicates the non-functionalized carbon atoms which connect to hydrogen and carbon (-C-H, -C-C). The standard binding energy of C₁ is 284.5 ± 0.1 eV [106]. Component C₂ displays the carbon atoms, which are attributed to another non-functionalized sp² and sp³ carbon atoms. C₂ has a binding energy from 284.5 to 286.5 eV [105, 106]. The C₃ peak is generally shifted about 1.5 eV from the C₂ peak and shows the carbon atom which bond to a carbonyl or two non-carbonyl atoms of oxygen (C=O or O-C-O). C₄ peak, corresponding to O-C-O, C=O bonds, is shifted about 3.00 eV from the C₂ peak and is difficult to obtain in XPS analysis of lignin [114, 115].

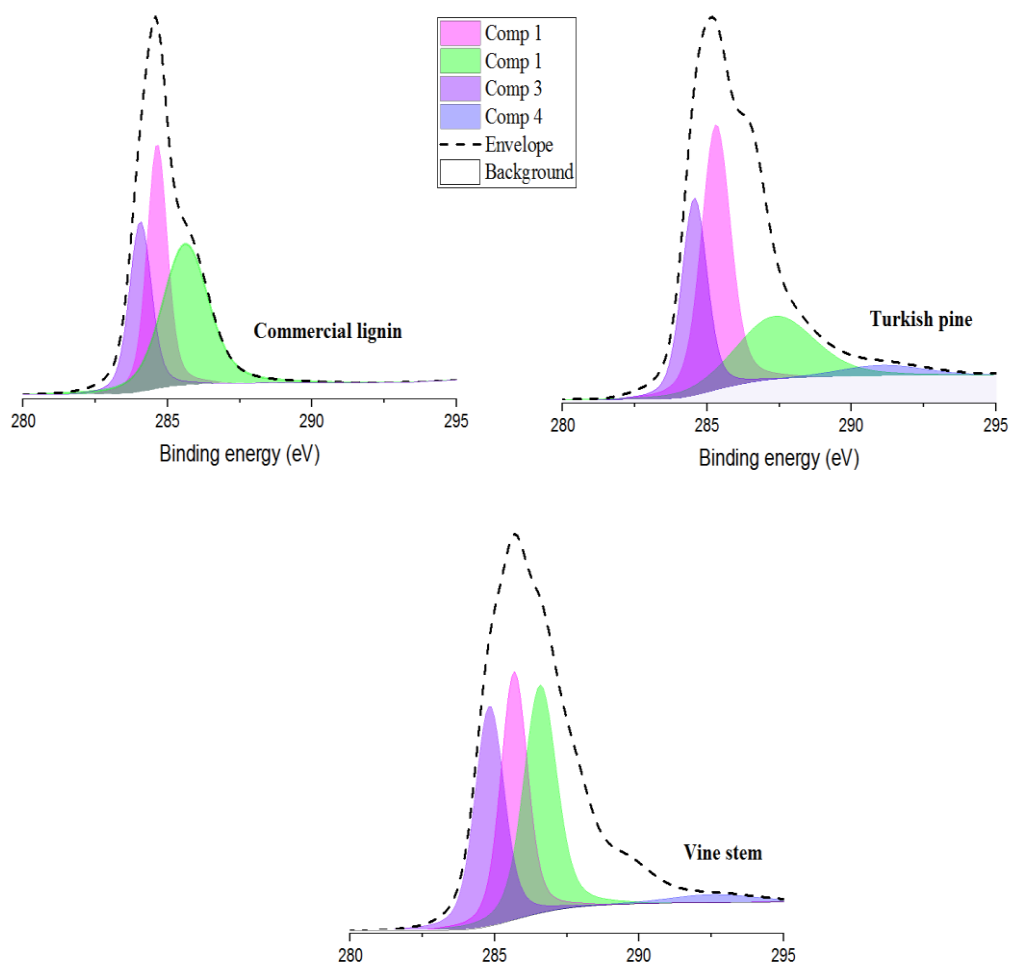


Figure 3.5: High-resolution C 1s spectra of three different types of lignin. The explanation of the components Comp 1–4 is mentioned in the text.

Figure 3.5 represents C1s spectra of three different kinds of lignin. The disparity of the intensity range, it is possible due to the carbon content of lignin and the extraction method of lignin. It is clear that the commercial lignin shows great carbon binding energy than the extracted lignins as well as it has high carbon content indicated in the table of elemental analysis (Table 3.2). Another reason of the difference of binding energy between commercial lignin and extracted lignins could mean that the contamination during extraction process of Turkish pine and vine stem.

In XPS analysis, O1s is usually low and its electron binding energy of 532 eV. Typically, O1s consists of two kinds of valence states: O₁ and O₂ (Figure 3.6). O₁ peak, corresponding to C = O, C-O-C and C-O-H bonds, shows low binding energy while O₂ peak, corresponding to C-O has higher binding energy [115]. In literature, the C1s

peak is regularly presented with the fit parameters, yet the O1s peaks are discussed rarely. It could be attributed to the small peak shift in O1s spectra. This will be studied thoroughly in future works.

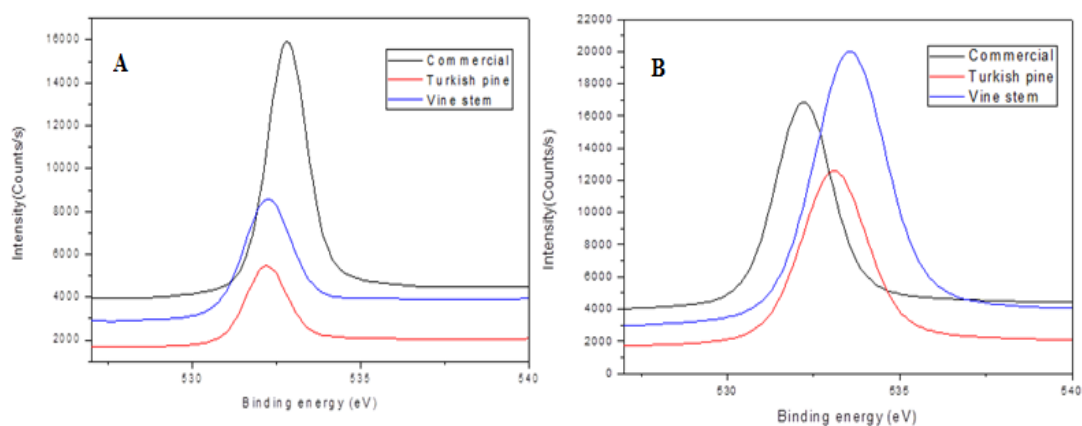


Figure 3.6: High-resolution O 1s spectra of three different types of lignin. A) O₁ peaks, and B) O₂ peaks.

3.2 Fabrication and Characterization of Nanofibers

3.2.1 Effect of polymer concentration and environmental parameters on electrospinning process

Nanofiber mats based on PAN and lignin were obtained later on electrospinning DMF dispersions of presented concentrations. The 1:1, 1:3, and 1:5 ratio PAN: Lignin solutions made nanofiber mats successfully. In the electrospinning process, the addition of lignin considerably influenced the morphology and diameter of nanofibers [116].

The primary purpose of the electrospinning in this study was to select the optimum parameter to obtain uniform, smooth and thin lignin-based nanofibers that are mainly based on the viscosity of PAN/lignin solutions. The optimum concentration of the polymer blends and their percentage was decided by comparing the electrospinnability of the solutions. Numerous concentrations of polymers (with polymer content ratio of 10 and 20 wt.%) were prepared and studied for their electrospinnability. The concentration 10 wt. % was attributed to an upper limit for solution concentration with

1:1 ratio of lignin, since further rising the lignin concentration resulted in lower viscose solutions.

When the amount of lignin is increased in PAN/lignin blends with low polymer content, the morphology of PAN/lignin nanofiber is highly influenced by the viscosity of blends (Figure 3.7).

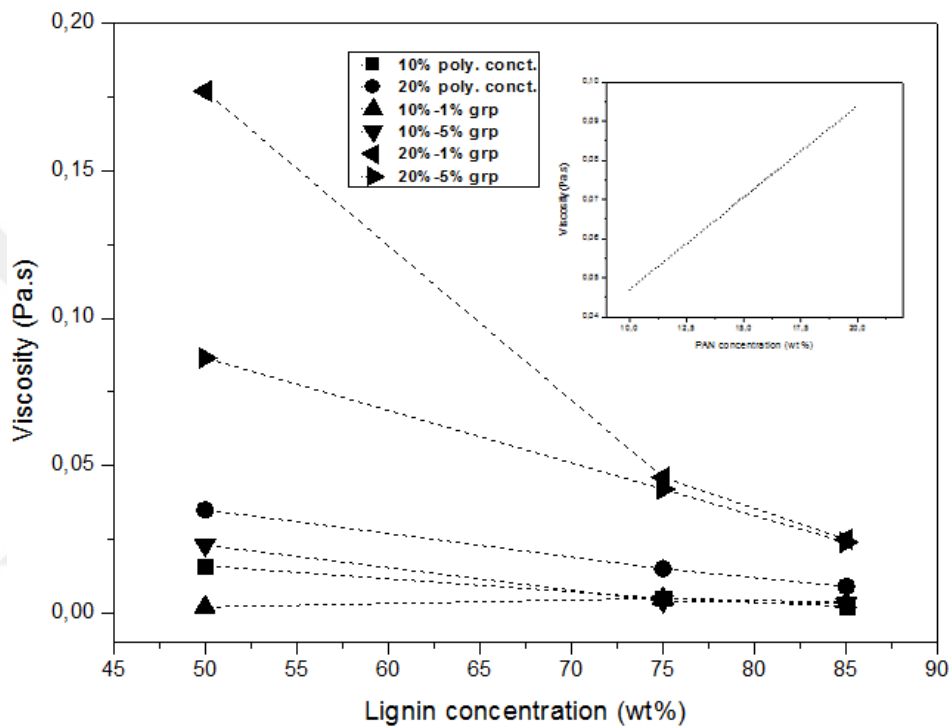


Figure 3.7: Viscosity and lignin concentration relationship for the PAN (inset graph) and PAN/Lignin solutions with 10 and 20 % wt. of total polymer concentration.

Figure 3.7 showed that the differences of the viscosity of PAN and PAN/lignin solutions with various polymer ratio. Using higher lignin content is decreased the viscosity even with higher polymer ratio in PAN/lignin solutions. The viscosity of PAN/lignin solution plays a significant role during the electrospinning process. The viscosity of PAN-lignin solutions decreased with the adding of lignin. At 1:5 PAN/lignin solution, a steep decrease in viscosity is remarkably noted. At this concentration, the morphology of the electrospun nanofibers alters from bead-free nanofibers to beaded nanofibers, as debated before.

Figure 3.7 shows the rheological behavior of PAN solutions with different concentrations at 10 and 20 wt. (%) respectively. The values of viscosity were

increased with rising of the concentration of PAN solution. These distinctions can be attributed to polymer configurations and polymer-solvent interactions [117]. The PAN/lignin solutions with higher concentrations of polymer concentration indicated higher viscosities, yet it was observed to be the viscosity of the polymer solutions decreased with growing lignin concentration (Figure 3.7). The reducing of viscosity against shear rate is because of entangled chain organizes in polymer arrangement [118].

Electrospinning of PAN/lignin solutions with low polymer concentrations was not effective owing to the low interaction among the components and the solution just electro sprayed. As a result of increasing the polymer concentration, viscosity of the PAN/lignin solution improved considerably for electrospinning process.

Contrary to the situation of 20 % polymer solution, some beading takes place upon electrospinning at 10 % polymer solutions (Figure 3.8 and 3.9). Based on SEM images, it is observed that electrospinning of PAN/lignin solutions is challenging and it results in figuration spherical droplets with fewer fiber formations.

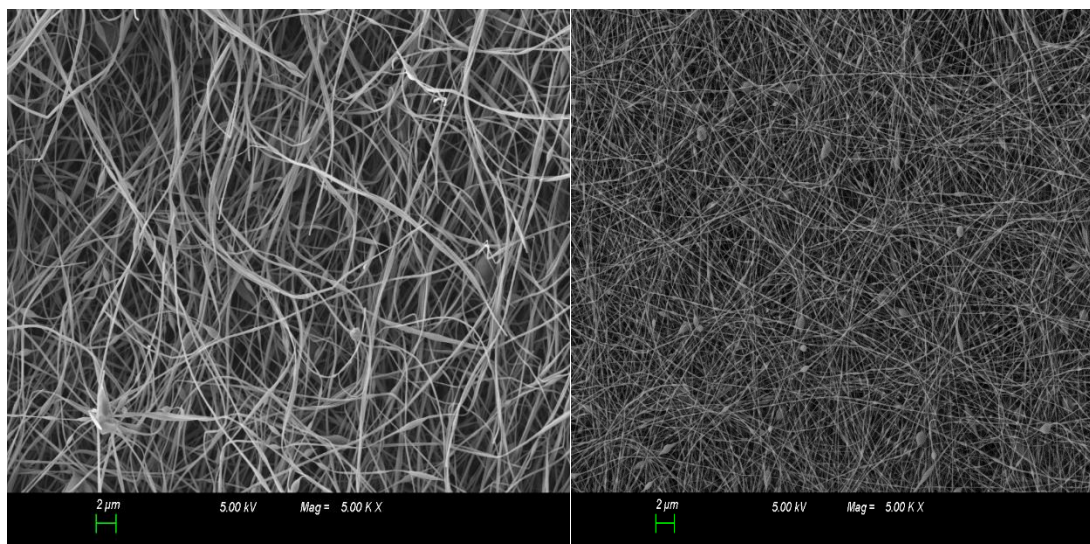


Figure 3.8: SEM images of nanofibers of 10PAN (left) and 10C1 (right).

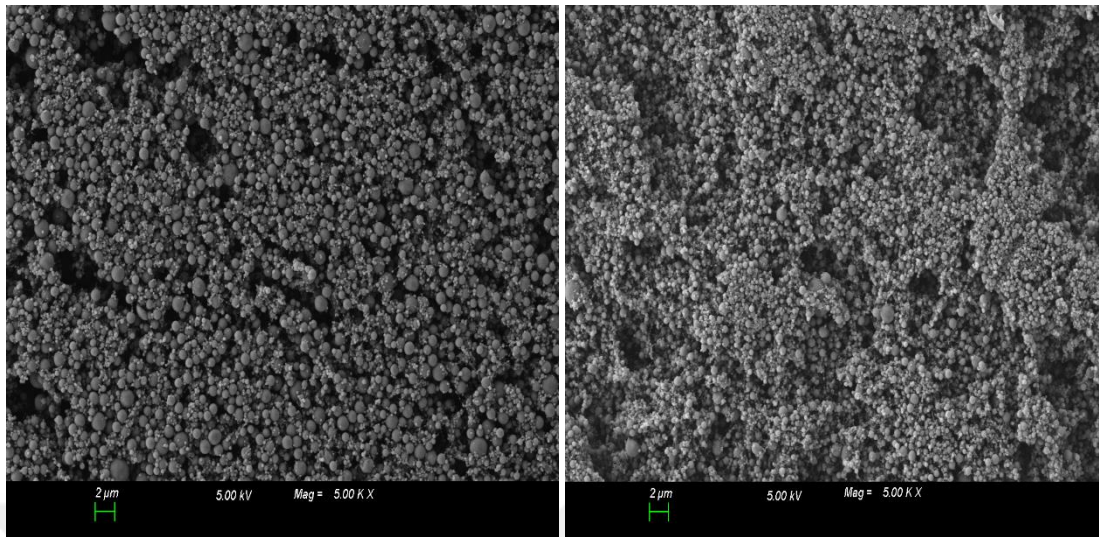


Figure 3.9: SEM images of nanofibers of 10C3 (left) and 10C5 (right).

According to SEM image of PAN/lignin nanofibers polymer concentration 20 wt. (%), the lignin in 20C1 concentration was smoothly electrospun and produced bead-free nanofibers (Figure 3.10). Similarly, uniform and mostly bead-free nanofibers were achieved upon the adding of high lignin content up to 20C3 (Figure 3.11). PAN/lignin blend of 1:5 weight ratio was hard to electrospun owing to the onset of phase separation and the considerably lower viscosity of the polymer solution. The SEM images of PAN/lignin nanofibers show that uniform, circular nanofibers with an average diameter of 120 nm were produced when the lignin contents were 3 (weight ratio) over PAN. The uniform morphology shifted to a beaded morphology when the concentration was 20C5 (Figure 3.11).

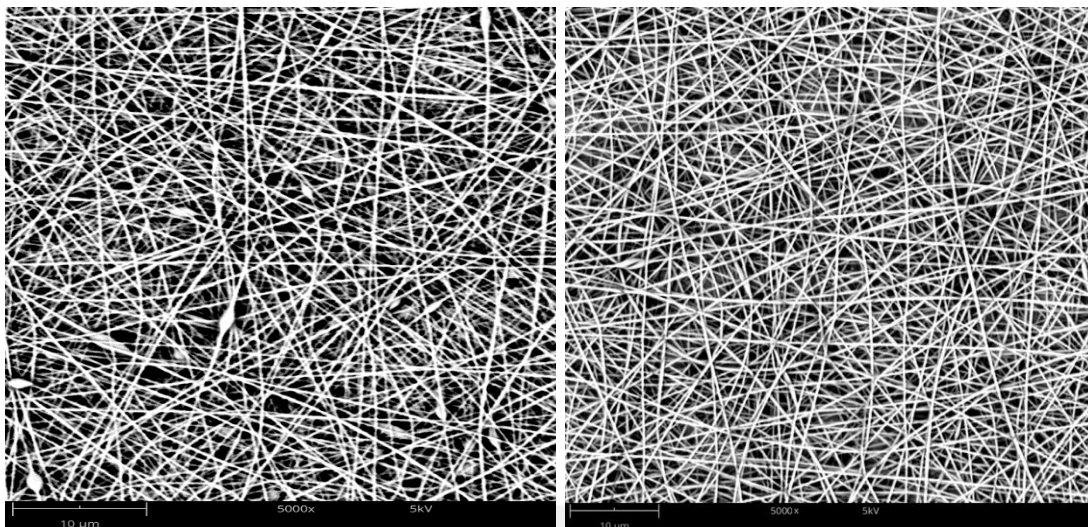


Figure 3.10: SEM images of nanofibers of 20PAN (left) and 20C1 (right).

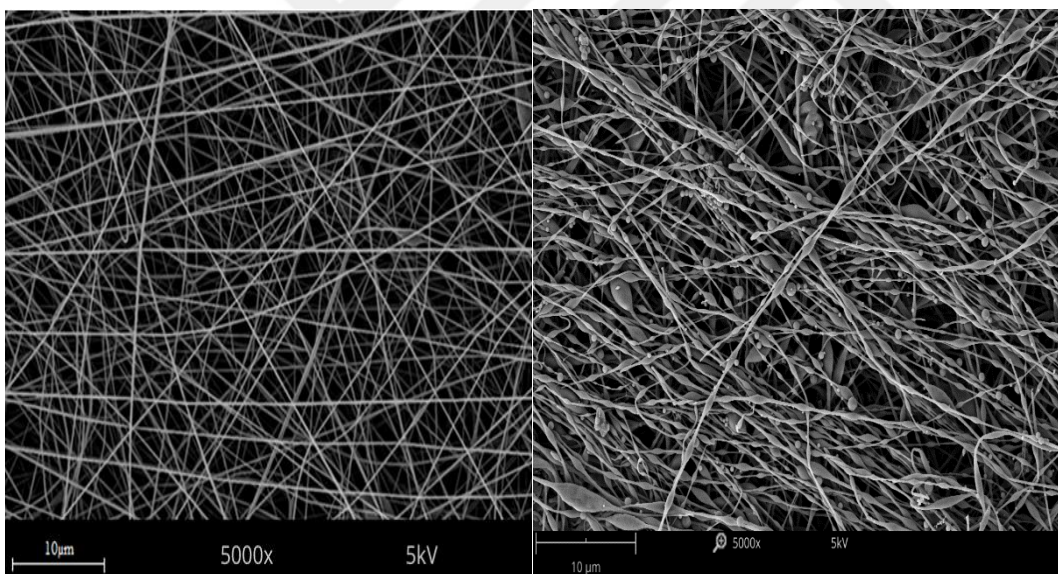


Figure 3.11: SEM image of nanofibers of 20C3 (left) and 20C5 (right).

When the polymer concentration was decreased, the formation of nanofibers was effected. More uniform nanofibers were composed with the enhancement of the PAN concentration because of its viscosity [117].

Except for low polymer concentration, the ambient parameters are also investigated to effect on electrospinnability of PAN/lignin solutions. Temperature and humidity

influence the morphology of obtained nanofibers. The electrospinning system commonly consists of the closed system which has a fan to supply a homogeneous relative humidity (RH) and temperature [119]. For the duration of electrospinning process, the fan is shut down to avoid that airflow disturbing the formation of the nanofibers. Furthermore, the average diameter nanofibers fabricated by electrospinning alter tremendously through difference of humidity and temperature. When temperature increases, solvent evaporation raises in the course of electrospinning process [120, 121]. For this reason, the viscosity of PAN/lignin solution changes. When the humidity goes up, the diameter of nanofibers increases.

As can be seen from the SEM results, humidity and temperature are highly influenced the electrospinning process and smooth nanofibers were obtained without bead formation even they have same percentages of PAN and lignin with same polymer concentration.

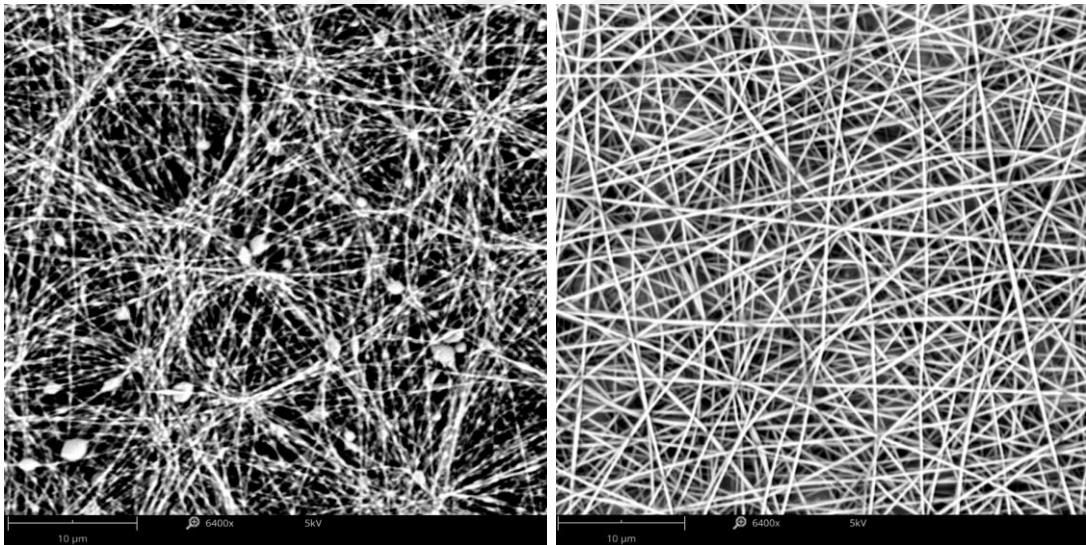


Figure 3.12: PAN/Lignin nanofibers of 20C1 without dehumidifier (left) and with dehumidifier (right) system during electrospinning.

Figure 3.12 showed that the PAN/lignin nanofibers were affected by temperature and humidity when they were exceeded 40 °C and 70% in the course of electrospinning. These images supplied a correlation of forming beads and spherical shapes with increasing temperature and humidity.

3.2.2 Effect of graphene on electrospinning process

GRPs were accustomed develop conductive (PAN/Lignin/GRP) nanofibers of various compositions. The concentrations of PAN and lignin are given as proportional weight fraction in the several nanofibers and the % of GRP is applied based on total polymers. PAN/Lignin/GRP nanofiber precursor dispersions are argued in more detail in the succeeding sections.

In this work, we concentrate on dispersions with weight ratios of the PAN/lignin of 1:1, 1:3 and 1:5 (1 and 5% GRP loading depends on total polymers). The morphology of the PAN/Lignin/GRP nanofibers for 1:5 PAN/lignin ratios was considerably influenced by the addition of GRPs (Figure 3.14). Without graphene, electrospinning was difficult when the lignin concentration was increased to 5 over PAN.

We successfully obtained better nanofiber formation with high lignin content by adding graphene in comparison to literature (Figure 3.13 and Figure 3.14). This result can be interpreted to mean, that of difficulties of electrospinning process for PAN/lignin ratio of 1:5 can be overcome by increasing the conductivity of blends. Furthermore, nanofibers with a diameter of 110 ± 20 and 105 ± 12 nm were achieved at the identical GRP concentrations verified, 1 and 5% GRP, respectively.

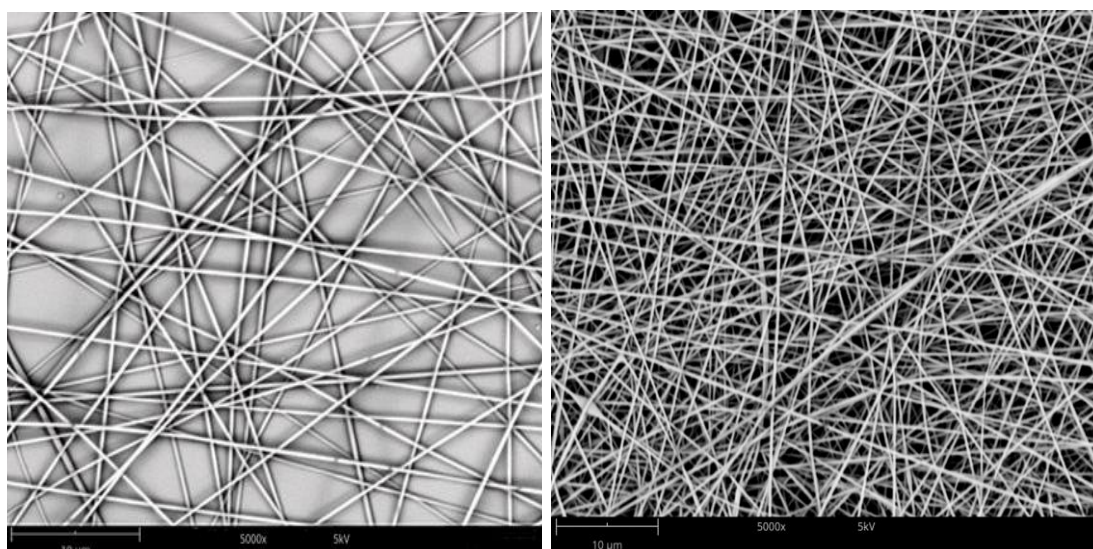


Figure 3.13: SEM image of nanofibers 20C1-1G (left) and 20C3-1G (right).

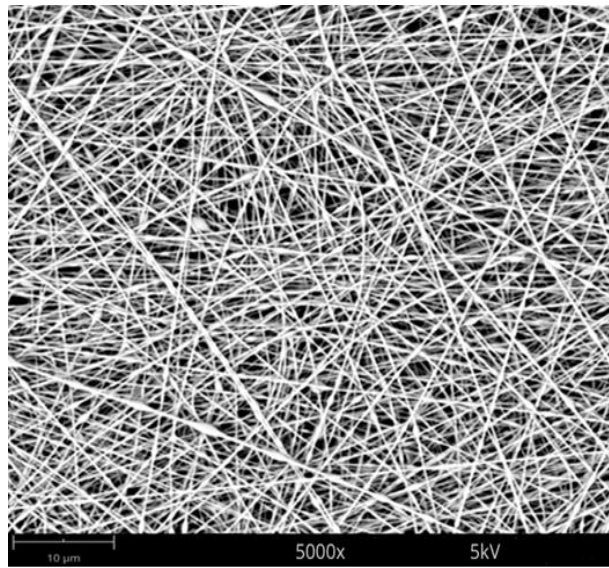


Figure 3.14: SEM image of nanofibers 20C5-1G.

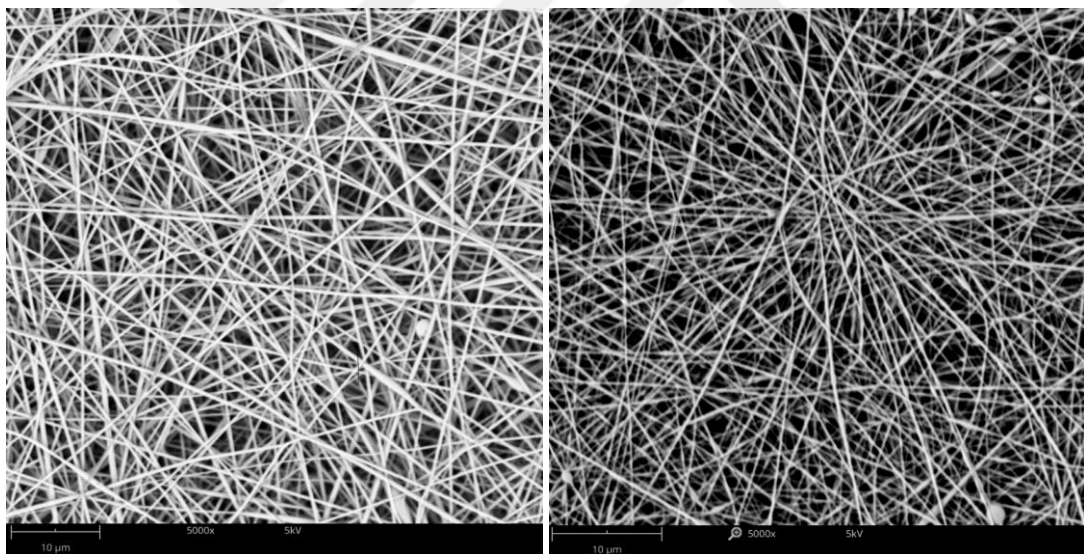


Figure 3.15: SEM image of nanofibers 20C1-5G (left) and 20C3-5G (right).

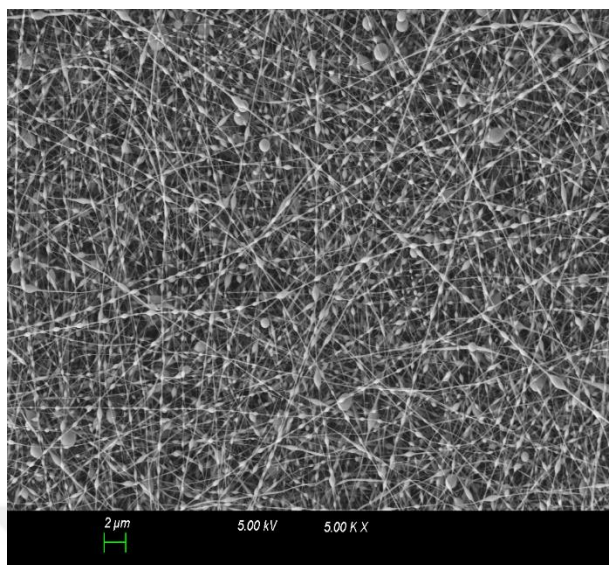


Figure 3.16: SEM image of nanofibers 20C5-5G.

Particularly, a decrease in nanofiber diameter is detected with the addition of GRP but a few beads were detected at the highest lignin content with 5% GRP. The shapes of the beads altered from nanofiber to spherical as the concentration was raised from 1 to 5% (Figure 3.15 and Figure 3.16). The dispersion of graphene may be required to provide a homogeneous in PAN/Lignin blend when the amount of graphene was enhanced to 5%.

Additionally, the SEM observation distinctly shows that a good affinity between PAN, lignin, and graphene resulted in the homogenized fibers without beads [122]. Furthermore, the increase in graphene concentration in PAN/Lignin also decreased the diameter of the nanofiber.

When graphene was added to PAN/Lignin solutions, the viscosity was decreased depends on the concentration of graphene. Figure 3.7 show that higher concentration of graphene is a reason to reduce the viscosity of PAN/Lignin/Graphene solutions.

In this work, we examine the role of the interactions between the dispersed GRPs and the PAN/lignin solution through measuring the apparent shear stress of the dispersions as a function of the shear rate (Figure 3.17).

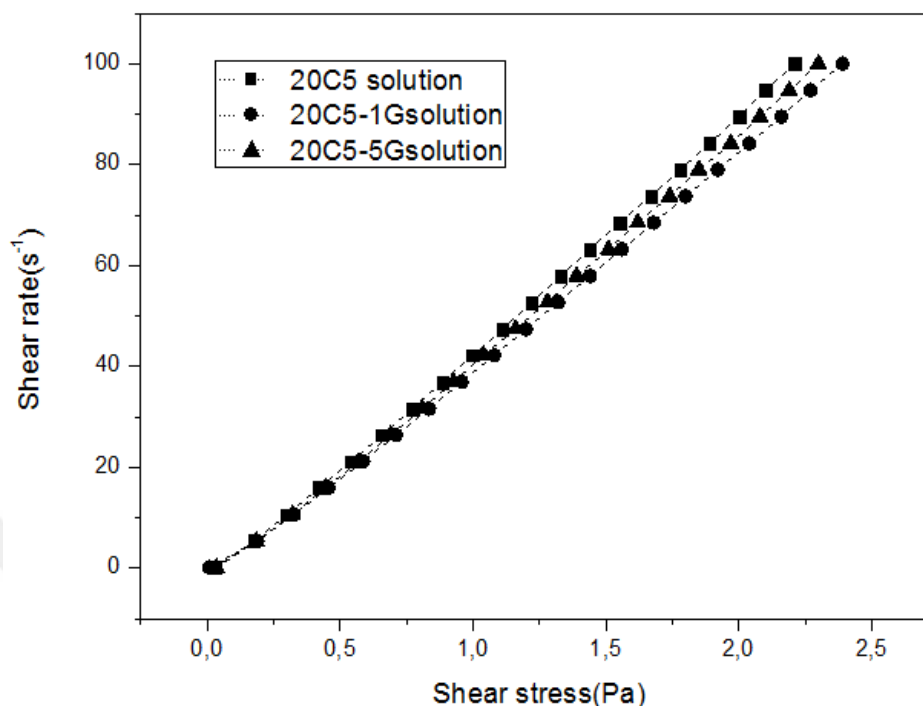


Figure 3.17: Shear rate and shear stress relationship for the 20C5 (1% and 5% wt.) solutions.

The results show a Newtonian behavior that is well represented by a power law relationship between shear stress (τ) and shear rates (du/dy), $\tau = \mu du/dy$.

The viscosity of the PAN/lignin solutions increased with the addition of GRP, which was especially carried out in the solutions of adding 1% graphene. There are some studies which have presented that the viscosity of dispersions of polymers reinforced with nanomaterials enhances the substance of the dispersed phase [123, 124].

3.2.3 Experimental design

For statistical analysis, two-way ANOVA statistical analysis was used to investigate the effects of the solution concentration on nanofiber diameter and conductivity (presented in Table 3.6). The analysis of variance completed for the factorial design shown those characterization variables, which have the most substantial effect on the response. According to Montgomery, the F-ratio is initially extracted from the statistical tables. For $\alpha=0.05$ (confidence level 95%), the F-ratio was 18.5 [125].

If the extracted F-ratio is lower than the calculated one, the statistical meaning of the result is finished. The ANOVA showed that the calculated F-ratio didn't exceed the presented values in Table 3.6. Nevertheless, all of the variables affect the response concluded their two-way interactions, the variability of whole factors was remarkable in some degree the variance of error and all of them have considerable consequences on the nanofiber diameters and conductivity [126]. In this study, the experimental results are compared to the results of the statistical analysis to confirm the consistency of the experimental data and analysis. Together these results provide evidence that the controlled polymer concentration affects the nanofiber diameter and their electrical conductivity.

Table 3.6: Experimental design results.

Std Order	Run Order	Pt Type	Blocks	L/P ratio	Grp %	Polymer concent. (wt.%)	Diameter (nm)	Conductivity ($\mu\text{S/m}$)
5	1	1	1	5	1	10	150	1,74
7	2	1	1	5	5	10	200	1,52
6	3	1	1	5	1	20	220	13,6
3	4	1	1	1	5	10	250	1,15
8	5	1	1	5	5	20	175	8,06
4	6	1	1	1	5	20	150	6,79
2	7	1	1	1	1	20	125	9,28
1	8	1	1	1	1	10	230	1,20

P value = $0,001845 < 0,05$

3.2.4 Electrical conductivity analysis

The electrical properties of nanofibers are essential for future applications as an electrode in biosensor or batteries. For this purpose, electrochemical impedance spectroscopy (EIS) has been utilized to characterize the electrolyte with their interface with electrodes. The evaluated impedance can be employed to study and qualitatively find out the electronic/ionic conductivity in the electrode or the surface films [127].

From, Table 3.7 displays the comparison of PAN/Lignin nanofibers of different concentration of graphene at 1% and 5%, we interestingly monitored that the conductivity of nanofibers indicates non-linear behavior.

Table 3.7: Conductivity results of nanofibers.

Sample Code	Conductivity ($\mu\text{S/m}$)
20C1	4,95
20C1-1G	9,28
20C1-5G	6,79
20C3	9,27
20C3-1G	19,2
20C3-5G	13,3
20C5	12,2
20C5-1G	13,6
20C5-5G	8,06

Pooled St. Dev. = 1,845

By adding 1% of graphene, the conductivity of PAN/Lignin nanofibers increases higher than that of the PAN/Lignin nanofibers reinforced with 5% of graphene. Table 3.7 shows that the maximum conductivity of PAN/Lignin/GRP nanofibers is obtained to be $\sim 19,2 \mu\text{S m}^{-1}$ for 20C3-1G nanofiber. It seems that increased lignin content is enhanced the conductivity of nanofibers than pure PAN nanofibers. However, this result also displays that the electrical conductivity is affected by the formation of beads during the electrospinning process. Thus, the electric current could not pass forward on the PAN/Lignin nanofibers with higher lignin content because of beads [122].

3.2.5 FTIR of nanofibers

To advance understanding the chemical behavior of the PAN/Lignin blends, the intermolecular interactions of PAN with lignin was examined with FTIR. FTIR spectra of the PAN and PAN/Lignin nanofibers, Figure 3.18, display the PAN specific peaks such as the stretching vibration of nitrile groups (-CN-) at 2243 cm^{-1} and the stretching vibration and bending vibration of methylene (-CH₂-) peaks at 2930 and 1453 cm^{-1} ,

respectively [128, 129]. The peaks at 2243 cm^{-1} and 2930 cm^{-1} perform in the PAN/Lignin nanofibers nearly at the same wavenumbers. However, the intensity of these peaks is diminished considerably with an increase in lignin content. Also, Liu et al. have shown that the peak at 1614 cm^{-1} corresponds to the formation of the C=N bond, results from lignin interaction with PAN [130].

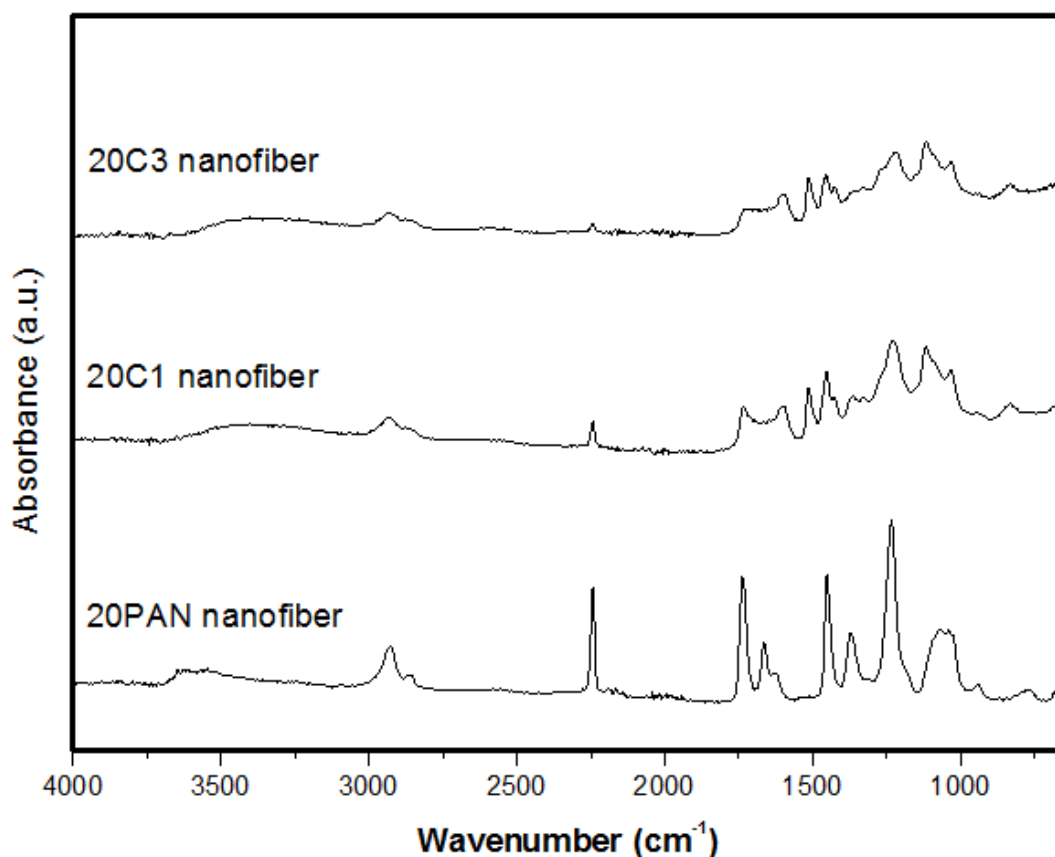


Figure 3.18: FTIR multilayer spectra of the PAN nanofiber and PAN/lignin nanofibers with different lignin content.

The peak at 1670 cm^{-1} is because of the oxidation of the as-received PAN in the air, which results in the formation of carboxyl (C=O) groups. The peaks at 1251 and 1360 cm^{-1} are described to the aliphatic CH group vibrations of different modes in CH and CH₂, respectively [131]. Increasing lignin concentration substantially affect these peaks for PAN/Lignin nanofibers and the intensity of peaks decreased by means of increasing the lignin content due to the interaction the PAN and lignin.

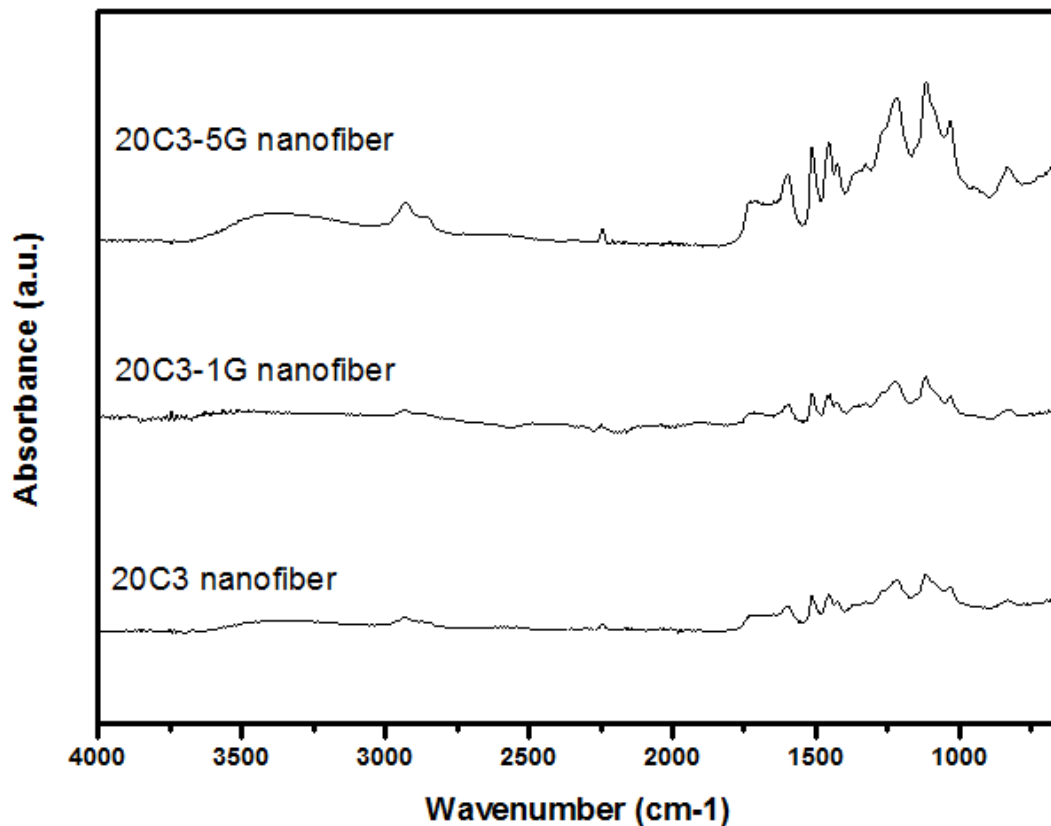


Figure 3.19: FTIR spectra of the PAN/lignin and PAN/Lignin/GRP nanofibers with different lignin content.

At 1 and 3 lignin ratio, the PAN/lignin nanofiber displayed a new band, 1110 cm^{-1} , as compared to 1118 cm^{-1} in the PAN and lignin nanofibers (see in Figure 3.18). Kadla et al. indicated that this new peak in C–O–C band region can be detected variations in the hydroxyl-stretching band region of the PEO/lignin blends [60]. On the other hand, this may be due to the mechanism of interaction between the PAN and lignin.

Figure 3.19 shows the functional group of the fabricated graphene reinforced PAN/Lignin nanofibers. In for the FTIR spectrum of graphene, one of the characteristic peaks observed at $3450\text{--}3500\text{ cm}^{-1}$ corresponds to the strong vibrations of OH group [60]. Also, the vibration of water molecules or non-oxidized graphitic parts was detected at $\sim 1600\text{ cm}^{-1}$ [132]. More, the peak resembled CO bond stretching was obtained at 1040 cm^{-1} in FTIR spectrum of graphene powder [133, 134].

In the FTIR spectrum of PAN/Lignin/GRP nanofibers with different graphene content, the characteristic band at $3500\text{--}3700\text{ cm}^{-1}$ could be described to the reaction between O-H band corresponding to graphene band. Furthermore, the observed band at 1600 cm^{-1} in PAN/Lignin/GRP nanofibers with 5% is higher intensity than the intensity of PAN/Lignin/GRP nanofibers with 1% for indicating the existence of graphene in the nanofibers.

3.2.6 XRD of nanofibers

The crystalline properties of electrospun nanofibers are significant when the materials are developed for industrial requests. For this reason, XRD patterns were utilized to examine the phase structure of the nanofibers. Figure 3.20, Figure 3.21 and Table 3.8 display the corresponding X-ray diffraction patterns and the relative degree of crystallinity of the PAN, PAN/Lignin, and PAN/Lignin/GRP nanofibers.

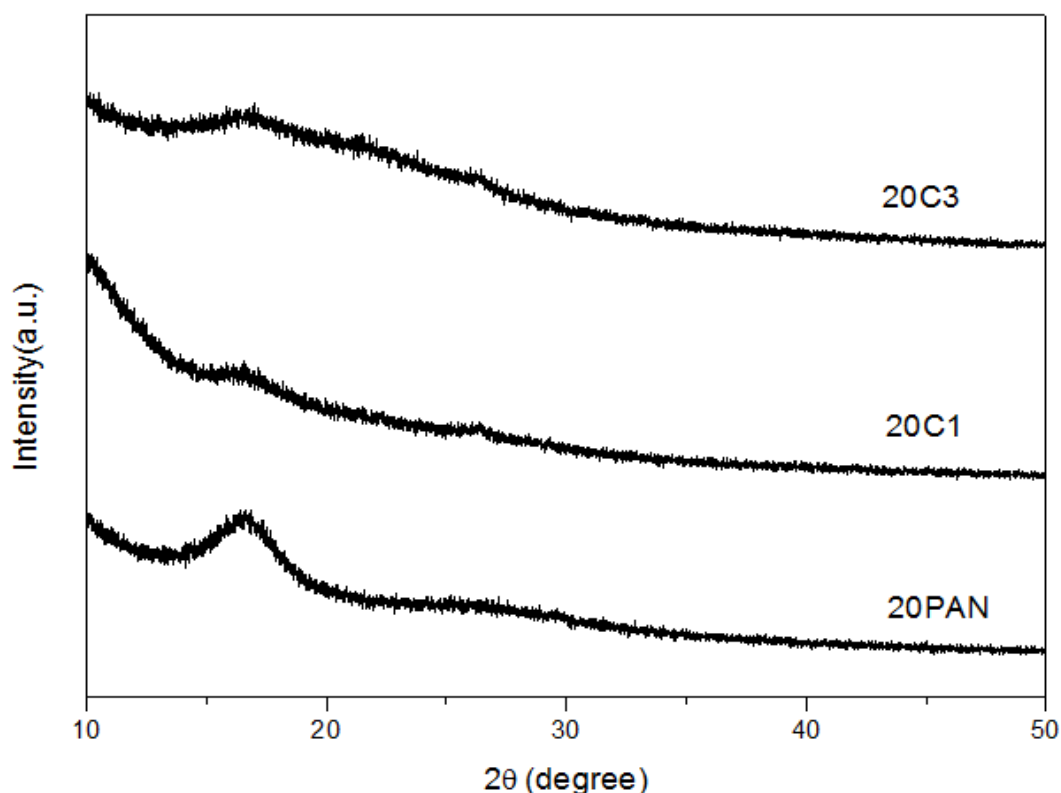


Figure 3.20: XRD of PAN/Lignin nanofibers at different concentrations.

In PAN nanofiber pattern, diffraction peak about the 2θ of 17° can be assigned to (100) the PAN polymer phase because of the amorphous nature [135, 136]. Nevertheless,

the intensities of peaks at 17° were diminished with the increase of lignin content in PAN-based nanofibers. From Figure 3.35 it can be detected that the XRD pattern of PAN and PAN/Lignin nanofibers displays a round peak at a diffraction angle around the 2θ of $26^\circ\sim 27^\circ$ owing to (114) crystallographic planes of graphene [57].

Figure 3.21 indicates the XRD pattern of the graphene and the diffraction peaks at 26.5 and 42.5 represented by (002) and (001), show the crystal planes of graphene [138, 139]. The broad graphene peak at 26.5 in the 20C3-5G XRD spectra can be pointed to disperse graphene in comparison with the lower concentration of graphene filled PAN/Lignin nanofibers [122, 137]. Although the intensity of peak being weak can be ascribed to a low concentration of graphene in the PAN/Lignin nanofibers, from the detected XRD peaks approve the nano-graphene sheets are inside the PAN/Lignin nanofiber (Figure 3.21).

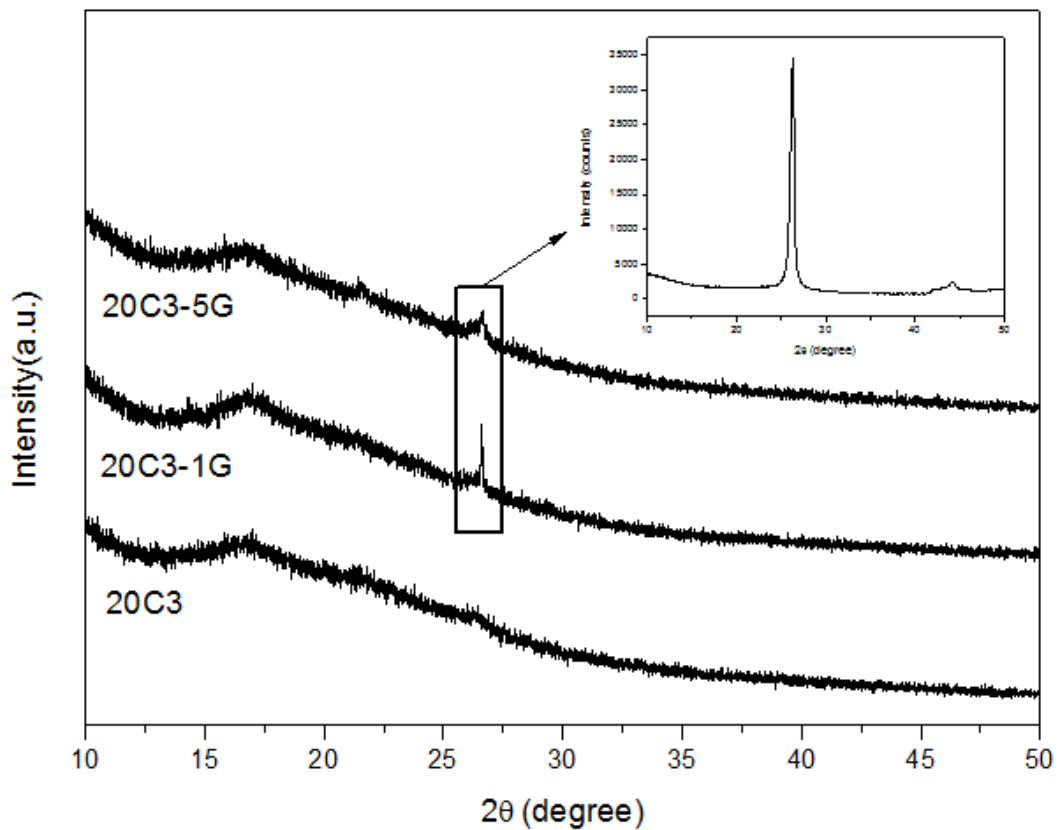


Figure 3.21: XRD pattern of PAN/Lignin nanofibers with and without graphene at several concentrations.

Table 3.8: Degree of nanofiber crystallinity by XRD patterns.

Sample Codes	Crystallinity %
20PAN	39.3
20C1	36.7
20C3	32.2
20C3-1G	28.5
20C3-5G	27.6

As it can be understood from the Table 3.8, the percentage of crystallinity values was decreased with the adding of lignin content. Lignin, is biopolymer consisted of amorphous phenyl propylene, may be used to explain the increasing lignin concentration of PAN nanofiber is owing to lesser the percentage of crystallinity on the PAN nanofiber [140].

Considering the crystallinity of nanofibers reinforced with graphene, Table 3.8 indicates that crystallinity reduced from 32.2% to 28.5, by adding 1% graphene to PAN/Lignin (1:3). Furthermore, the falling of crystallinity proceeds with rising graphene amount up to 5%. Owing to the high aspect ratio of graphene sheets, graphene can be readily passed through polymer chains. In this way, the crystallization process may be interrupted and reason to decrease crystallinity of PAN/Lignin/GRP nanofibers [141].

3.2.7 TGA of nanofibers

A TGA analysis was employed to determine the temperature of carbonization of PAN/lignin and PAN/lignin/graphene nanofibers in the next stage of thesis. For this reason, thermal stability of the PAN/lignin and PAN/lignin/graphene nanofibers was determined by means of thermogravimetric analysis (TGA).

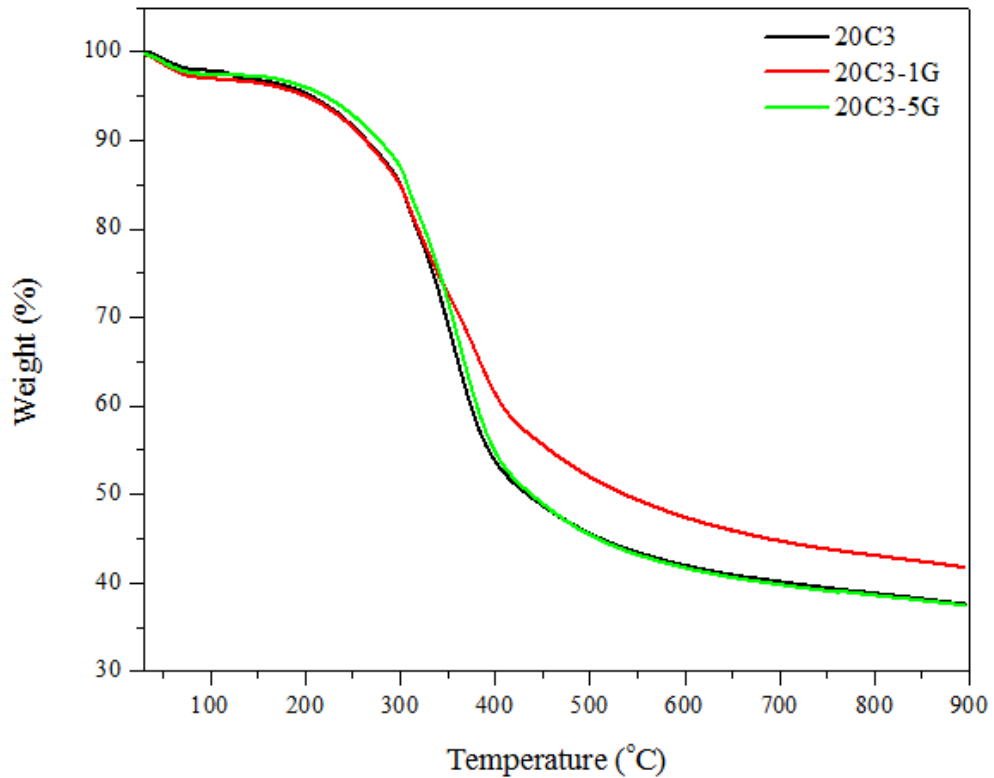


Figure 3.22: TGA analyses of three types of nanofibers.

As it can be seen in Figure 3.22, the first degradation temperature of all nanofibers takes place at similar temperatures. The decomposition temperature of PAN/lignin nanofibers increases with greater concentration of graphene. However, the thermal stability of 20C3-1G nanofibers are better than the 20C3 and 20C3-5G nanofibers (Figure 3.22).

These results proved that the thermal stability of the PAN/lignin nanofibers by adding graphene with 1% wt. has improved, compared to the PAN/lignin and PAN/lignin/graphene. This is caused by the existence of graphene with large surface area that behave as barrier and a thermal insulation [141]. For the PAN/lignin, the major weight loss of 60% (Figure 3.22) happens in a similar temperature range of 420 °C with that of PAN/lignin/graphene nanofibers. The lowest weight loss was recorded in 20C3-1G nanofibers after heated to 900 °C, which makes these nanofibers a promising precursor for production carbon nanofibers.

3.2.8 AFM of nanofibers

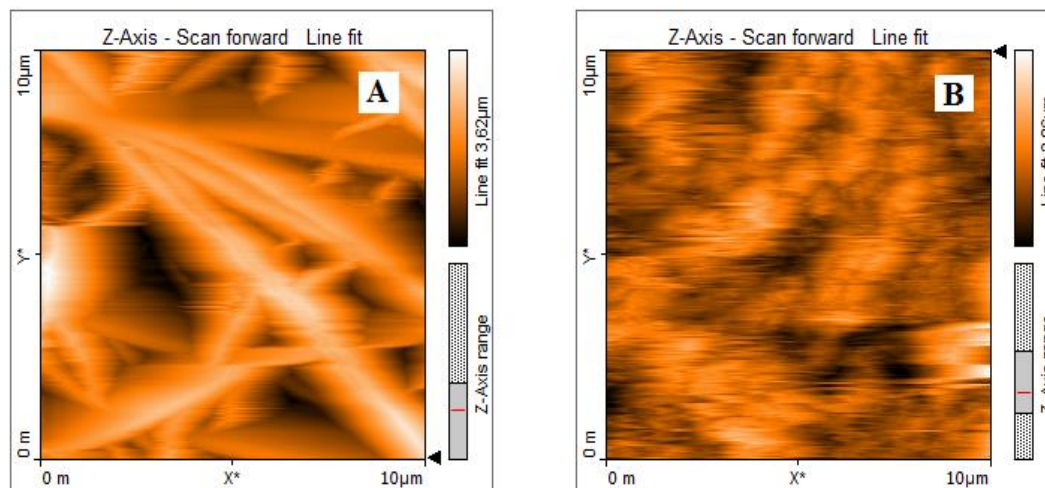


Figure 3.23: AFM analyses of a) 20C1-1G and b) 20C1 of nanofibers.

Atomic force microscope (AFM) images of PAN/lignin/graphene and PAN/lignin nanofibers A, and B are shown in Figures 3.23. Owing to complications associated with imaging individual nanofibers, AFM analyses were performed on reference 20C1-1G and 20C1 samples for detecting phase separation of polymers and graphene.

As it can be seen in Figure 3.23, the AFM images indicate phase separation in the PAN/lignin/graphene nanofibers (Figure 3.22a), but no phase separation is detected in the PAN/lignin nanofibers (Figure 3.22b).

3.3 Thermal Stabilization and Carbonization

Lignin-based carbon nanofiber fabrication has numerous advantages in comparison with other carbon nanofibers. These advantages consist of its high carbon content and low cost except for being a renewable resource. Considering the thermal stabilization and carbonization process, lignin has a shorter stabilization time and lesser stabilization temperature because of its high oxygen content. However, it is difficult to obtain and purify uniform lignin in the course of isolation so carbonization process can be hard with this complex material [13].

In this work, we investigated the differences of carbonized mats when graphene was used to obtain a uniform and smooth PAN/Lignin nanofibers. This could pave the

way for comparing PAN/Lignin and PAN-Lignin/Graphene nanofibers depend on carbonized mats. To find out best heating conditions of carbonization, Table 2.2 is a summary of conditions used for PAN/Lignin and PAN/Lignin/GRP nanofibers before. Detecting proper heating conditions is essential as nanofibers can be curled or melt when oxidation is too fast or high heating rate is conducted to nanofibers [53].

Figure 3.24 showed that the summary of all process from powder lignin to lignin-based carbon nanofiber. We can see clearly the physical differences of nanofibers such as color and shrinkage in the nanofiber after carbonization process.



Figure 3.24: Sample preparation for thermal processing, (a) lignin powder, (b) electrospun PAN/Lignin nanofibers, (c) horizontal tube furnace (d) placement of carbon nanofibers in the ceramic boat after carbonization, (e) carbonized nanofibers.

3.3.1 SEM of carbon nanofibers

Morphology of PAN/Lignin nanofibers with several ratios which had been reinforced with graphene was investigated for thermal stabilization and carbonization by using SEM. In order to avoid the melting of lignin in the course of the carbonization T_g of lignin should exceed its degradation temperature. The thermal stabilization was utilized for this purpose. So, after thermal stabilization and carbonization, the final PAN/Lignin and PAN/Lignin/GRP carbon nanofibers were fabricated as presented in following figures. However, in contrast to PAN/Lignin carbon nanofibers, PAN/Lignin/GRP carbon nanofibers had a superior conservation of morphology after

thermal stabilization and besides after carbonization, they kept their flexible fibrous configuration.

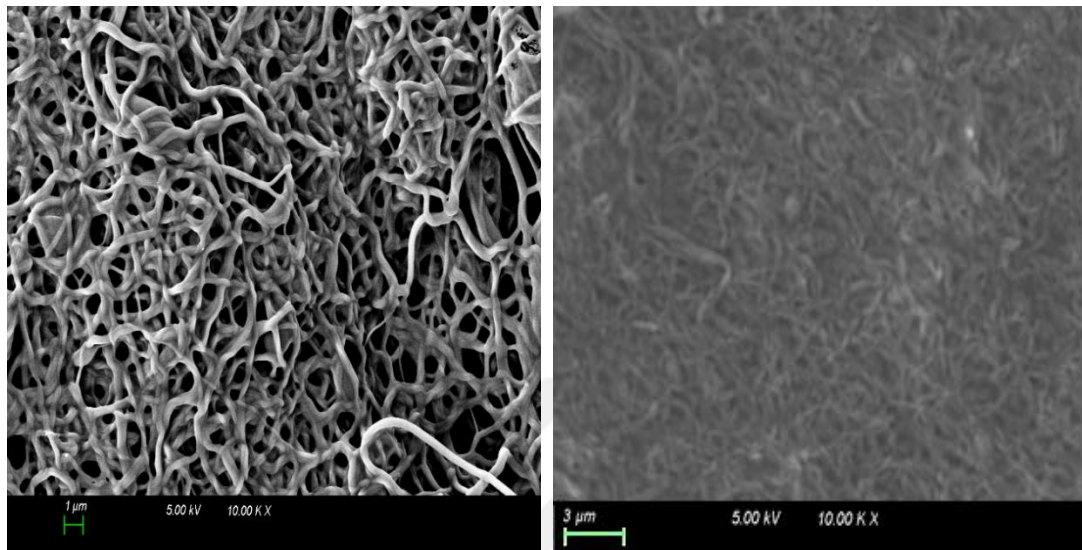


Figure 3.25: 900 °C – 2 °C/min – 1 h, 20C1-1G (left) and 20C3-1G (right).

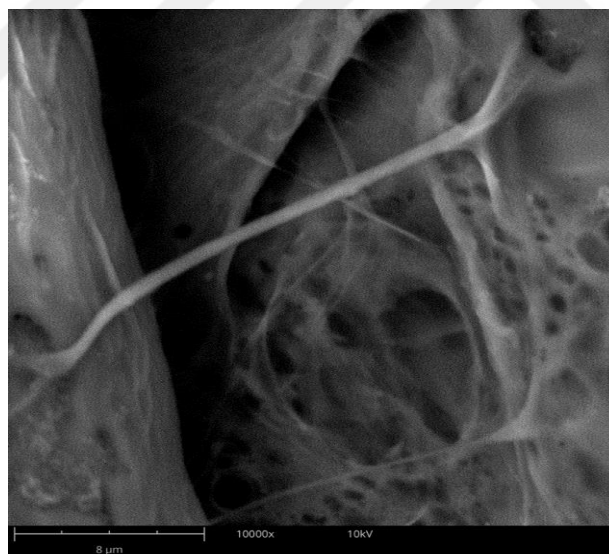


Figure 3.26: 900 °C – 2 °C/min – 1 h, 20C5-1G.

Figure 3.24 and Figure 3.26 display that increased lignin content in PAN/Lignin/GRP nanofibers is a reason to lose fibrous configuration on the surface. With highest lignin content, it is clearly difficult to maintain the carbon nanofiber morphology in carbonized mat (Figure 3.26).

Higher temperatures or longer residence times may be used to further remove the residual non-carbon amount. The stabilization yield for the lignin-based fibers was less than for PAN-based fibers which were ascribed to the ease of expelling volatile compounds in lignin at stabilization temperatures. Owing to the already-oxidized state of lignin, degradation, for instance, demethoxylation was originated at ~ 200 °C by running off CO and CO₂ in the course of the stabilization of the precursor fibers [24, 142].

SEM images of carbonized nanofibers without and with graphene are shown in Figure 3.27.

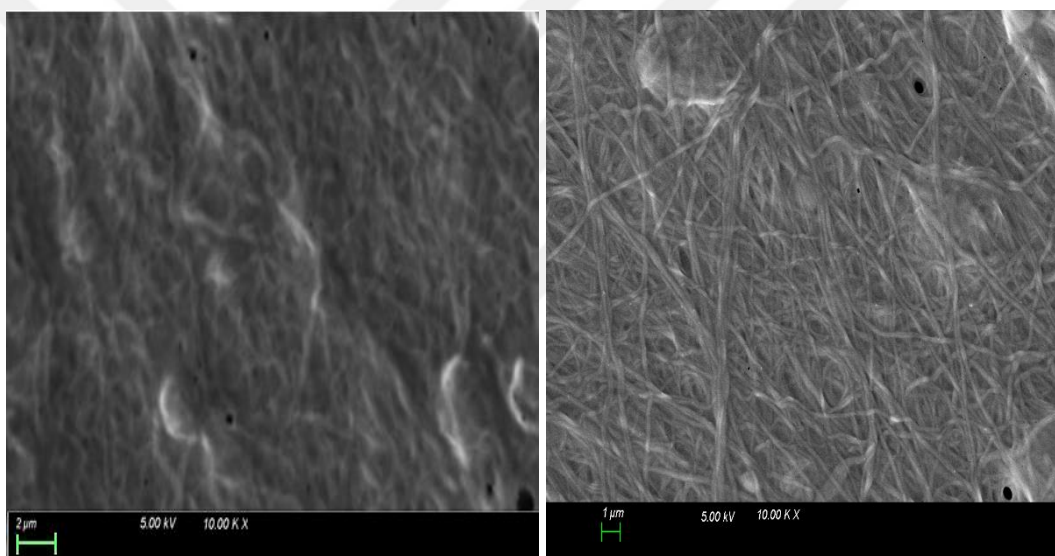


Figure 3.27: 800 °C – 2 °C/min – 2 h, 20C3 (left) and 20C3-5G (right).

From Figure 3.27, we can understand that PAN/Lignin nanofibers carbonized at 800 °C had a rough surface compared to PAN/Lignin/GRP nanofibers carbonized at 800 °C. However, they do not have great morphological alterations, subsequently evaporation of other atoms with a low amount of carbon during carbonization.

The imperfections of the resulting lignin-based carbon nanofibers can meaningfully affect the mechanical properties but improve other performance like surface area and porosity.

EDS

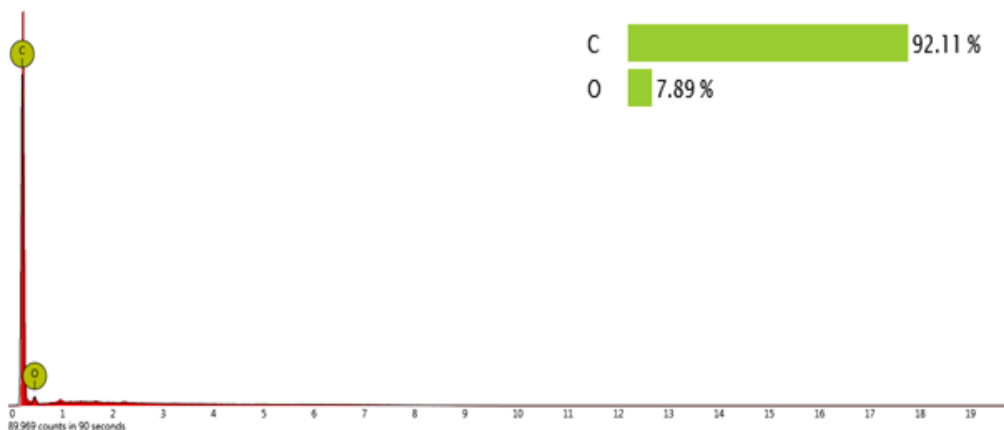


Figure 3.28: EDS of the PAN/Lignin nanofibers.

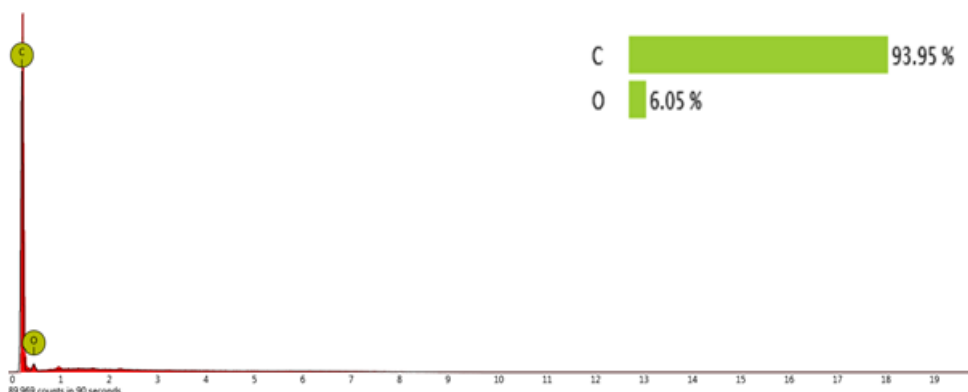


Figure 3.29: EDS of the PAN/Lignin/Graphene carbon nanofibers.

Generally, the major elements found in the lignin-based nanofibers were carbon, oxygen, and sulfur. In fabrication carbon nanofibers, the carbon content is a significant issue in a carbon fiber precursor. Owing to this reason, we used the soda lignin which is sulfur-free as a precursor for carbon nanofibers. Although the results of the elemental analysis showed that the commercial lignin has a very low amount of sulfur, the EDS data indicates the carbon nanofibers have only carbon and oxygen (Figure 3.28 and Figure 3.29). Thus, the O and C relate to the lignin molecule itself, whereas S residues do not remain from lignin. It can be considered that this low sulfur content

was reduced by means of thermal treatment, which possibly might be owing to the extrication of SO₂ gas throughout the carbonization [140].

The EDS results indicated a higher percentage of carbon in the PAN/Lignin/GRP carbon nanofibers. The carbon amount of all carbonized nanofibers was steadily above 90%, representing that the approximately carbonization temperature of 900 °C allows an adequate transformation of lignin-based to carbon materials (Figure 3.28).

The diameters of the carbon nanofibers convert smaller compared to those of the representing electrospun nanofibers. However, the last diameter of nanofibers did not display a dependence on the carbonization temperature or the first diameter [51].

For PAN/Lignin/GRP nanofibers, higher lignin content resulted in a better reduction in nanofiber diameter even smaller carbon nanofibers below 100 nm (Figure 3.30). Investigation of the nanofibers by RAMAN exhibited an accomplished appearance of graphene after carbonization.

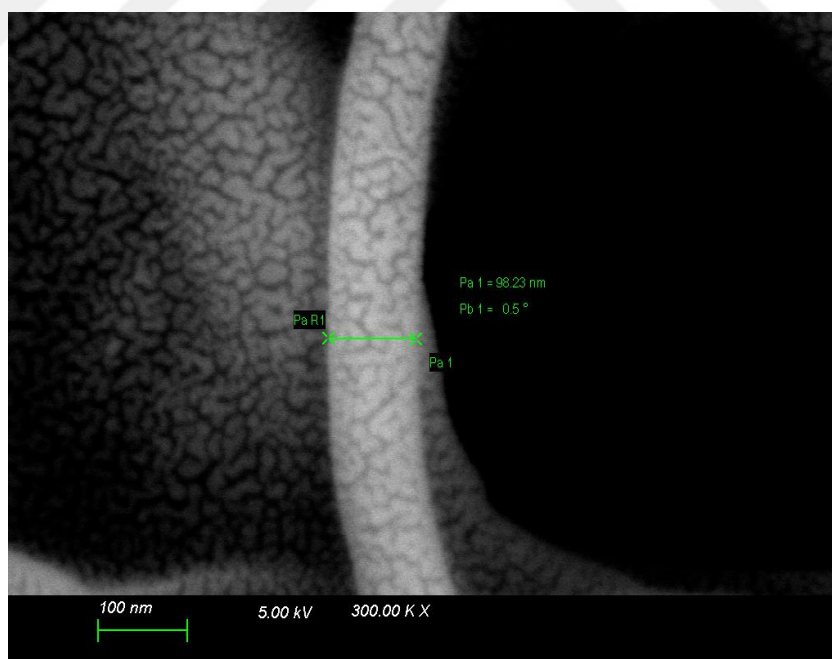


Figure 3.30: 900 °C – 1 °C/min – 1h -20C1-1G.

3.3.2 RAMAN of carbon nanofibers

Raman spectroscopy is a vital analysis for the characterization of carbonized materials. The obtained Raman spectrum of carbonized PAN/Lignin/GRP nanofibers (20C3-1G) at 800 °C and 900 °C in Figure 3.32 evidently displays a prominent two peaks, G band and D band. G band, at 1575 cm^{-1} , which shows the sp^2 hybridization of carbon and stretching mode in the graphite plane [143].

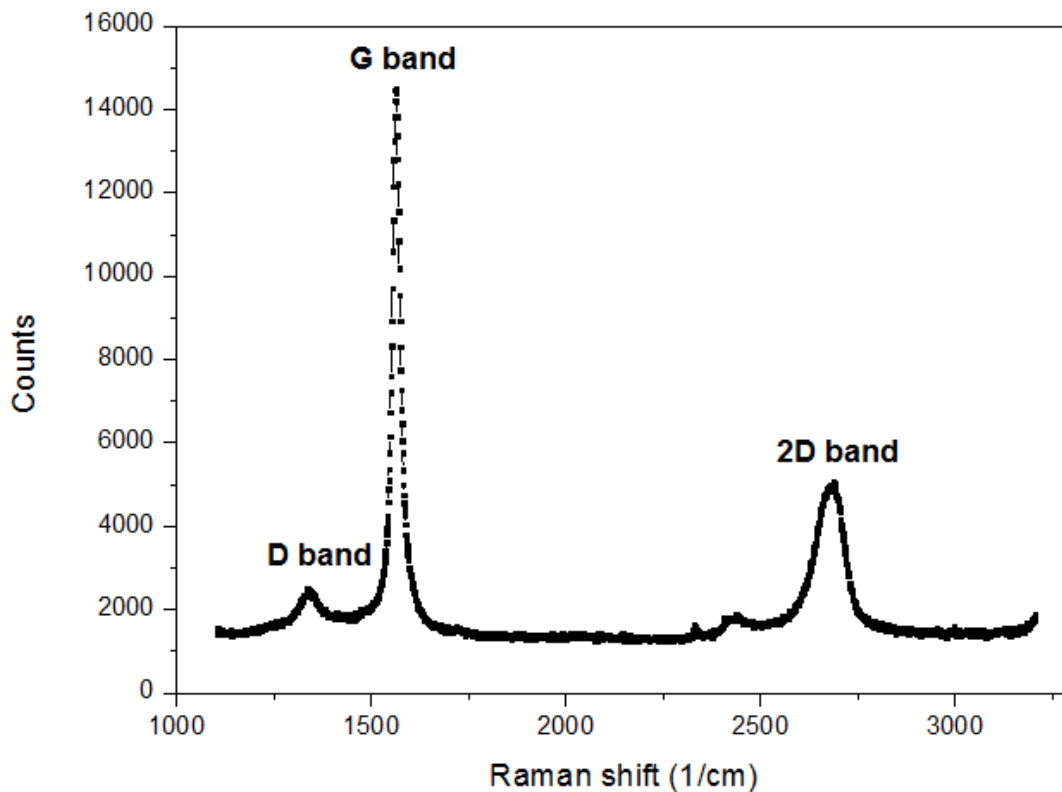


Figure 3.31: Raman spectrum of graphene.

Another band which has been described to appear in the range of 1330 cm^{-1} is called as D band and is associated with the sp^3 hybridization of carbon in polycrystalline graphite. It indicates the existence of turbostratic carbon which is a disorderly structure or characterizes deficiencies in the graphitized structure. According to Raman spectrum, the results indicated by increasing the temperature, D and G bands transform narrower and intensity of the D and G band enhances.

The 2D band detected at 2680 cm^{-1} demonstrates an increment in the number layers of graphene sheets [134]. Thus, Figure 3.31 shows that the graphene used in this study is multilayer based on the 2D band.

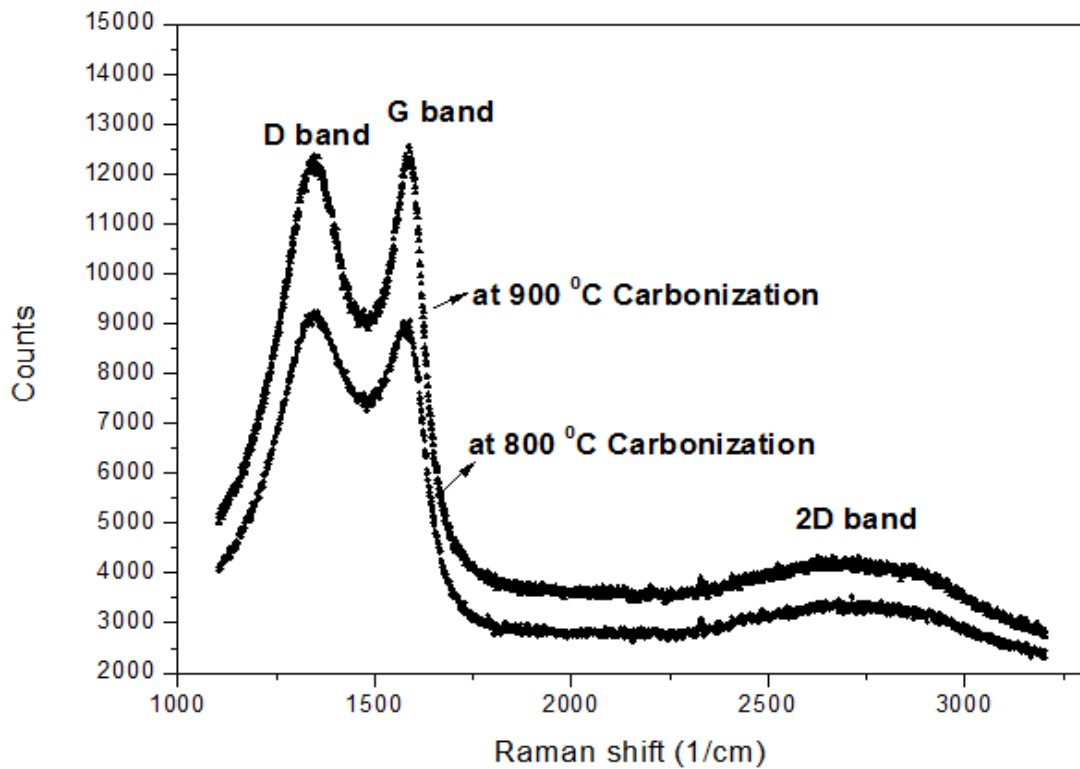


Figure 3.32: Raman spectra of the carbonized nanofibers (20C3-1G) at different temperatures.

The ratio of D band height to G band height which is as well presented as $R=I(D) / I(G)$ indicates the alignment of the graphitic part and in addition to a degree of graphitization. Lower numbers of R point the more sp^2 carbons [145].

The R values are lower for PAN/Lignin/GRP nanofibers carbonized at higher temperatures (as shown below).

$$R=I(D) / I(G)$$

$$R@900 < R@800$$

The ratio of the D to G band intensities (I_D/I_G) is commonly corresponding the crystallite size (La) [146], where $La = (2.4 \times 10^{-10}) \times \lambda^4 I_{laser} (I_D/I_G)^{-1}$. Consequently, the lower ratio of I_D/I_G is caused by higher crystallite size depending on the lower amount of defects. Figure 3.32 indicates that the crystallite size is greater in carbonization process at 900 °C in comparison to at 800 °C.

3.4 Characterization of CNF/SPE and CNF-G/SPE

In this work, the characterization of modified SPE via CNF and CNF-G was completed both by EIS and CV.

EIS measurements were to understand electrochemical properties at the electrode-electrolyte interface demonstrates the modification of carbon nanofiber and graphene reinforced carbon nanofiber on screen-printed electrode.

The complex impedance, Z, consists of the real and imaginary impedance (Z' and $-Z''$). Figure 3.33 displays the semicircle diameter in the Nyquist diagrams with the equivalent circuit units of charge transfer resistance (R_{ct}), Warburg impedance (W), solution resistance (R_s) and double layer capacitance (Cdl).

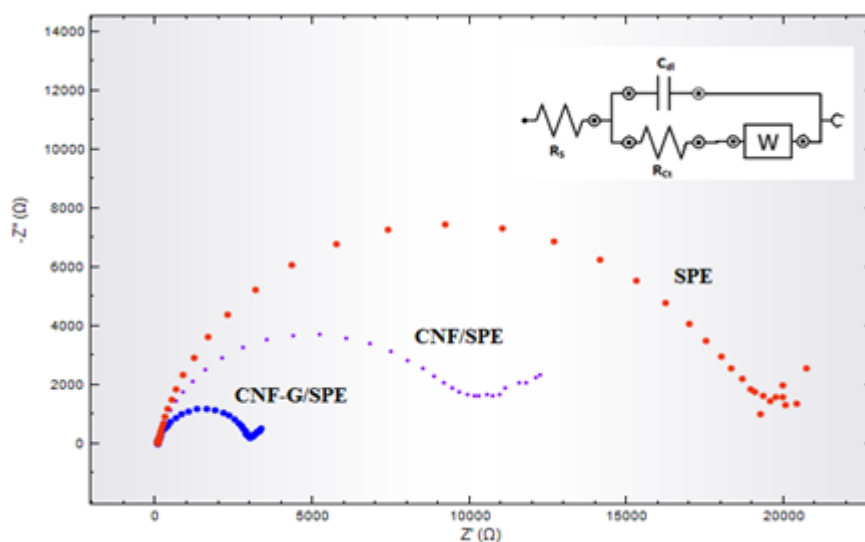


Figure 3.33: Nyquist plots of SPE, CNF/SPE, and CNF-G/SPE.

As shown in Figure 3.31, the Randles circuit model was used to fit of impedimetric measurements, the diameter of the Nyquist plot semicircle at SPE is higher compared to the obtained diameters of CNF-G/SPE and CNF/SPE. The differences in the Nyquist

plot indicate that electrical conductivity of carbon nanofibers is better than unmodified SPE. Furthermore, graphene improves the electrical conductivity of carbon nanofibers because of good electron transfer properties [146].

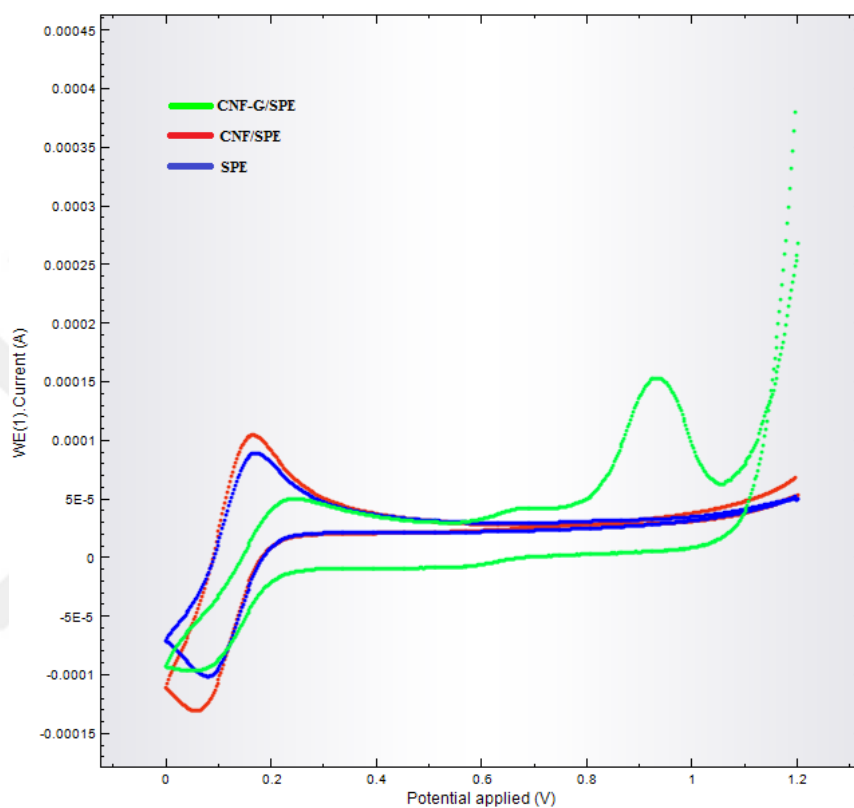


Figure 3.34: Cyclic voltammograms of three screen-printed electrodes.

As shown in Figure 3.34, comparing with SPE, the redox current increased at CNF and CNF-G modified SPE. The electroactive surface area (A) can be calculated to use the Randles-Sevcik equation:

$$I_p = (2,69 \times 10^5) n^{3/2} A C D^{1/2} \nu^{1/2}$$

I_p : peak current, A

n: electron transfer number

A: electrode area, cm^2

D: diffusion coefficient, cm^2/s

C: concentration, mol/cm^3

γ : scan rate volt/sec

According to Figure 3.34, the oxidation current at SPE was enhanced by carbon nanofiber and graphene [146, 147]. However, we will focus on the different scan rates to figure out the certain reason for improvement at oxidation current.

DPV measurements were to understand the electrochemical behavior of the modified electrodes in PBS against the certain concentrations of acetaminophen.

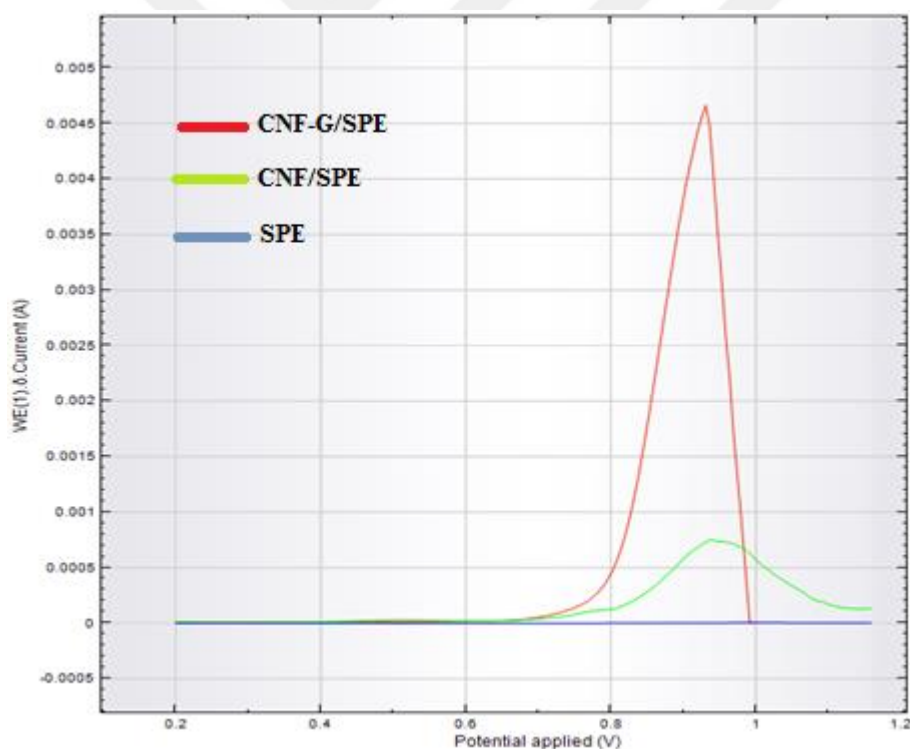


Figure 3.35: DPV voltammograms of the acetaminophen for three screen-printed electrodes.

The peak current for the oxidation of acetaminophen increased with detecting of acetaminophen as shown in Figure 3.35. With the same concentration of acetaminophen, the peak current was changed because of the detection limit of modified electrodes (CNF-G/SPE and CNF/SPE). However, the A-ferin forte tablet

consists of Acetaminophen, Triprolidine Hydrochloride Pseudoephedrine Hydrochloride. So, the obtained peak currents cannot compare with literatures which related to the detection of acetaminophen.





4. CONCLUSION

The aim of this Ph.D. thesis extracted lignin from two different Turkish resources compared with commercial lignin and produced low-cost carbon nanofiber based on lignin using as an electrode material. Graphene was used to enhance electrical conductivity and reduce the diameter of lignin-based carbon nanofibers.

In this work, the lignocellulosic biomass has been used as a resource for lignin extraction. The type of biomass should be affected the lignin amount obtained by extraction method. Chemical compositions of three different lignin examined present work are dissimilar from those submitted elsewhere because of the dependence of chemical composition of lignocellulosic biomass on locality and species. The extracted lignin from Turkish resources and commercial lignin were chemical, thermally and structurally characterized and compared. The data obtained characterization methods were discussed related to their origin and the extraction procedures. In spite of the fact that the glass transition temperature of all lignins was very close, the T_g of the extracted lignins is higher than commercial lignin's T_g . As a result, the extraction process of lignin was successful with high yield for biomass of vine stem over Turkish pine, but commercial lignin has greater carbon content than extracted lignins. Thus, commercial lignin will give researchers some advantages over extracted lignins for the manufacture of carbon fiber.

Nanofibers were manufactured from electrospinning dispersions of numerous concentration containing lignin and PAN in DMF. By improving the process, PAN/lignin nanofibers of average 150 nm diameter with uniform and circular were produced using the electrospinning when the lignin contents were 5 wt.% over PAN. The morphology of the nanofibers was observed by SEM and correlated to the critical impact of solution rheology. Consideration of the PAN/Lignin nanofibers with FTIR provided a hint for the blending of the two polymers by intermolecular interactions. XRD showed that different concentration of lignin can be played an essential role in nanofiber crystallinity improvement by electrospinning process. Lignin-based carbon nanofibers with graphene were produced for the first time by the electrospinning and

carbonization process. The graphene sheets filled in the PAN/Lignin carbon nanofibers improved the degree of graphitization of pure PAN/Lignin carbon nanofibers. However, the results indicated that the conservation of morphology of nanofibers could be influenced by the high lignin content in PAN/Lignin/GRP nanofibers. This study demonstrated that the reduction in diameter of PAN/Lignin/GRP nanofibers was dependent on the carbonization temperature such as 900 °C and high lignin content in nanofibers.

The last part of this thesis was to use CNF and CNF-G for developing the conductivity of disposable screen-printed electrodes. The characterization of CNF/SPE and CNF-G/SPE in contrast to unmodified SPE was firstly performed by EIS and CV. After measuring the electrical conductivity properties of electrodes, the CNF and CNF-G were clearly increased the conductivity of the screen-printed electrode. Novel modified electrodes combining CNF and CNF-G were developed and used for the electrochemical detection of acetaminophen.

To the best of our knowledge, the biosensor for specific recognition of biomolecules based on CNF-G/SPE was fabricated for the first time in this thesis.

5. REFERENCES

- [1] **Bognitzki, M., Czado, W., Frese, T., Schaper, A., Hellwig, M., Steinhart, M., Greiner, A. and Wendorff, J. H.** (2001). Nanostructured Fibers via Electrospinning, *Adv. Mater.* 13, 70-72.
- [2] **Gouma, P.** (2010). Nanomaterials for chemical sensors and biotechnology, *Singapore: Pan Stanford.*
- [3] **Köhler, J. M., Fritzsche, W.** (2004). Nanotechnology: an introduction to nanostructuring techniques, *Weinheim: Wiley-VCH.*
- [4] **Wei, P., Zhang, L., Lu, Y., Man, N., Wen, L.** (2010). C60 (Nd) nanoparticles enhance chemotherapeutic susceptibility of cancer cells by modulation of autophagy, *Nanotechnology*, 21(49): 495101.
- [5] **Drexler, K. E.** (1992). Nanosystems: Molecular Machinery, Manufacturing, and Computation, *New York: John Wiley & Sons.*
- [6] **Cao, G.** (2004). Nanostructures & nanomaterials: synthesis, properties & applications, *London: Imperial College Press.*
- [7] **Vollath, D.** (2008). Nanomaterials: An Introduction to Synthesis, Properties and Applications, *Wiley-VCH Verlag GmbH & Co. KGaA Weinheim.*
- [8] **Wen, Y.** (2004). Novel Continuous Carbon and Ceramic Nanofibers and Nanocomposites, Ph.D. Dissertation, Department of Mechanical & Materials Engineering, 116 University of Nebraska-Lincoln.
- [9] **Frank, E., Steudle, L. M., Ingildeev, D., Spörl, J. M., and Buchmeiser, M. R.** (2014). Carbon fibers: precursor systems, processing, structure, and properties, *Angew. Chem. Int.* 53, 5262-5298.
- [10] **Huang, X.** (2009). Fabrication and properties of carbon fibers, *Materials*, 2, 2369–2403.
- [11] <http://www.indiantextilejournal.com/articles/FAdetails.asp?id=5331>
- [12] **Hammel, E., Tang, X., Trampert, M., Schmitt, T., Mauthner, K., Eder, A., et al.** (2004). Carbon nanofibers for composite applications, *Carbon*, 42(5–6), 1153–8.
- [13] **Kadla, J. F., Kubo, S., Gilbert, R.D., Venditti, R.A.** (2002). Lignin-based carbon fibers for composite fiber applications, *Carbon*, 40(15), 2913–2920.
- [14] <http://www.news.cornell.edu/stories/May07/nanofibers.fashion.aj.html>
- [15] **Fong, H., Chun, I., Reneker, D. H.** (1999). Carbon Nanofibers from Polyacrylonitrile and Mesophase Pitch, *Journal Of Advanced Materials*, 40, 4585–4592.
- [16] **Wang, Y., Serrano, S., Santiago-Avilé's, J. J.** (2003). Raman characterization of carbon nanofibers prepared using electrospinning, *Synthetic Metals*, 138, 423–427.

- [17] **Baker, D.A., Gallego, N.C., Baker, F.** (2012). On the characterization and spinning of an organic-purified lignin toward the manufacture of low-cost carbon fiber, *Journal of Applied Polymer Science*, 124, 227-234.
- [18] Low Cost Carbon Fiber Overview, (2011). [PowerPoint slides]. Retrieved from http://energy.gov/sites/prod/files/2014/03/f11/lm002_warren_2011_o.pdf
- [19] **Chen, T., Dai, L.** (2013). Carbon nanomaterials for high-performance supercapacitors, *Mater. Today*, 16(7/8), 272-280.
- [20] **Thunga, M., Chen, K., Grewell, D., Kessler, M. R.** (2014). Bio-renewable precursor fibers from lignin/polylactide blends for conversion to carbon fibers, *Carbon*, 68, 159–166.
- [21] **Luckachan, G. E., Pillai, C. K. S.** (2011). Biodegradable polymers, A review on recent trends and emerging perspectives, *J. Polym. Environ.*, 19 (3), 637–676.
- [22] **Kubo, S., Kadla, J. F.** (2005). Lignin-based carbon fibers: Effect of synthetic polymer blending on fiber properties, *J. Polym. Environ.*, 13 (2), 97–105.
- [23] **Baker, D.A. and Rials, T.G.** (2013). Recent advances in low-cost carbon fiber manufacture from lignin, *Journal of Applied Polymer Science*, 130, 713-728. doi: 10.1002/app.39273.
- [24] **Ruiz-Rosas, et al.** (2010). The production of submicron diameter carbon fibers by the electrospinning of lignin, *Carbon*, 48, 696-705.
- [25] **Duval, A., Lawoko, M.** (2014). A Review on Lignin-Based Polymeric, Micro and Nano-Structured Materials, *Reactive and Functional Polymer*, 85, 78-96.
- [26] **Koch, G.** (2008). Raw Material for Pulp. Handbook of Pulp. Wiley-VCH Verlag GmbH, 21-68.
- [27] **Calvo-Flores, F.G., Dobado, J. A.** (2010). Lignin as renewable raw material. *Chemosuschem*, 3 (11), 1227-1235.
- [28] **Seydibeyoglu, M.O.** (2012). A novel partially biobased PAN- lignin blend as a potential carbon fiber precursor, *Journal of Biomedicine and Biotechnology*, 1-8.
- [29] **Kubo, S., Kadla, J.F.** (2006). Carbon fibers from lignin-recyclable plastic blends. Encyclopedia of chemical processing, *Taylor & Francis, U.K.*, 317-331.
- [30] **Ragauskas, A.J., Williams, C.K., Davison, B.H., Britovsek, G., Cairney, J., Eckert, C.A., Frederick, Jr. W.J., Hallet, J. P., Leak, D.J., Liotta, C.L., Mielenz, J.R., Murphy, R., Templer, R., Tschaplinski, T.** (2006). The path forward for biofuels and biomaterials, *Science*, 311, 484-489.
- [31] **Picart, P., de María, P. D., Schallmey, A.** (2015). From gene to biorefinery: microbial β - etherases as promising biocatalysts for lignin valorization, *Front Microbiol*, 6, 916.
- [32] **Li, Y., and Sarkanen, S.** (2002). Alkylated Kraft Lignin-Based Thermoplastic Blends with Aliphatic Polyesters, *Macromolecules*, 35(26), 9707–9715.
- [33] **Gogoi, S. B.** (2010). Adsorption of a Lignin-Based Surfactant on Nahorkatiya Porous Media, *Indian Chem. Eng.*, 52, 325–335.

- [34] **Wang, M., Leitch, M., Xu, C.** (2009). Synthesis of phenol–formaldehydesol resins using organosolv pine lignins, *Eur Polym J.*, *45*, 3380–8.
- [35] **Mankar, S. S., Chaudhari, A. R., Soni, I.** (2012). Lignin in phenol–formaldehyde adhesives, *Int J Knowl Eng.*, *3*(1), 116–8.
- [36] **Strassberger, Z., Tanase, S., and Rothenberg, G.** (2014). The pros and cons of lignin valorisation in an integrated biorefinery, *RSC Adv.*, *4*, 25310–25318.
- [37] **Young, R. A.** (1994). Comparison of the properties of chemical cellulose pulps, *Cellulose*, *1*(2), 107–130.
- [38] **Mabee, W.E., Gregg, D.J., Arato, C., Berlin, A., Bura, R., Gilkes, N., Mirochnik, O., Pan, X., Pye, E.K., Saddler, J. N.** (2006). Updates on Softwood-to-Ethanol Process, *Applied Biochemistry and Biotechnology*, *129-132*, 55–70.
- [39] **Pan, X., Arato, C., Gilkes, N., Gregg, D., Mabee, W., Pye, K., Xiao, Z., Zhang, X., Saddler, J.** (2005). Biorefining of softwoods using ethanol organosolv pulping: preliminary evaluation of process streams for the manufacture of fuel-grade ethanol and co-products. *Biotechnology and bioengineering*, *90*, 473–81.
- [40] **Pan, X., Xie, D., Yu, R. W., Lam, D., Saddler, J. N.** (2007). Pretreatment of Lodgepole Pine Killed by Mountain Pine Beetle Using the Ethanol Organosolv Process: Fractionation and Process Optimization, *Industrial & Engineering Chemistry Research*, *46*, 2609–2617.
- [41] **Mansouri, N-EE., Salvadó, J.** (2006). Structural characterization of technical lignins for the production of adhesives: application to lignosulfonate, kraft, soda-anthraquinone, organosolv and ethanol process lignins, *Ind Crop Prod.*, *24*(1), 8–16.
- [42] **Laurichesse, S., Avérous, L.** (2014). Chemical modification of lignins: towards biobased polymers, *Prog Polym Sci.*, *39*, 1266–1290.
- [43] Low cost carbon fiber from renewable resources, (2010), [PowerPoint slides]. http://www1.eere.energy.gov/vehiclesandfuels/pdfs/merit_review_2010/lightweight_materials/lm005_baker_2010_o.pdf.
- [44] High Strength Carbon Fibers, (2010), [PowerPoint slides], https://www.hydrogen.energy.gov/pdfs/review10/st093_paulauskas_p.
- [45] **Otani, S., Fukuoka, Y., Igarashi, B., Sasaki, K.** (1969). Method for producing carbonized lignin fiber, US Pat.3, 461,082.
- [46] **Reneker, D.H, Yârin, A.L.** (2008). Electrospinning jets and polymer nanofibers, *Polymer*, *49*, 2387-2425.
- [47] **Dallmeyer, I., Ko, F., Kadla, J.F.** (2010). Electrospinning of technical lignins for the production of fibrous networks, *J. Wood Chem. Technol.* *30*, 315–329.
- [48] **Hosseinaei, O., Harper, D.P., Bozell, J.J., Rials, T.G.** (2016). Role of physicochemical structure of organosolv hardwood and herbaceous lignins on carbon fiber performance, *ACS Sustain. Chem. Eng.*, *4*, 5785–5798.
- [49] **Bissett, P. J., Herriott, C.W.** (2010). Fiber dope solution, useful for producing fibers e.g. precursor, oxidized and carbonized fibers, which are useful in e.g. composite

materials, comprises lignin and polyacrylonitrile or polyacrylonitrile copolymer in an organic solvent, patent WO2012003070-A1.

[50] **Ma, X., Kolla, P., Zhao, Y., Smirnova, A.L., Fong, H.** (2016). Electrospun lignin-derived carbon nanofiber mats surface-decorated with MnO₂ nanowhiskers as binder-free supercapacitor electrodes with high performance, *J. Power Sources*, 325, 541-548.

[51] **Choi, D. I., Lee, J.-N., Song, J., Kang, P.-H., Park, J.-K., Lee, Y. M.** (2013). Fabrication of polyacrylonitrile/lignin-based carbon nanofibers for high-power lithium ion battery anodes, *J. Solid State Electr.*, 17 (9), 2471-2475.

[52] **Ago, M., Okajima, K., Jakes, J.E., Park, S., Rojas, O.J.** (2012). Lignin-Based electrospun nanofibers reinforced with cellulose nanocrystals, *Biomacromolecules*, 13 (3), 918-926.

[53] **Lai, C., et al.** (2014). Free-standing and mechanically flexible mats consisting of electrospun carbon nanofibers made from a natural product of alkali lignin as binder-free electrodes for high performance supercapacitors, *J. Power Sources*, 247, 134-141.

[54] **Hu, S., Hsieh, Y.-L.** (2013). Ultrafine microporous and mesoporous activated carbon fibers from alkali lignin, *J. Mater. Chem. A*, 1 (37), 11279-11288.

[55] **Mousavioun, P., Doherty, W. O. S., George, G.** (2010). Thermal stability and miscibility of poly(hydroxybutyrate) and soda lignin blends, *Ind. Crops Prod.*, 32, 656-661.

[56] **Oroumei, A., Fox, B., Naebe, M.** (2015). Thermal and rheological characteristics of biobased carbon fiber precursor derived from low molecular weight organosolv lignin, *Acs Sustain. Chem. Eng.*, 3 (4), 758-769.

[57] **Seo, D. K., Jeun, J. P., Bin Kim, H., Kang, P. H.** (2011). Preparation and characterization of the carbon nanofiber mat produced from electrospun pan/lignin precursors by electron beam irradiation, *Rev. Adv. Mater. Sci.* 28, (1), 31-34.

[58] **Xu, X., Zhou, J., Jiang, L., Lubineau, G., Chen, Y., Wu, X-F., Piere, R.** (2013). Porous core-shell carbon fibers derived from lignin and cellulose nanofibrils, *Mater. Lett.* 109, 175-178.

[59] **Xu, X., Zhou, J., Jiang, L., Lubineau, G., Payne, S.A., Gutschmidt, D.**(2014). Lignin-based carbon fibers: carbon nanotube decoration and superior thermal stability, *Carbon* 80, 91-102.

[60] **Kadla, J. F., Kubo, S.** (2004). Lignin-based polymer blends: analysis of intermolecular interactions in lignin-synthetic polymer blends, *Composites Part A*, 35(3), 395-400.

[61] **Liu, J., Yue, Z., Fong, H.** (2009). Continuous nanoscale carbon fibers with superior mechanical strength, *Small*, 5, 536-42.

[62] **Reneker, D. H., Yarin, A., Fong, L. H., and Koombhongse, S.** (2000). Bending instability of electrically charged liquid jets of polymer solutions in electrospinning, *J. Appl. Phys.*, 87, 4531-4547.

- [63] **Teo, W.E., Inai, R., Ramakrishna, S.** (2011). Technological advances in electrospinning of nanofibers, *Science and Technology of Advanced Materials*, 12,1-19.
- [64] **Gupta, P., Elkins, C., Long, T. E., Wilkes, G. L.** (2005). Electrospinning of linear homopolymers of poly (methyl methacrylate): exploring relationships between fiber formation, viscosity, molecular weight and concentration in a good solvent, *Polymer*, 46, 4799–4810.
- [65] **McKee, M. G., Wilkes, G. L., Colby, R. H., Long, T. E.** (2004). Correlations of Solution Rheology with Electrospun Fiber Formation of Linear and Branched Polyesters, *Macromolecules*, 37, 1760–1767.
- [66] **Thompson, C. J., Chase, G. G., Yarin, A. L., Reneker, D. H.** (2007). Effects of parameters on nanofiber diameter determined from electrospinning model, *Polymer*, 48, 6913–6922.
- [67] **Casper, C. L., Stephens, J. S., Tassi, N. G., Chase, D. B., Rabolt, J. F.** (2004). Controlling Surface Morphology of Electrospun Polystyrene Fibers: Effect of Humidity and Molecular Weight in the Electrospinning Process, *Macromolecules*, 37, 573–578.
- [68] **Theron, S. A., Zussman, E., Yarin, A. L.** (2004). Experimental investigation of the governing parameters in the electrospinning of polymer solutions, *Polymer*, 45, 2017–2030.
- [69] **Bhardwaj, N., Kundu, S.C.** (2010). Electrospinning: A fascinating fiber fabrication technique, *Biotechnology Advances*, 28, 325-347.
- [70] **Dong, X., Lu, C., Zhou, P., Zhang, S., Wang, L., Li, D.** (2015). Polyacrylonitrile/lignin Sulfonate Blend Fiber for Low-cost Carbon Fiber, *RSC Advances*, 5, 42259-42265.
- [71] **Liu, H. C., Chien, A. T., Newcomb, B. A., Liu, Y., Kumar, S.** (2015). Processing, Structure, and Properties of Lignin- and CNT-Incorporated Polyacrylonitrile-Based Carbon Fibers, *ACS Sustain. Chem. Eng.*, 3 (9), 1943-1954.
- [72] **Bissett, P. J., Herriott, C. W.** (2014). Lignin/polyacrylonitrile-containing dopes, fibers, and methods of making same, US Pat. 8771832.
- [73] **Bissett, P. J., Herriott, C. W.** (2012). Lignin/polyacrylonitrile-containing dopes, fibers, and methods of making same, US Pat. 0003471.
- [74] **Zhao, X., Cheng, K., Liu, D.** (2009). Organosolv pretreatment of lignocellulosic biomass for enzymatic hydrolysis, *Appl Microbiol Biotechnol*, 82, 815–827.
- [75] **Brodin, I., Ernstsson, M., Gellerstedt, G., and Sjöholm, E.** (2012). Oxidative stabilisation of kraft lignin for carbon fibre production, *Holzforschung*, 66, 141-147.
- [76] **Li, Y., Cui, D., Tong, Y., and Xu, L.** (2013). Study on structure and thermal stability properties of lignin during thermostabilization and carbonization, *Int. J. Biol. Macromol.*, 62, 663-669.

- [77] **Lallave, M. et al.** (2007). Filled and hollow carbon nanofibers by coaxial electrospinning of alcell lignin without binder polymers, *Adv. Mater.*, *19*(23), 4292-4296.
- [78] **Lin, J., Kubo, S., Yamada, T., Koda, K., and Uraki, Y.** (2012). Chemical thermostabilization for the preparation of carbon fibers from softwood lignin, *Bioresources*, *7*(4), 5634-5646.
- [79] **Braun, J.L., Holtman, K. M., Kadla, J.F.** (2005). Lignin-based carbon fibers: Oxidative thermostabilization of kraft lignin, *Carbon*, *43*, 385-394.
- [80] **Mainka, H.** (2015). Raman and X-Ray Photoelectron Spectroscopy: A Useful Tool for the Chemical Characterization of the Conversion Process of Lignin to Carbon Fiber, http://speautomotive.com/SPEA_CD/SPEA2015/pdf/RF/RF1.pdf.
- [81] **Bao, Q., et al.** (2010). Graphene–Polymer Nanofiber Membrane for Ultrafast Photonics, *Adv. Funct. Mater.*, *20*, 782–791.
- [82] **Chang, Y., Han, G., Li, M., Gao, F.** (2011). Graphene-modified carbon fiber mats used to improve the activity and stability of Pt catalyst for methanol electrochemical oxidation, *Carbon*, *49*(15), 5158–5165.
- [83] **Gao, G. Z., Ko, F., Kadla, J. F.** (2015). Synthesis of noble monometal and bimetal-modified lignin nanofibers and carbon nanofibers through surface-grafted poly (2- (dimethylamino)ethyl methacrylate) brushes, *Macromol. Mater. Eng.*, *300*, 836-847.
- [84] **Meyer, J. C., Geim, A. K., Katsnelson, M. I., Novoselov, K. S., Booth, T. J., Roth, S.** (2007). The structure of suspended graphene sheets, *Nature*, *446*, 60.
- [85] **Yang, W., Ratinac, K.R., Braet, F. et al.** (2010). Carbon Nanomaterials in Biosensors: Should You use Nanotubes or Graphene? *Angew. Chem. Int. Ed.* *49*, 2114-2138.
- [86] **Ouyang, S., Ding, Z. H., Shao, K., Li, Z. E., Xu, L. P.** (1992). Quantitative analysis method of the main chemical compositions in ramie, *Standard of Chinese textile industry*. FZ/T30001-92, 93–101.
- [87] **Zhang, J., Zhang, H., and Zhang, J.** (2014). Evaluation of liquid ammonia treatment on surface characteristics of hemp fiber, *Cellulose*, *21* (1), 569-579.
- [88] **Hatakeyama, T., Nakamura, K., Hatakeyama, H.** (1982). Studies on heat capacity of cellulose and lignin by differential scanning calorimetry, *Polymer*, *23*, 1801-1804.
- [89] **Stenius, P.** (2000). Forest Products Chemistry, *Helsinki: Fapet Oy*.
- [90] **Malherbe, S. and Cloete, T.** (2002). Lignocellulose Biodegradation: Fundamentals and Applications, *Reviews in Environmental Science and Biotechnology*, *1*, 105-114.
- [91] **Prasad, A., S. Singh, and H.C. Joshi** (2007). Ethanol as an alternative fuel from agricultural, industrial and urban residues, *Resources, Conservation and Recycling*, *50*, 1-39.

- [92] **Guimarães, J. L., Frollini, E., da Silva, C.G., Wypych, F., Satyanarayana, K.G.** (2009). Characterization of banana, sugarcane bagasse and sponge gourd fibers of Brazil, *Industrial Crops and Products*, 30(3), pp. 407-415.
- [93] **McKendry, P.** (2002). Energy production from biomass (part 1): An overview of biomass, *Bioresource Technology*, 83 (1), 37–46.
- [94] **Kubo, S., Kadla, J. F.** (2004). Poly (Ethylene Oxide)/Organosolv Lignin Blends: Relationship between Thermal Properties, Chemical Structure, and Blend Behavior, *Macromolecules*, 37(18), 6904-6911.
- [95] **Morais, J.P.S., de Freitas Rosa, M., Nascimento, L. D., do Nascimento, D.M., Cassales, A. R.** (2013). Extraction and characterization of nanocellulose structures from raw cotton linter, *Carbohydrate Polymers*, 91, 229–235.
- [96] **Gordobila, O., Delucis R., Egüés, I., Labidi, J.** (2015). Kraft lignin as filler in PLA to improve ductility and thermal properties, *Industrial Crops and Products*, 72, 46-53.
- [97] **Kubo, S. and J. F. Kadla.** (2005). Hydrogen Bonding in Lignin: A Fourier Transform Infrared Model Compound Study, *Biomacromolecules*, 6(5), 2815-2821.
- [98] **Hergert, H. L.** (1960). Infrared Spectra of Lignin and Related Compounds. II. Conifer Lignin and Model Compounds^{1,2}, *The Journal of Organic Chemistry*, 25(3), 405-413.
- [99] **Liu, Q., Wang, C. S., Zheng, Y., Luo, Z., Cen, K.** (2008). Mechanism study of wood lignin pyrolysis by using TG–FTIR analysis, *J. Anal. Appl. Pyrolysis*, 82, 170–177.
- [100] **Derkacheva, O., and Sukhov, D.** (2008). Investigation of Lignins by FTIR Spectroscopy, *Macromolecular Symposia*, 265(1), 61-68.
- [101] **Li, Z., Qiu, X., Pang, Y., Ouyang, X., Lou, H.** (2009). Adsorption performance of calcium lignosulfonates on surface of solid particle, *Journal of Chemical Engineering of Chinese Universities*, 23, 466.
- [102] **Sjöström, E.** (1981). *Wood Chemistry: Fundamentals and Applications*, ISBN 0-12-647481-18.
- [103] **Boeriu, C.G., Bravo, D., Gosselink, R.J.A., van Dam, J.E.G.** (2004). Characterisation of structure-dependent functional properties of lignin with infrared spectroscopy, 6th International Lignin Institute conference, 20, 205-218.
- [104] **El Mansouri, N. E., Yuan, Q., and Huang, F.** (2011). Characterization of alkaline lignins for use in phenol-formaldehyde and epoxy resins, *BioResources*, 6(3), 2647–62.
- [105] **Sahoo, S., Seydibeyoğlu, M. Ö., Mohanty, A. K., and Misra, M.** (2011). Characterization of industrial lignins for their utilization in future value added applications, *Biomass and Bioenergy*, 35, 4230–4237.
- [106] **Yang, H., Yan, R., Chen, H., Lee, D. H., Zheg, C.** (2007). Characteristics of hemicellulose, cellulose, and lignin pyrolysis, *Fuel*, 86, 1781–8.

- [107] **Tejado, A., Pena, C., Labidi, J., Echeverria, J. M., Mondragon, I.** (2007). Physico-chemical characterization of lignins from different sources for use in phenol-formaldehyde resin synthesis, *Bioresour Technol*, 98, 1655–63.
- [108] **Brebu, M., Vasile, C.** (2010). Thermal degradation of lignin—a review, *Cellul. Chem. Technol.*, 44, 353–363.
- [109] **Feldman, D.** (2002). Lignin and its polyblends – a review, In *Chemical, Modification, Properties, and Usage of Lignin* (T. Q. Hu, ed.), 81-99, *Kluwer Academic/Plenum Publishers, New York*.
- [110] **Chung, Y., Olsson, J.V., Li, J.R., Curtis, W.F., Waymouth, R.M., Billington, S.L., Sattely, E.S.** (2013). A renewable lignin-lactide copolymer and application in biobased composites, *Sustainable Chem. Eng. I*, 1231–1238.
- [111] **Norambuena, M., et al.** (2016). Optimization of Experimental Variables to Modify Lignin from *Eucalyptus globulus* under Alkaline Catalysis, *Bioresources*, 11(1),1828-1842.
- [112] **Mohamad, M., Zakaria, N., Sipaut, C., Sulaiman, O., and Hashim, R.** (2011). Chemical and thermal properties of lignins from oil palm biomass as a substitute for phenol in a phenol formaldehyde resin production, *Carbohydrate Polymers*, 86 (1), 112-119. ISSN 0144-8617.
- [113] **Johansson, L.S., Campbell, J.M., Koljonen, K., Stenius, P.** (1999). Evaluation of surface lignin on cellulose fibers with XPS, *Applied Surface Science*, 144–145, 92–95.
- [114] **Wysocki, M., Klapiszewski, L., Moszyński, D., Bartczak, P., Szatkowski, T., Majchrzak, I., Siwińska-Stefańska, K., Bazhenov, V.V., Jesionowski, T.** (2014). Modification of Chitin with Kraft Lignin and Development of New Biosorbents for Removal of Cadmium(II) and Nickel(II) Ions, *Mar Drugs*, Apr, 12(4), 2245–2268.
- [115] **Huang, C., Yang, Q., Wang, S.** (2012). XPS Characterization of Fiber Surface of Chemithermomechanical Pulp Fibers Modified by White-Rot Fungi, *Asian Journal of Chemistry*, 24 (12), 5476-5480.
- [116] **Buchko, C. J., Chen, L. C., Shen, Y., Martin, D. C.** (1999). Processing and microstructural characterization of porous biocompatible protein polymer thin films, *Polymer*, 40(26), 7397–7407. doi:10.1016/s0032-3861(98)00866-0 24.
- [117] **Shenoy, S. L., Bates, W. D., Frisch, H. L., and Wnek, G. E.** (2005). Role of chain entanglements on fiber formation during electrospinning of polymer solutions: good solvent, non-specific polymer-polymer interaction limit, *Polymer*, 46(10), 3372–3384.
- [118] **Kopperud, H. M., Hansen, F. K., and Nystrom, B.** (1998). Effect of surfactant and temperature on the rheological properties of aqueous solutions of unmodified and hydrophobically modified Poly(acrylamide), *Macromolecular Chemistry Physics*., 199, 2385-2394.

- [119] **Hardick, O., Stevens, B., Bracewell, D. G.** (2011). Nanofibre fabrication in a temperature and humidity controlled environment for improved fibre consistency. *J Mater Sci.*, *46*, 3890–3898.
- [120] **De Vrieze, S., Van Camp, T., Nelvig, A., Hagström, B., Westbroek, P., De Clerck, K.** (2009). The effect of temperature and humidity on electrospinning, *J Mater Sci.*, *44*, 1357–1362.
- [121] **Zampetti, E., Muzyczuk, A., Macagnano, A., Pantalei, S., Scalese, S., Spinella, C., Bearzotti, A.** (2011). Effects of temperature and humidity on electrospun conductive nanofibers based on polyaniline blends, *J Nanopart Res.*, *13*, 6193–6200.
- [122] **Ramalingam, K. J., et. al.** (2014). Electrical measurement of PVA/graphene nanofibers for transparent electrode applications, *Synthetic Metals*, *191*, 113-119.
- [123] **Rahatekar, S. S., Koziol, K. K. K., Butler, S. A., Elliott, J. A., Shaffer, M. S. P., Mackley, M. R., Windle, A. H.** (2006). Optical microstructure and viscosity enhancement for an epoxy resin matrix containing multiwall carbon nanotubes, *J. Rheol.*, *50*, 599–610.
- [124] **Jaber, E., Luo, H., Li, W., Gersappe, D.** (2011). Network formation in polymer nanocomposites under shear, *Soft Matter*, *7*, 3852–3860.
- [125] **Montgomery, D. C.** (1991). Design and Analysis of Experiments. *John Wiley & Sons, Inc: New York*.
- [126] **Saligheh, O., Eslami-Farsani, R., Khajavi, R., Forouharshad, M.** (2013). The study of processing parameters on impact behavior of high performance polyethylene fiber cross-ply composites by Taguchi method, *Fiber. Polym.*, *14*, 1864.
- [127] **Soboleva, T., Xie, Z., Shi, Z., Tsang, E., Navessin, T., Holdcroft, S.** (2008). Investigation of the through-plane impedance technique for evaluation of anisotropy of proton conducting polymer membranes, *J. Electroanal. Chem.*, *622*, 145–152.
- [128] **Mathur, R. B., Bahl, O. P., Sivaram, P.** (1992). Thermal degradation of polyacrylonitrile fibres, *Curr. Sci.*, *62*(10), 662-669.
- [129] **Panapoy, M., Dankeaw, A., Ksapabutr, B.** (2008). Electrical Conductivity of PAN-based. Carbon Nanofibers Prepared by Electrospinning Method, *Int. J. Sci. Technol.* *13*, 11.
- [130] **Liu, H. C., Chien, A. T., Newcomb, B. A., Liu, Y., Kumar, S.** (2015). Processing, structure, and properties of lignin-and CNT-incorporated polyacrylonitrile-based carbon fibers, *ACS Sustainable Chemistry & Engineering*, *3* (9), 1943-1954.
- [131] **Arshad, S. N., Naraghi, M., and Chasiotis, I.** (2011). Strong carbon nanofibers from electrospun polyacrylonitrile, *Carbon*, *49*(5), 1710.
- [132] **Heidari, M., Bahrami, S. H., Mohammadi, M. R.** (2015). Preparation and Characterization of Electrospun PCL/Gelatin Nanofibers Containing Graphene Nanoparticles, The 13th Asian Textile Conference, 486 -1108.

- [133] **Yuan, X.** (2011). Enhanced interfacial interaction for effective reinforcement of poly (vinyl alcohol) nanocomposites at low loading of graphene, *Polym. Bull.*, 67 1785–1797.
- [134] **Si, Y., Samulski, E.T.** (2008). Synthesis of Water Soluble Graphene, *Nano Lett.* 8(6), 1679–1682.
- [135] **Xu, Y., Bai, H., Lu, G., Li, C., Shi, G.** (2008). Flexible Graphene Films via the Filtration of Water-Soluble Noncovalent Functionalized Graphene Sheets, *J. Am. Chem. Soc.*, 130(18), 5856–5857.
- [136] **Nirmala, R., Jeon, K., Navamathavan, R., Kim, B. S., and Khil, M. S.** (2013). Fabrication and characterization of II-VI semiconductor nanoparticles decorated electrospun polyacrylonitrile nanofibers, *J. Colloid. Interface. Sci.*, 397, 65-72.
- [137] **Saud, P. S., et. al.** (2015). Synthesis and Characterization of Photocatalytic and Antibacterial PAN/Ag₂CO₃ Composite Nanofibers by Ion Exchange Method, *Fibers and Polymers*, 16(6), 1336–1342.
- [138] **Zhang, C., Zhu, X., Wang, Z., Sun, P., Ren, Y., Zhu, J., Zhu, J., Xiao, D.** (2014). Facile synthesis and strongly microstructure-dependent electrochemical properties of graphene/manganese dioxide composites for supercapacitors, *Nanoscale Res Lett.*, 9(1), 490.
- [139] **Sahatiya, P., and Badhulika, S.** (2015). One step in-situ single aligned Graphene-ZnO nanofiber for UV sensing, *RSC Advances.*, 5(100), 82481-82487.
- [140] **Goudarzi, A., Lin, L-T., Ko, F. K.** (2014). X-Ray Diffraction Analysis of Kraft Lignins and Lignin-Derived Carbon Nanofibers, *J. Nanotechnol. Engineer. Med.*, 5(2), 021006.
- [141] **Hoor, F. A., Morshedian, J., Ahmadi, S., Rakhshanfar, M., Bahramzadeh, A.** (2015). Effect of Graphene Nanosheets on the Morphology, Crystallinity, and Thermal and Electrical Properties of Super Tough Polyamide 6 Using SEBS Compounds, *Journal of Chemistry*, 6 pages.
- [142] **Harish Kumar, R. N.** (2014). Temperature: Stabilization in Oxidation stage during Carbon Fibre production, *International Journal of Engineering Science Invention*, 3 (8), 23-27.
- [143] **Ferrari, A. C., Robertson, J.** (2000). Interpretation of Raman spectra of disordered and amorphous carbon, *Physical Review B.*, 61(20), 14095-14107.
- [144] **Lucchese, M. M., et al.** (2010). Quantifying ion-induced defects and Raman relaxation length in graphene, *Carbon*, 48, 1592–1597.
- [145] **Cançado, L. G., et al.** (2006). General equation for the determination of the crystallite size La of nanographite by Raman spectroscopy, *Appl Phys Lett*, 88, 163106.
- [146] **Kilic, T., Kaplan, M., Demiroglu, S., Erdem, A., Ozsoz, M.** (2016). Label-free electrochemical detection of microRNA-122 in real samples by graphene modified disposable electrodes, *J. Electrochem. Soc.*, 163 (6), 227-233.

[147] **Sun, J., Liu, Y., Lv, S., Huang, Z., Cui, L., Wu, T.** (2016). An Electrochemical Sensor Based on Nitrogen-doped Carbon Nanofiber for Bisphenol A Determination, *Electroanalysis*, 28 (3), 439-444.





Name : Sibel Demirođlu Mustafov,
Postal Address : İzmir Kâtip Çelebi University,
Material Science and Engineering
Çiđli Ana Yerleşkesi 35620 Çiđli, İzmir
Birth Date and Place : 27 September 1983, Amasya, Turkey
Phone : +90 507 412 72 75
e-mail : sbldemiroglu@gmail.com

EDUCATION

Ph.D.	2013-	İzmir Kâtip Çelebi University, İzmir, Turkey Nanotechnology
M.Sc.	2009	Rovira i Virgili University, Tarrogon, Spain Nanotechnology
B.Sc.	2008	Ege University, İzmir, Turkey Bioengineering

WORK EXPERIENCE

05/2016-11/2016	Doctoral Research Fellow , Guelph University, Guelph Canada, School of Engineering with Prof. Amar Mohanty. Worked on lignin based nanofiber and biocomposites.
05/2015-05/2017	Project Assistant , İzmir Kâtip Çelebi University, İzmir, Turkey.
09/2010-09/2011	Teaching Turkish and web designer , Turkish Language Center, İzmir, Turkey.
07/2006-09/2006	Summer Intern , CNR with Dr. Giuseppe Torzillo,

Florence, Italy, Worked on production hydrogen by using microalgae.

PROJECTS

0774.STZ.2014 Industry Project funded by Ministry of Technology, “Halogen Free Flame Retardants for Paint Industry”, Researcher, 05/2015-05/2017, \$95,000

2015-TDR-FEBE-0011İzmir Kâtip Çelebi University, “The production of graphene enhanced lignin-PAN nanofibers for biosensor applications”, Scientific Research Projects, Researcher, 08/2015-06/2016

GRANTS

BDDC, Guelph University, Canada-Visiting Scholar, May-November (6 months)

VIBes in bioscience, 17-19 September 2014, Antwerp-Belgium (Travel Grant)

Rovira i Virgili University, Spain- Master Fellowship

Hands-on experiences on

- Carbonization furnace
- Thermal stabilization oven
- Electrospinning
- Thermogravimetric Analysis (TGA)
- Differential Scanning Calorimetry (DSC)
- Fourier-transform infrared spectroscopy (FTIR)
- Electrochemical analyses- Autolab (Potentiostat/Galvanostat)
- Contact angle
- Rheometry
- Scanning Electron Microscopy (SEM)
- X-Ray Diffraction (XRD)
- Sonicator
- Limiting Oxygen Index Testing (LOI)
- Viscosimetry

- Polymerase Chain Reaction (PCR)
- Gel electrophoresis

PUBLICATIONS

THESIS

Ph.D. Thesis “Nanocomposites with graphene”, 2013-

M.Sc. Thesis “Development of solid-contact needle-type ion-selective microelectrodes using carbon nanotubes”, 2009.

BS. Thesis “Development of a cost- effective photobioreactor design for mass cultivation of microalgae”, 2008.

BOOK CHAPTERS

1. **Sibel Demiroğlu**, M. Özgür Seydibeyoğlu, Manjusri Misra, Amar K. Mohanty, “The Use of Nanotechnology for Fiber Reinforced Composites” in the book “Fiber Technology for Fiber Reinforced Composites”, Woodhead Publishing, Elsevier, 2017.
2. Metehan Atagür, **Sibel Demiroğlu**, M. Özgür Seydibeyoğlu, “Flame retardancy of composites and nanocomposites based on PU polymers” in the book “Polyurethane Blends and IPNs”, Elsevier, 2017.

PEER REVIEWED JOURNAL PUBLICATIONS

1. Seydibeyoglu MO, **Demiroglu S**, Atagur M, Yanar Ocaktan S, Modification of Clay Crystal Structure with Different Alcohols, Scientific Research Publishing, 2017, 8 (11), 709-715.
2. **Demiroglu S**, Erdogan F, Akın E, Karavana HA, Seydibeyoglu MO, Natural Fiber Reinforced Polyurethane Rigid Foam, GUJ Sci., 2017, 30(2),97-109.

3. Kavur AE, **Demiroglu S**, Seydibeyođlu MO, Bařer O, Güzeliř C, řahin S, Design and Implementation of Chaotic System Based Robust Delta Robot for Blending Graphene Nanoplatelets, IEEE Conference Paper, 2016, DOI: 10.1109/MMAR.2016.7575139.
4. Kilic T, Kaplan M, **Demiroglu S**, Erdem A, Ozsoz M, Label-Free Electrochemical Detection of MicroRNA-122 in Real Samples by Graphene Modified Disposable Electrodes, J. Electrochem. Soc., 2016,163 (6), 227-233.
5. Seydibeyođlu MO, **Demirođlu Mustafafov S**, Kavur AE, Bařer O, Isler Y, Güzeliř C, řahin S, A New Method for Preparing Nanocomposites, Chaotic Mixing for Graphene Nanocomposites, Beilstein Journal of Nanotechnology, under review, 2017.
6. **Demiroglu Mustafafov S**, Misra M, Mohanty A, Seydibeyoglu MO, Extraction and Characterization Lignin from Different Biosources, in preparation for Biomass and Bioenergy
7. **Demiroglu Mustafafov S**, Misra M, Mohanty A, Seydibeyoglu MO, Processing and Characterization of Graphene Enhanced Lignin-PAN Nanofibers in preparation for Carbon.
8. **Demiroglu Mustafafov S**, Misra M, Mohanty A, Seydibeyoglu MO, Fabrication and Characterization of Lignin-Based Carbon Nanofiber Reinforced Graphene in preparation for Journal of Biobased Materials and Bioenergy.
9. **Demiroglu Mustafafov S**, Sabankay M, Özveren N, Seydibeyoglu MO, The Use of Microalgae in Various Application: Past, Present and Future Projections, in preparation for Algal Research.

CONFERENCES/PRESENTATIONS

Oral Presentations

1. **S. Demiroglu**, O. Seydibeyoglu, “Polyurethane Foams in Biomedical Applications”, 1st International Congress on Green Chemistry and Sustainable Technologies, 30-03 October 2015, Çeřme, Izmir-Turkey.

2. **S. Demiroglu**, F. Erdoğan, A. Ayvalık, E. Akın, M. O. Seydibeyoglu, “Polyurethane Foam Reinforced Natural Fibers”, 1st International Congress on Green Chemistry and Sustainable Technologies, 30-03 October 2015, Çeşme, Izmir-Turkey.
3. **S. Demiroglu**, O. Seydibeyoglu, “Characterization of Various Lignins from Different Resources”, 1st International Congress on Green Chemistry and Sustainable Technologies, 30-03 October 2015, Çeşme, Izmir-Turkey.
4. M. S. Ozsoz, **S. Demiroglu**, M. Kaplan, T. Kılıc, “Cancer Biomarker MicroRNAs Detection Based on Graphene by Electrochemical Method in Cell Lysates”, Pittcon Conference and Expo, 12 March 2015, New Orleans, USA.

Posters and Workshops

1. **S. Demiroglu**, M. O. Seydibeyoğlu, M. Misra, A. K. Mohanty, Development of Biosensor by Using Low Cost BioRefinery Lignin, Bioeconomy Research and Innovation Forum Collaborating to Advance Ontario's Bioeconomy, 24 October 2016, Guelph, Canada, poster.
2. Kavur A.E, **Demiroglu S**, Seydibeyoğlu M.O, Başer O, Güzeliş C, Şahin S, Design and Implementation of Chaotic System Based Robust Delta Robot for Blending Graphene Nanoplatelets, MMAR 2016, August 29-September 1, Miedzzydroje, Poland, Poster.
3. **S. Demiroglu**, A.E Kavur, C. Güzeliş, O. Başer, M.O Seydibeyoğlu, S. Şahin, A Novel Approach to Prepare Graphene Nanocomposites via Chaotic Mixing, ISBBB 2016, May 31-June 3, Guelph, Canada, Poster.
4. **S. Demiroglu**, S.Y. Yıldız, O. Seydibeyoglu, M.S. Ozsoz, Electrochemical biosensor based on graphene, 2nd International Congress on Biosensor, Gediz University, 10-12 June 2015, Izmir-Turkey, Poster.
5. S. Y. Yıldız, F. C. Sendan, M. Yıldız, **S. Demiroglu**, O. Seydibeyoglu, E. Aydın, Functionalized Carbon Nanotube Based Biosensors for Cancer Detection, 2nd International Congress on Biosensor, Gediz University, 10-12 June 2015, Izmir-Turkey, Poster.

6. **S. Demiroglu**, M. Kaplan, M.S. Ozsoz, III. International Workshop and Training Course on Electrochemistry, 03-07 June 2014, Ayvalık-Turkey (Course Instructor)
7. **S. Demiroglu**, M. Senisik, M. Kaplan, T. Kılıc, M. S. Ozsoz, “The importance of miRNA in the cancer diagnosis”, Medicine Faculty of Ege University, 07 November 2013 Izmir-Turkey, Poster.
8. **S. Demiroglu**, M. Conk Dalay, Undergraduation thesis, “Comperation of Photobioreactors for Microalgae/ Cyanobacteria Production”, Bioengineering Department of Ege University, 01-02 May 2007, Izmir-Turkey, Poster.